Adaptable Electrically Steerable Antenna Array with Diverse Switchable Polarization

by

Jorden Mark Labossiere

A thesis submitted to the Faculty of Graduate and Postdoctoral Affairs in partial fulfillment of the requirements for the degree of

Master of Applied Science

in

Electrical Engineering

Department of Electronics
Faculty of Engineering
Carleton University
Ottawa, Ontario

Abstract

Adaptability is essential for antenna systems, especially those operating in harsh or unpredictable environments. Adaptable electrically steerable antennas (AESA) provide this flexibility. AESA use in radar systems is expanding due to new technologies that enable higher power and more miniaturized implementations. Polarization diversity is another way of adding adaptability to radar systems.

System-level analysis of a typical radar system was performed to determine the specifications for a series of 4x4 switchable polarization AESA arrays meant to operate from 9.4 to 9.5 GHz. These arrays were designed on a multilayer Rogers Duroid PCB. Sub-components such as a microstrip feeding network, patch antennas, switches and hybrid couplers were integrated on the same PCB utilizing both sides of the board. Simple 4x4 linear and 4x4 circular polarized arrays were designed and fabricated on this chosen package. These single-polarization arrays were compacted into a single low-profile PCB that measures 2.5x2.5 inches. The measurements of both single-polarization arrays closely matched the simulated results, which helped correct issues with the design process before adding more polarization states. Measurements show that these modularly scalable 2.5x2.5-inch PCBs can achieve a gain of between 12 and 21 dB depending on how many boards are tiled together.

A technique for increasing the bandwidth of a single patch antenna through resistive loading was also explored. Using commercially packaged resistors to load a single patch resulted in a bandwidth increase of 400 MHz.

Once simple single-polarization arrays were verified, two switchable polarization arrays, one linear and one circular, were designed and simulated. These switchable

polarization arrays utilized the same PCB setup as the previous two arrays but with the addition of an SPDT and 90º hybrid coupler. A method for miniaturizing a hybrid coupler through capacitive loading is also presented. The miniaturized coupler had a central area of around 135x120 mils, a sound reduction from a conventional coupler of 230x215 mils shown in reference [9]. Simulation of the switchable polarization arrays showed promising results of an array that can switch between either vertical or horizontal linear polarization or between LHCP and RHCP with up to 16 dB of gain.

Due to global supply chain disruption and related production delays, the fabricated switchable polarization antenna arrays were not measurement ready at the time of writing. Once received, they can be measured and the results published later.

Acknowledgments

The professors at the Department of Electronics at Carleton University challenged me in unique ways. Those who pushed the hardest helped prove that I can accomplish great things if I stay focused, have a plan and trust my abilities.

My supervisor and mentor, Rony E. Amaya, whose guidance has expanded my skillset and opened up many research and work opportunities.

My high school physics teacher Eric Lorenzen whose passion for science inspired me to pursue engineering as a career.

My mother, Elizabeth Clark who raised and supported me throughout my academic career from elementary and high school up to this point.

My late father, Joel Labossiere, who I always looked up to as a child and still do to this day. While he passed long before I decided to pursue a career in engineering, his example is the one I try to follow in my professional career.

Table of Contents

List of Tables

List of Figures

List of Abbreviations

AESA	Active Electrically Steerable Antenna
EIRP	Effective Isotropic Radiated Power
HPBW	Half Power Beam Width
LHCP	Left Hand Circular Polarization
PCB	Printed Circuit Board
POC	Proof of Concept
Q	Quality Factor
QWT	Quarter Wave Transformer
RHCP	Right Hand Circular Polarization
SOP	System on Package
SPDT	Single Pole Double Throw
VNA	Vector Network Analyzer
VSWR	Voltage Standing Wave Ratio

Chapter 1: Introduction

1.1 Motivation

Technologies used in industrial and military aerospace applications are held to a higher standard than those used in commercial systems, requiring more specialized packaging processes. Adaptability is essential for antenna systems, especially those operating in harsh or unpredictable environments. The current design approach is to build systems that always function under their worst-case specifications. This design approach results in overdesigned radar systems with redundancies that increase the size and price of the whole system [1] [2]. A better approach would be to design adaptive antenna systems for use in different environments. This approach is otherwise known as Active Electrically Steered Antennas (AESA). AESA is not a new technology, but its use in radar systems is expanding due to new technologies that enable higher power and more miniaturized implementations. AESA has a few advantages over conventional radar systems. Beam steering makes tracking and searching completely independent, dramatically improving system detection capabilities. It enables simultaneous mode implementation. Steering the beam electrically rather than mechanically increases the reliability and makes platform installation easier. AESA also offers an improved power budget, lower losses and beam-shaping capabilities, enabling the radiation pattern to adapt to the environment [3].

In addition to AESA, polarization diversity has gained significant interest in radar systems. Polarization diversity can benefit radar system performance by enhancing channel capacity and reducing multipath interference since a multipolar system can receive and transmit multiple pieces of data simultaneously at different polarizations [4] [5]. Pattern diversity can also improve the radiation coverage of multiple objects, and it is

also helpful for autonomous vehicles, moving target detection, and satellite links [6][7]. The antenna is often designed to have the same polarization as the received signal in conventional radar systems, and the antenna may be designed to transmit and receive waves at multiple polarizations in more complex radar systems. Waves of different polarization can be transmitted separately, using a switch to direct energy to the different parts of the antenna. Circularly polarized signals can be created by feeding two linear polarized signals from the antenna with similar magnitude and 90° phase shift [8].

Switchable polarization antennas have been done before, but two areas where they can be improved are system-on-package (SOP) and miniaturization [9]-[12]. The designs seen in [9] and [10] show good integration but can be improved by reducing the size of their packaged components. Other designs such as [11] can benefit from adding switching components on the package. System On Package (SOP) integration benefits from not committing to one given technology that allows incorporation of various components while getting the benefits of each one, which results in designs with lower cost and faster development time [13].

1.2 Methodology and Thesis Objectives

This thesis was initially part of a project tailored towards supporting surveillance of Canadian coastal borders. The work planned for this thesis was based on an X-band radar platform with a center frequency of 9.45 GHz. Initially, research was done in collaboration with a Canadian company to develop the system specifications for the project. The proposed research initially focused on developing technologies for adaptive wireless systems operating in harsh conditions. The research plan included:

- System analysis of full AESA to develop specifications of each subcomponent.
- Use of active MMIC beamformer to support AESA arrays. This will initially be done using a commercially purchased part, and a replacement will then be designed in gallium nitride (GaN) with all unnecessary components removed.
- Arrays can be used for both low and high-power applications depending on the power limitations of the circuitry involved.
- Implement a scalable 4x4 AESA array that can be used to form larger arrays by tiling multiple 4x4 array boards together in different shapes.
- Testing and calibration of the final system.

Due to global events, this company dropped the project and research was forced to continue independently. The target goals presented in this thesis also had to be scaled down significantly. The accomplishments achieved are presented as follows.

- System analysis of full AESA to develop specifications of subcomponents.
- Implement a 4x4 linear polarized array that can be tiled to form larger arrays. Called Proof of Concept 1 (POC1).
- Implement a 4x4 circular polarized array that can be tiled to form larger arrays. Called Proof of Concept 2 (POC2).
- Testing of POC1 and POC2
- Designs of two different switchable polarization boards (POC3), one linear and one circular, by integrating packaged components such as an SDPT and miniaturized hybrid coupler on the antenna PCB.
- Design of a miniaturized 90° degree hybrid coupler.

1.3 Thesis Organization

This thesis will follow the process of designing an AESA system on PCB technology along with packaged components in order to achieve the end goal of having an antenna array with switchable polarization on a small package.

Chapter 2 will summarize the needed background concepts needed for the research done in this thesis. Concepts such as patch antenna functionality, antenna arrays, different polarization types, and package components such as hybrid couplers, SDPTs and antenna measurement will be discussed.

Chapter 3 discusses POC1, which is the first attempt at making a simple linearly polarized patch array on the desired substrate before adding any additional components or polarization types.

Chapter 4 discusses POC2, which is similar to POC1 but with the added twist of making a circularly polarized patch array instead of linearly polarized.

Chapter 5 will discuss POC3, which attempts to make two different switchable polarization boards, one linear and one circular, by integrating packaged components such as an SDPT and miniaturized hybrid coupler on the antenna PCB.

Chapter 6 will conclude this thesis with a re-summary of the accomplished contributions and a discussion of future work and possible expansions on the research already done.

Chapter 2: Theoretical Background

This chapter will discuss the theoretical operation of several sub-components that comprise the overall switchable polarization AESA system. These include microstrip patch antennas, antenna arrays, wave polarization, integrated circuit switches, hybrid couplers and antenna measurement techniques. An explanation of how each sub-component contributes to achieving the overall goal of a diversely polarized antenna system will also be provided.

2.1 Patch Antennas

A patch antenna consists of a flat sheet of metal separated from another sheet of metal that acts as a ground plane with a dielectric material connecting the two. Patch antennas give off radiation via the fringing fields along the edges [14].

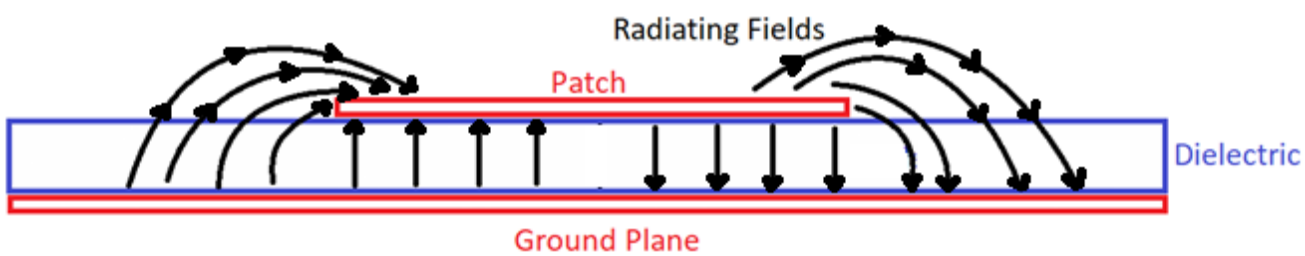

Figure 2.1: Patch Antenna Geometry with Fringing Fields.

Microstrip antennas are quick and cheap to manufacture and design because of this simple 2D geometry. They are beneficial at high frequencies because the short wavelengths mean that the size of the antenna is usually compact [15].

One advantage of patch antennas is the ability to have diverse polarizations. Patch antennas can be easily designed to have vertical, horizontal, right-hand circular (RHCP)

or left-hand circular (LHCP) polarization. This can be done using multiple feed points, allowing the polarization to be set based on the amplitude and phase of each input [16]. This property makes patch antennas perfectly suited for a system that requires switchable polarization.

The important substrate characteristics for patch antennas are the dielectric constant ε_r, the loss tangent $\tan\delta$ and the height of the dielectric substrate h. Substrates with high $\tan\delta$ will increase dielectric loss and therefore lower the efficiency. Thicker substrates will have higher radiated power and better bandwidth but a higher dielectric loss. The dielectric constant plays a similar role as the thickness. Lower values of ε_r will increase the radiated power via the fringing fields at the patch edges. Therefore, it is recommended to select a substrate that has a low ε_r and $\tan\delta$ with the thickness adjusted to get the desired bandwidth [15].

2.1.1 Radiation Pattern

The directivity of an antenna is defined as how well the emitted radiation is concentrated in a single direction. It is a ratio of the maximum radiation intensity in the main beam to the average radiation intensity in all directions [14]. Figure 2.2 below gives a visual representation of antenna radiation.

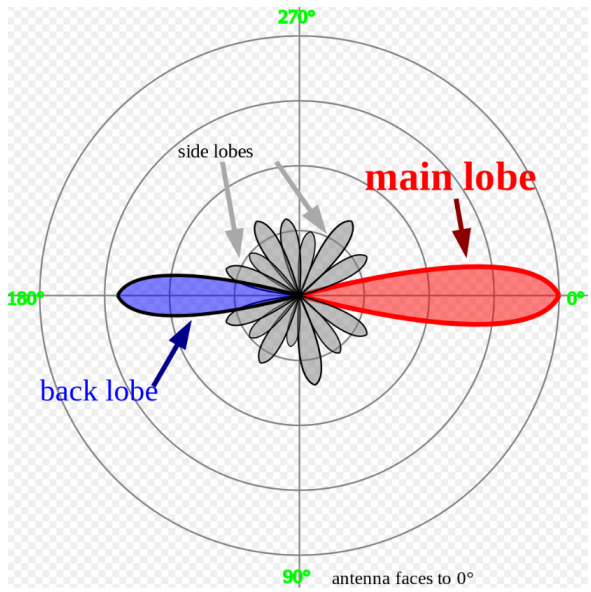

Figure 2.2: Typical Antenna Radiation Pattern [17].

The most prominent lobe is the main lobe, with the most significant radiation intensity. Side lobes are located to the side of the main, while the lobe directly behind is called the back lobe. Radiation patterns are typically plotted in spherical coordinates and represented by two planes; the x-y or azimuthal plane containing the phi-component of the pattern and the x-z or elevation plane containing the theta-component of the pattern. A visual representation of these planes is given in Figure 2.3 below.

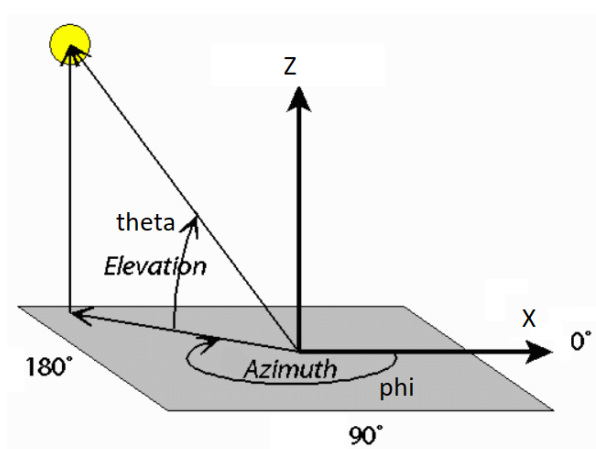

Figure 2.3: Visual Representation of Spherical Coordinate System.

Radiation efficiency is the ratio of the total power radiated by an antenna to the input power of the antenna. Patch antennas cannot radiate 100% of the input power due to conductive and dielectric loss in the substrate [14]. Other factors that can degrade radiation efficiency are impedance mismatches at the input port of the antenna and any gain or phase imbalances between ports for multi-input antennas [16].

Antenna gain is the combination of directivity and efficiency, as shown in Equation 2.1 [14].

$$G = \eta D \tag{2. 1}$$

Gain describes how well the antenna actually radiates in a single direction when all of its losses are considered. It should be noted that when there is no direction specified, the gain is assumed to be the peak gain in the direction of the main lobe [14].

2.1.2 Bandwidth

The bandwidth of an antenna can be defined in multiple ways depending on the desired characteristics. Typically, the bandwidth of an antenna describes the frequency range over which the antenna can adequately radiate or receive a signal. When no specific preference is given, the impedance bandwidth is used [14].

Impedance bandwidth is based on the losses an antenna experiences if mismatched to the feeding line. The load reflection coefficient Γ_L represents this loss where the antenna meets the feeding network. Figure 2.4 shows the reflection coefficient where Z_o represents the feeding network and Z_L represents the antenna.

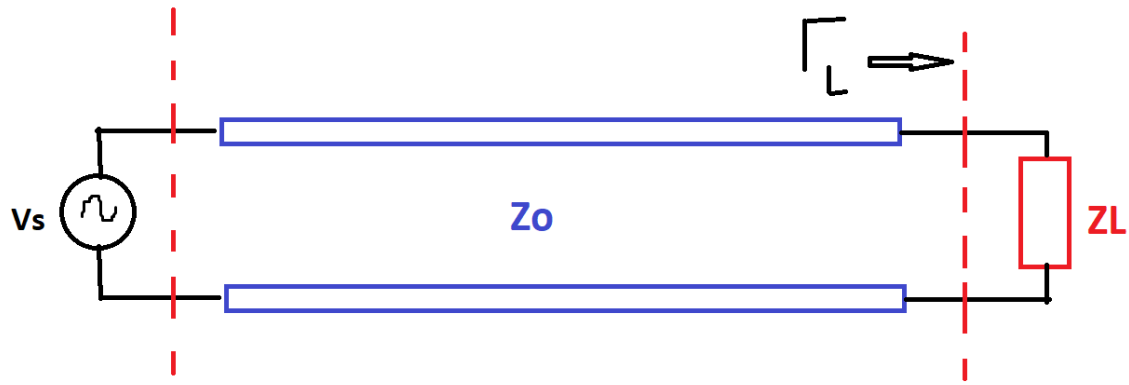

Figure 2.4: Microstrip Reflection Coefficient Due to Load Mismatch.

Equations 2.2-2.4 show how the reflection coefficient is calculated and determines the impedance bandwidth through voltage standing wave ratio (VSWR) and return loss [18].

$$\Gamma_{\mathrm{L}} = \frac{Z_L - Z_o}{Z_L + Z_o} \tag{2. 2}$$

VSWR measures how much power delivered to the load gets reflected. It is a ratio between transmitted and reflected waves, and high VSWR indicates poor efficiency and high reflected energy.

$$VSWR = \frac{1 + \Gamma_{\mathrm{L}}}{1 - \Gamma_{\mathrm{L}}} \tag{2. 3}$$

The reflection loss is another way to represent the power lost or reflected from the load due to mismatches.

$$RL = -20\log_{10}(\Gamma_{\mathrm{L}}) \tag{2. 4}$$

Impedance bandwidth specifies the difference between the upper and lower frequency where the antenna accepts more than 90% of the input power. This percentage corresponds to a return loss of below -10 dB or a VSWR of less than 2.0 [19].

2.2 Antenna Arrays

A single microstrip patch antenna is enough to meet the requirements for specific applications. However, patch antennas can be combined to form arrays for applications that require higher gain or beam steering capabilities. A planar array formation is where antenna elements are placed side by side along a rectangular grid. Planar arrays have good beam control and are useful for applications that require thin pencil-like beams [20]. Figure 2.5 shows the standard configuration of a planar patch antenna array.

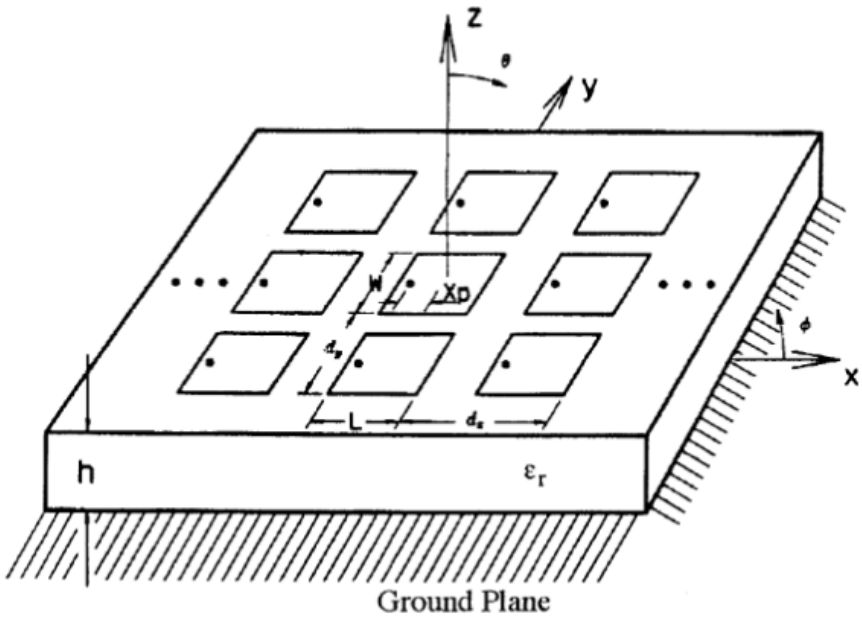

Figure 2.5: Infinite Planar Array of Microstrip Patches [14].

Antenna arrays achieve high gain and narrow beams through the superposition of the radiation patterns of the individual elements into a single pattern. The main beam of the array can be steered to cover a section of space via two methods. Mechanical steering requires the entire array to be physically rotated so the beam can cover the desired space. Electrical beam steering is achieved by controlling the signal phase fed to each antenna

element while the array remains stationary [20]. Figure 2.6 gives a visual representation of pattern superposition and electrical beam steering.

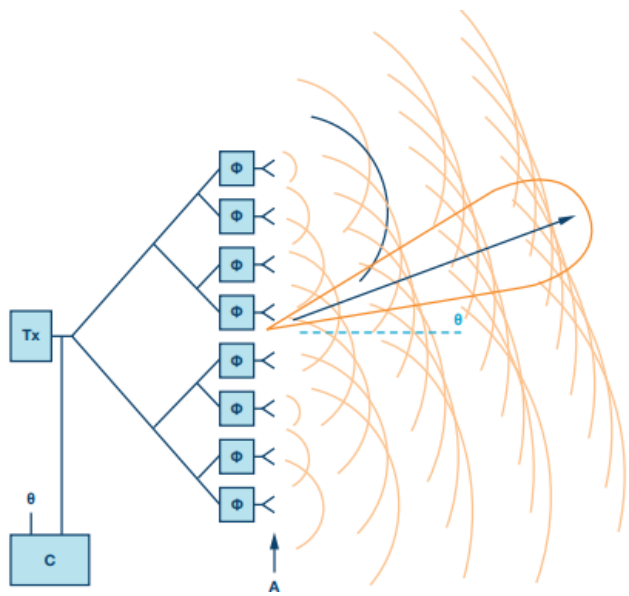

Figure 2.6: Diagram of Phased Array Elements Basic Theory [21].

Electrical steering has a few advantages over mechanical such as a lower profile, faster steering and multiple beams. Two parameters to keep in mind when designing an antenna array are the array gain and effective isotropic radiated power (EIRP). Array gain is directly proportional to the gain of each antenna element and the number of elements, as seen in Equation 2.5 below [21].

$$G_A = 10\log_{10}(N) + G_E \qquad \textbf{(2. 5)}$$

The EIRP of the array can also be thought of as the power a perfect isotropic antenna would have to radiate to achieve the same power measured at the receiver. EIRP is directly proportional to the transmitted power and gain of the antenna array, as seen in Equation 2.6 below [21].

$$EIRP_{dBm} = (P_t)_{dBm} + (G_A)_{dBi} \qquad \textbf{(2. 6)}$$

2.2.1 Element Spacing and Sidelobes

Sidelobes are an unavoidable part of all directional antennas. Diffraction effects in travelling waves that occur from discontinuities in radiating surfaces cause sidelobes in an antenna [22].

There is a particular type of sidelobe for antenna arrays called grating sidelobes. Grating sidelobes are caused by the spacing between antenna elements in the array. Since the goal of an antenna array is for the radiation patterns of each element to combine, spacing the elements far apart defeats this purpose. If the elements are too far apart, the array will radiate several small patterns instead of one prominent lobe. Grating sidelobes result from this phenomenon; they are residuals of the individual element patterns and get worse the further elements are separated. Grating sidelobes should be mitigated as much as possible since large sidelobes will mean lower power radiating in the main lobe [23]. Figure 2.6 shows the directivity of a broadside linear antenna array as a function of the element spacing in fractions of a wavelength. The antenna element type is not given since the principal applies to arrays with any antenna element.

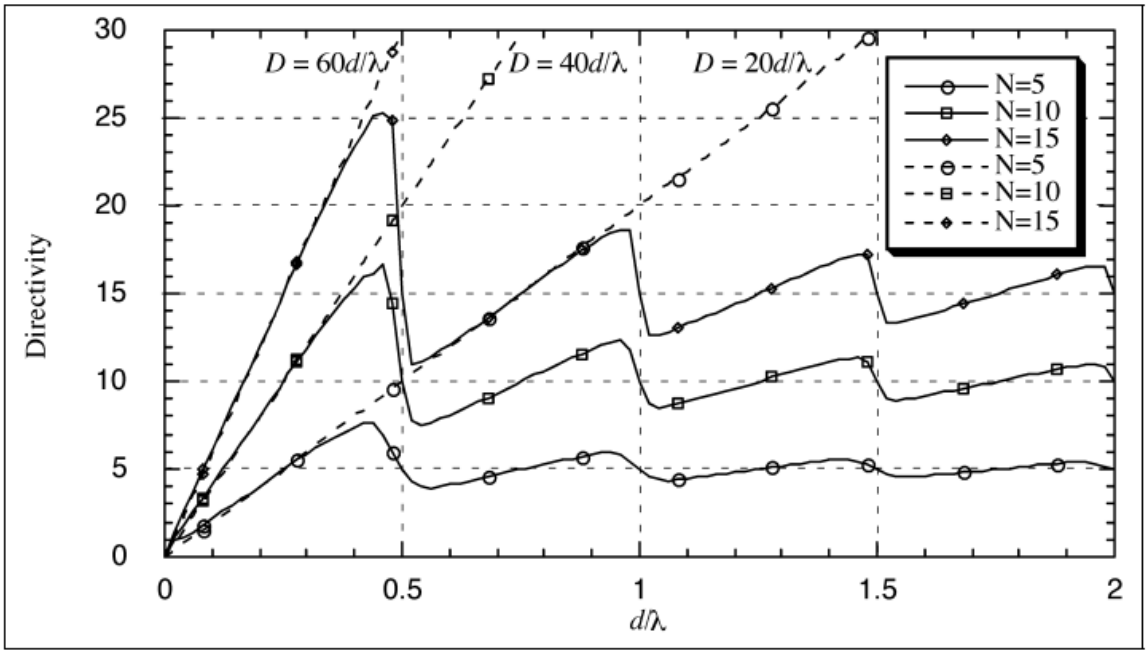

Figure 2.7: Directivity of Array vs. Element Spacing [23].

As seen in Figure 2.6, the directivity of an antenna array is highest when the elements are spaced just under 0.5λ apart. Typical arrays with elements radiating at equal power will have sidelobes around -13 dB below or about 20 times lower than the power of the main beam [22].

2.3 Polarization

In its most basic form, electromagnetic polarization refers to the direction in which an electromagnetic wave oscillates. Polarization is vital for antennas because they only transmit or receive energy at a particular polarization [24]. The two types of polarization of interest in this thesis are linear and circular polarization.

2.3.1 Linear Polarization

Linear polarization is the most common polarization type where the electric field vector of the travelling electromagnetic wave is confined to a single plane along the direction of propagation. The linear polarization direction is mainly relative and depends on the coordinate system used [24]. For instance, there are three different interpretations of linear polarization; vertical, horizontal and slant, represented in Figure 2.8.

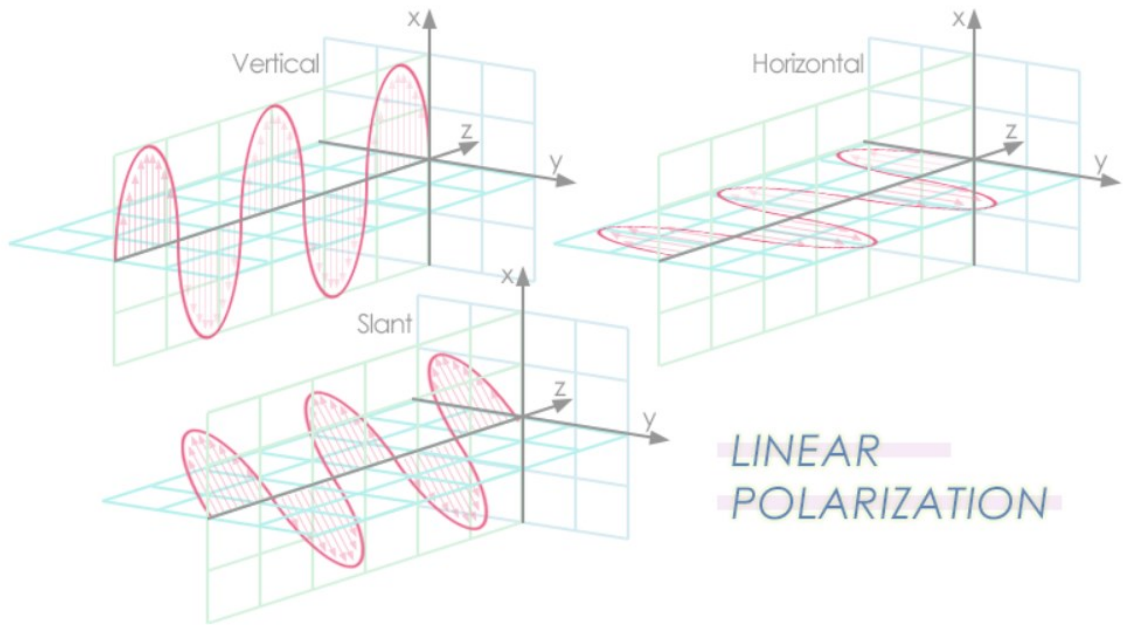

Figure 2.8: Vertical, Horizontal and Slant Linear Polarization [25].

For linear polarized antennas, there are two planes of interest; the co-polarized and cross-polarized planes. The co-polarized plane is the plane of space parallel to the antenna of interest's polarization, while the cross-polarized plane is orthogonal to the antenna's polarization. For instance, if a linearly polarized receiver antenna was oriented along the x-plane in Figure 2.8, then the x-plane is co-polarized and any signals travelling along it would be received by the antenna. Likewise, the y-plane would be cross-

polarized and any signals travelling along it would be rejected by the receiver antenna. If any slant polarized signals travelled towards the antenna, only a tiny portion existing in the co-polarized plane would be received [14].

2.3.2 Circular Polarization

Circular polarization refers to an electromagnetic wave that rotates flat in a perpendicular plane as it travels. A circularly polarized wave can be generated using two linearly polarized waves placed orthogonally with equal magnitude and a 90° phase shift between them. There are two variations of circular polarization, known as left-hand (LHCP) and right-hand circular polarization (RHCP). The difference between them is dependent on which direction they rotate clockwise or counterclockwise with respect to the direction of propagation. This difference can also be interpreted as two linear waves with a +90° or -90° phase shift to determine how the circular wave rotates [24]. Figure 2.9 provides a visual representation of LHCP and RHCP.

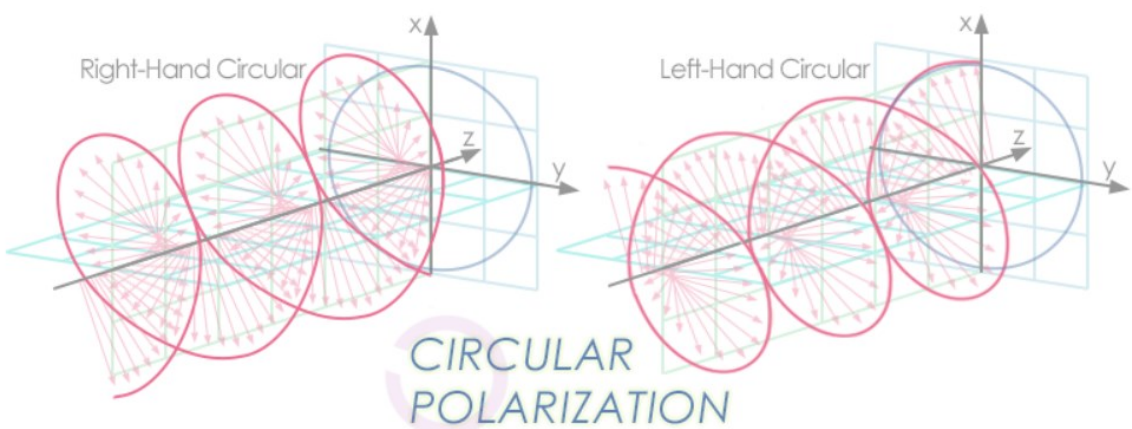

Figure 2.9: Left-Hand and Right-Hand Circular Polarization [25].

A key design parameter to consider when designing a circularly polarized antenna is the axial ratio. Axial ratio is defined as the difference between the electric field magnitude of the orthogonal portions of a circularly polarized wave. Ideally, the axial ratio of a circular antenna would be 1 dB indicating that the orthogonal components have the same magnitude, but for most antenna applications, an axial ratio of 3 dB or lower is considered acceptable [16].

2.4 Switches

The most straightforward type of RF switch is a single pole double throw (SPDT) switch. This switch has one input and can direct the input power to one of two output terminals. These simple switches are typically switched between their two paths using DC control voltages. One path will typically be enabled with a high voltage, while the other is enabled with a low voltage. The most important parameters to consider when selecting an SPDT are the return loss on each port, the insertion loss from the input to each of the output ports and the isolation between the output ports [26].

2.5 Hybrid Couplers

Power division is when an input signal is divided into output signals with lower power two or more times, and each time the power is split in two is equivalent to a 3 dB loss. Power splitting can be done using a 90º Hybrid Coupler, which comprises two sets of coupled output ports with a 90° phase shift and high isolation between them. Ideally, the power enters through one input port and is split equally between two output ports while the fourth port is isolated. This is done by arranging four quarter-wavelength

transmission lines in a square, with each port located at the four corners [27]. Figure 2.10 below shows the standard form of a 90º hybrid coupler.

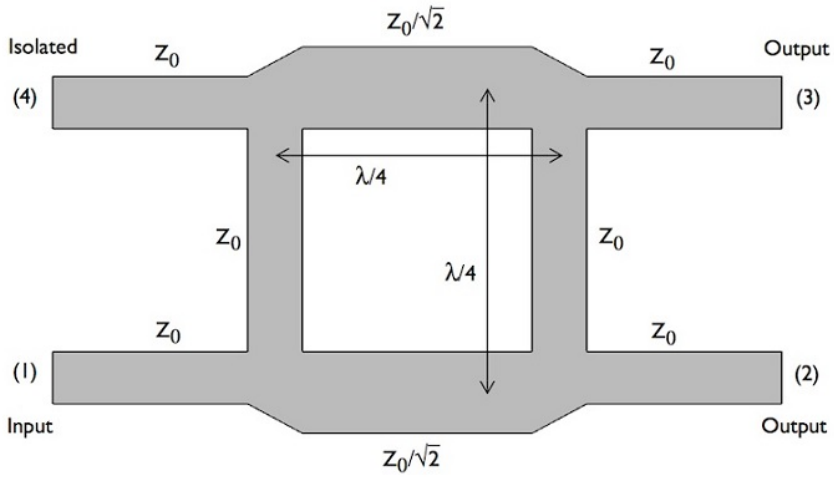

Figure 2.10: Standard Form of 90º Hybrid Coupler [28].

Hybrid couplers are particularly useful when designing circularly polarized antennas because they can provide two signals with roughly the same magnitude and a 90º phase shift between them. This method has the benefit of using standard transmission lines and can be fabricated directly on the substrate instead of using another packaged IC. However, this type of coupler uses a large amount of space on-chip because of its quarter-wavelength transmission lines. In order to fit a hybrid coupler on the selected substrate, a method of reducing the size will need to be found [29].

2.6 Antenna Measurement

Once each design in this thesis was fabricated, they were tested using equipment found in the labs at the Department of Electronics at Carleton University. The testing can be categorized into S-Parameter and Radiation Pattern measurements.

2.6.1 S-Parameter Measurements

The S-parameters of each antenna array are measured using an Agilent 8720ES Vector Network Analyzer (VNA) calibrated with an Agilent 85052D calibration kit. Calibration is done using short, open, and 50Ω broadband loads. Each antenna array is connected to the VNA via an SMA to SMPM cable. Due to the availability of only SMA calibration kits, an SMPM to SMA connector is connected to the end of the SMPM cable. It was judged that a connection adapter would have a lower loss and, therefore, a more negligible effect on the signal than the cable. While it is impossible to completely de-embed the antenna, the additional connector will allow the SMPM cable to be de-embedded. Figure 2.11 below shows the measurement setup for POC1 and POC2.

Figure 2.11: Test Setup for POC1 and POC2 (Single).

To assess the scalability of each antenna array design, the S-Parameters of an 8x8 array were also measured. This is done by adding a ZC4PD-153-S+ four-way power splitter/combiner. The common port of the power splitter is connected to the VNA, while the four split ports are connected to four antennas via four SMA to SMPM cables. Figure 2.12 shows the test setup for multiple antenna arrays tiled together.

Figure 2.12: Test Setup for POC1 and POC2 (Multiple).

For POC3, a pair of 3.3V watch batteries provided the DC bias for all circuitry on the antenna PCB. The DC ground was also connected to the RF ground on the SMPM cable. Otherwise, the testing setup and methodology are the same as the setup for POC1 and POC2. Figure 2.13 shows the test setup for POC3.

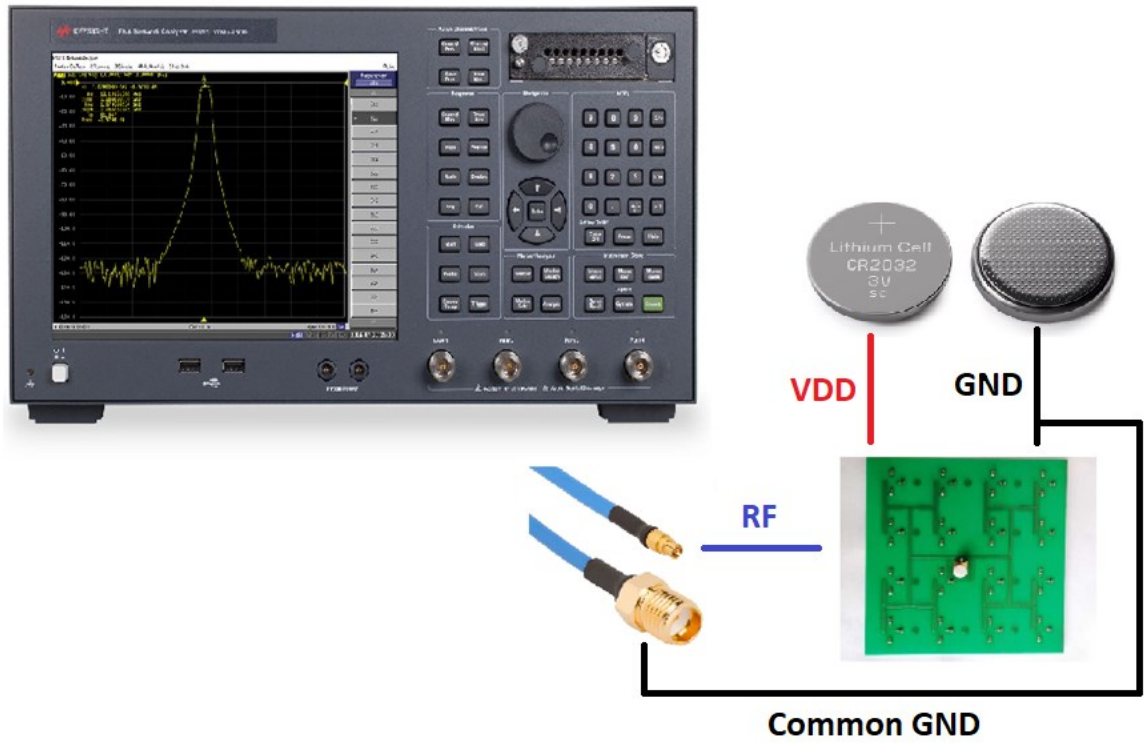

Figure 2.13: Test Setup for POC3.

2.6.2 Radiation Pattern Measurements

The radiation patterns of each antenna array were measured in the anechoic chamber at Carleton University. An SAV-0131831040-NF horn antenna with a nominal gain of 13 dBi was implemented as the standard gain horn (SGH) antenna. The center frequency for the radiation pattern is 9.45 GHz same as the S-Parameters.

A custom holder for the designed antenna arrays was 3D printed to fit the stand in the anechoic chamber. The holder consists of a slab that holds the antenna PCB, which is then slotted into a holder that fits the stand in the chamber. Figure 2.14 shows the custom holder.

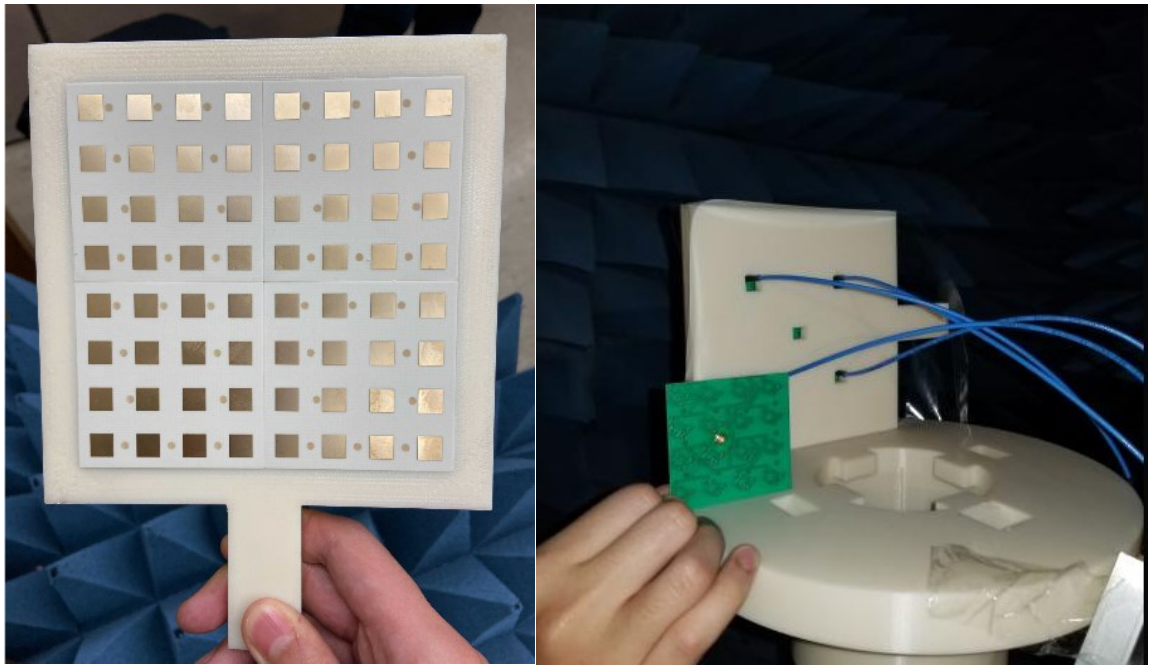

Figure 2.14: 3D Printed Antenna Holder.

The antenna holder shown in Figure 2.14 has holes in the back to allow for signal feeding of each antenna PCB and the DC biasing for POC3.

Chapter 3: Linearly Polarized Antenna Array

3.1 Introduction

Proof of Concept 1 (POC1) aims to design, simulate, and test a simple linearly polarized antenna array on the selected substrate. This development will be used to realize an antenna structure with a switchable polarization state. POC1 is the first step in this undertaking to identify potential challenges with substrate, feeding and patch antenna design before any additional polarization modes are added using packaged components.

This chapter will outline the design process of POC1, starting with the required specifications of the linearly polarized 4x4 patch antenna array. The specifications are used to design a single patch antenna that is to be used as the building block of a 4x4 antenna array that will be fabricated and tested later.

3.2 Specifications

This thesis was initially tailored towards supporting surveillance of Canadian coastal borders. The work planned for this thesis was based on an X-band radar platform with a center frequency of 9.45 GHz. Initially, research was done in collaboration with a Canadian company to develop the specifications in Table 3.1. This company later dropped the project and research was forced to continue independently. The initial plan utilized a part known as the ADAR1000, which is a 4-channel, X-band, beamforming chip for phased arrays [30]. Figure 3.1 shows a block diagram of the ADAR1000 and some of its features.

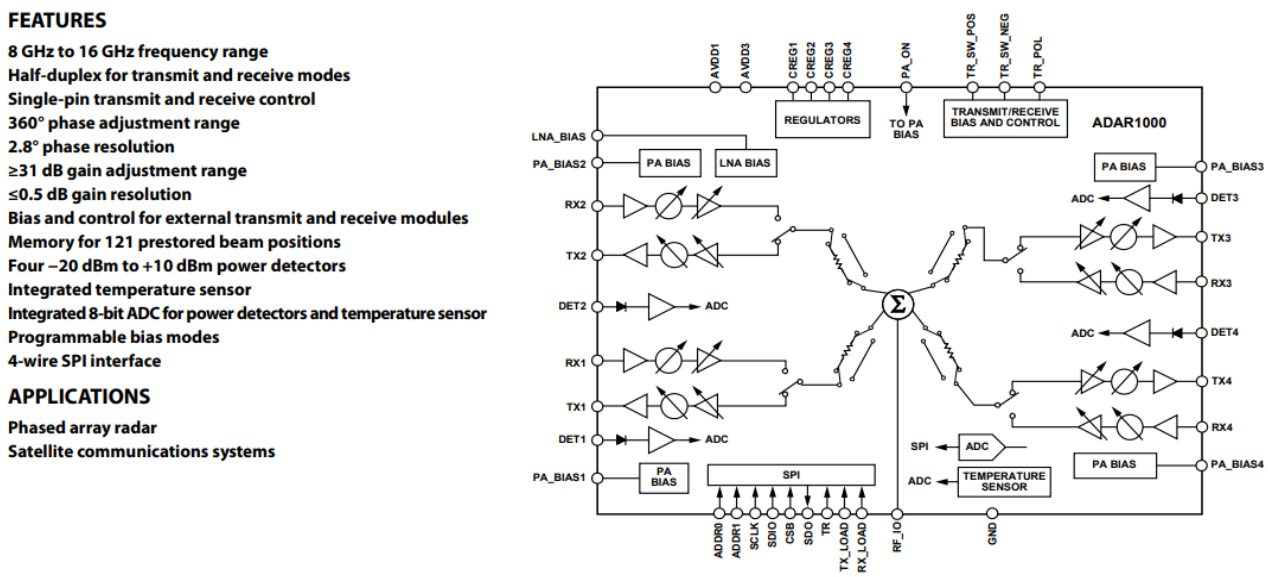

Figure 3.1: ADAR1000 Block Diagram and Key Features [30].

POC1 is meant to design a simple 4x4 antenna array with which the ADAR1000 can later be integrated. Figure 3.2 shows a hypothetical 4x4 phased array with switchable polarization using the ADAR1000 that served as the target end goal.

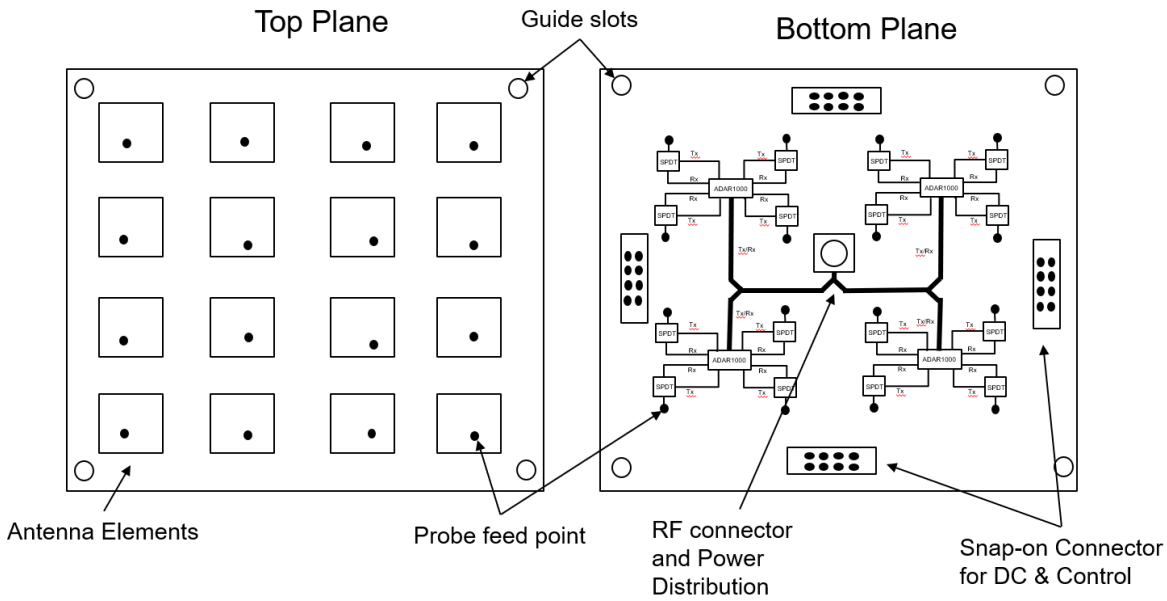

Figure 3.2: Target Design for 4x4 Switchable Polarization Phased Array.

As seen in Figures 3.1 and 3.2, the ADAR1000 has four beamforming chains with separate pins for transmitting and receiving for a total of eight signal ports. One ADAR1000 part has four beamforming chains, which means four ADAR1000 parts are needed for a 16-element array. A switching network must be included for each beamforming set to accommodate the separate Tx and Rx paths, as seen in Figure 3.2.

A preliminary RF system-level analysis was done in SystemVue using the ADAR1000 to determine the required specifications for the 4x4 antenna array. Figure 3.3 shows the SystemVue setup for the RF chain using the ADAR1000.

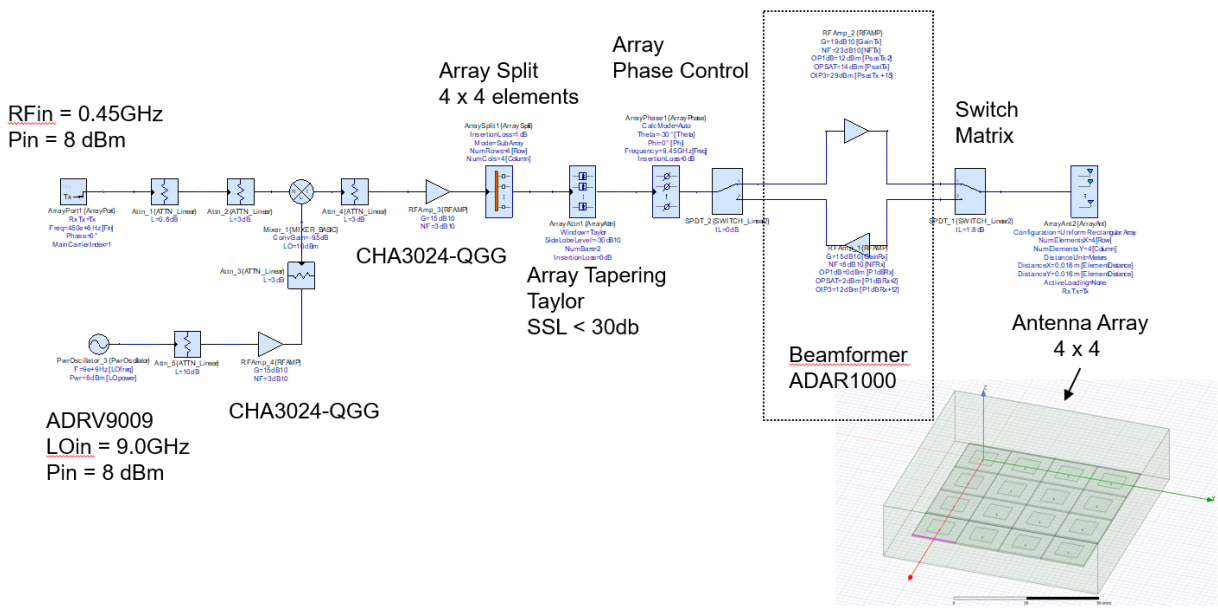

Figure 3.3: RF Chain of Proposed 4x4 Phased Array using ADAR1000.

Figure 3.4 shows the power and compression at each stage of the RF chain.

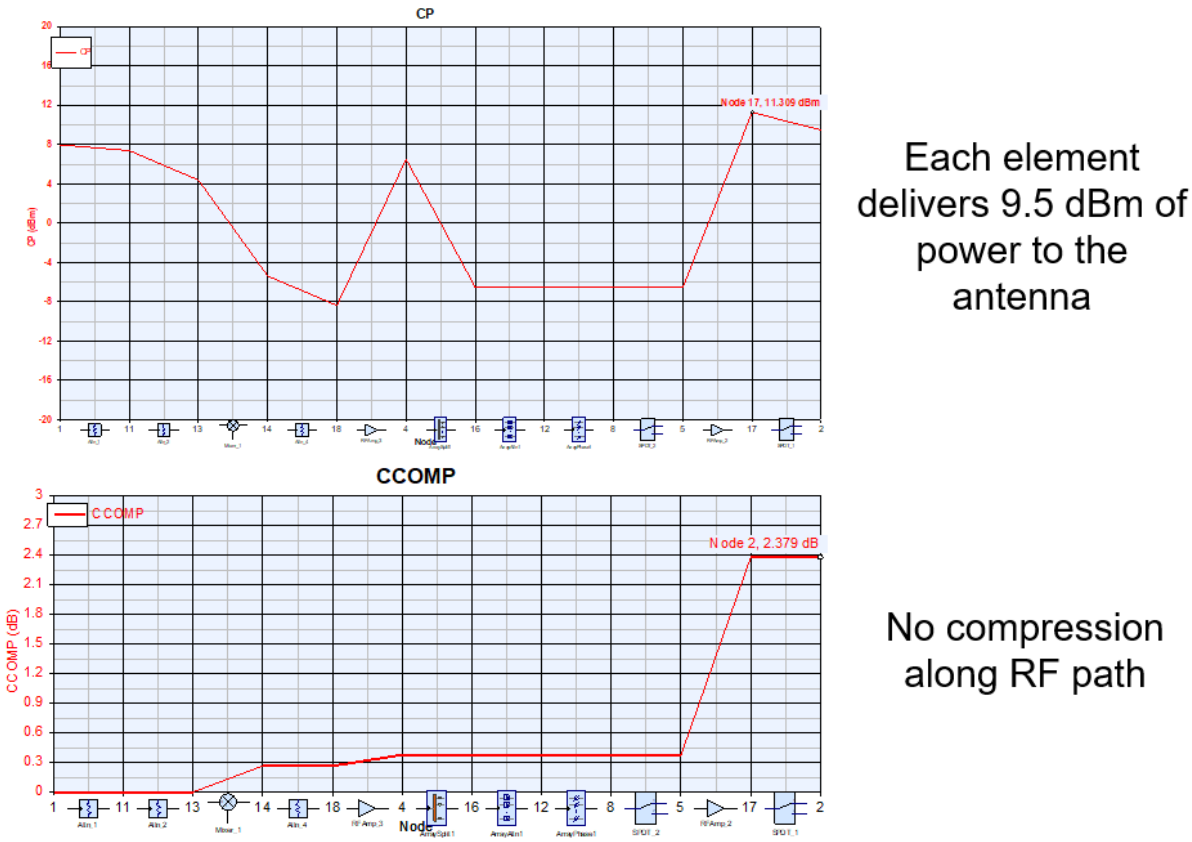

Figure 3.4: Power and Compression along the RF Chain.

Figure 3.5 shows a preliminary view of the radiation pattern of a 4x4 array connected to the RF chain.

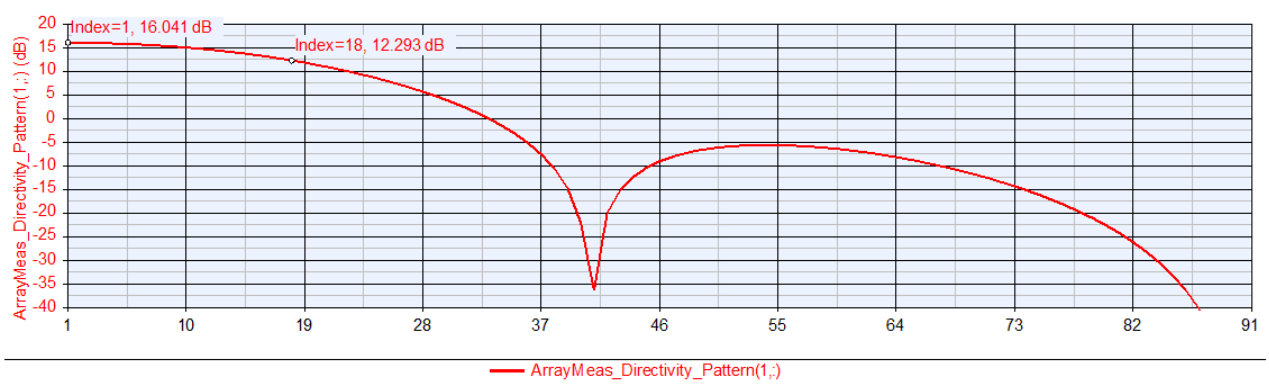

Index	BeamMeas_MainLobePhiBeamwidth (°)	ArrayMeas_EIRPAtThetaPhi (dB...
1	30.772	33.096

Figure 3.5: Preliminary Radiation Pattern of 4x4 Array and RF Chain.

As seen in Figures 3.4 and 3.5, the power delivered to the array is around 10 dBm, the nominal gain of the array is 16 dB, the HPBW is around 30º and the required EIRP is 33 dBm. Even though the nominal gain of the array is 16 dB, Equations 2.5-2.6 seen in Chapter 2 indicate that for 10 dBm of power delivered to a 16-element array, the minimum gain is closer to 11 dB. Table 3.1 shows a summary of the system specifications for POC1.

Table 3.1: POC1 System Specifications.

SECTION	TITLE/DESCRIPTION	SPECIFICATION				COMMENTS
1	**Antenna Array Specification**	Unit	Min	Nominal	Max	
1.1	Operating Frequency	GHz	9.4	9.45	9.5	
1.2	Gain of Antenna	dB	11	16		EIRP – Pin
1.3	EIRP	dBm		33		Keep fixed EIRP
1.4	HPBW	deg		30		
1.5	Input IF frequency	GHz		9.45		
1.6	Input IF power Pin	dBm		18		Varying the Pin to achieve fixed EIRP
1.7	Return Loss	dB			-10	
1.8	Side Lobe Level	dB		13		Below main lobe.
1.9	Efficiency	%	60			
1.10	System loss	dB		2		Insertion losses of 1/16 power divider and RF connector
1.11	Polarization type	Vertical Linear				
2	**Environmental Specifications**					
2.1	Operating Temperature	°C	-40	25	85	
3	**Physical Specifications**					
3.1	Dimensions (W x L)	mm		64 x 64		Rogers 4003 20 mil two layers

3.2.1 Substrate Selection and Practical Considerations

The substrate selected for the array designs was 20 mils thick Rogers Duroid 4003, which has an ε_r of 3.55 and a tanδ of 0.0027 at 10 GHz [31]. While Rogers has substrates with lower ε_r and tanδ, this substrate was selected for its lower price. Since the thesis goal is a PCB with patch antennas on one side and RF circuitry on the other, multiple substrate pieces will need to be stacked. Rogers 4450 prepreg was used to glue multiple pieces of 4003 together. This material was stipulated by the PCB foundry used to fabricate POC1. Figure 3.6 shows the substrate stackup for POC1.

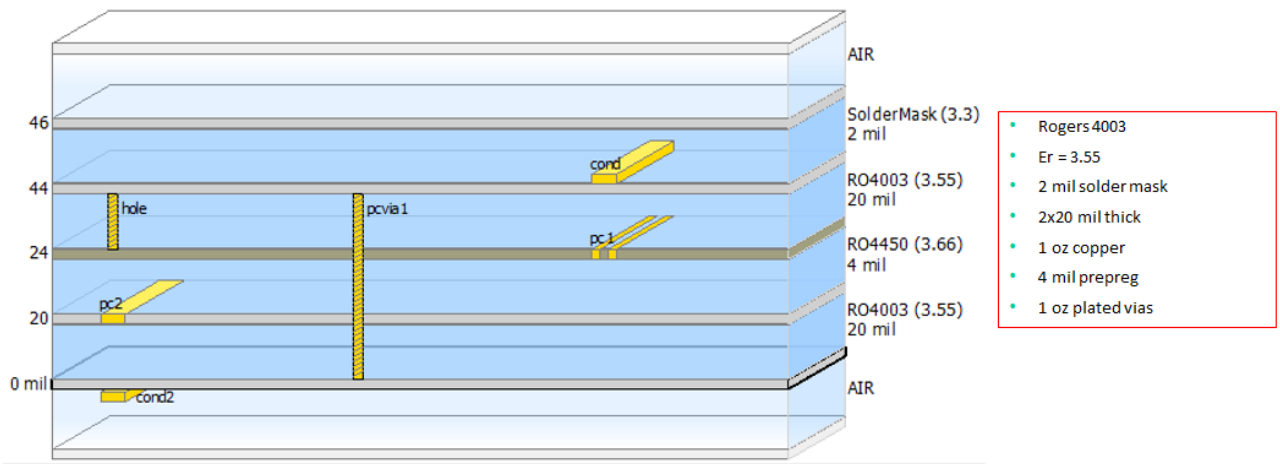

Figure 3.6: POC1 Substrate Stackup.

The guided wavelength on the selected RO4003 substrate is approximately 16.85 mm or 663 mil for the target operating band. While a spacing close to λ/2 is recommended to avoid grating sidelobes, elements in POC1 are spaced 625 mils or 0.95λ apart [20]. This value was chosen so that a PCB with 16 elements will be exactly 2.5 x 2.5 inches. A uniform size was decided upon because POC1 is the first steppingstone for the other array designs in this thesis; therefore, all antenna arrays should share the same board dimensions. This was done primarily for comparison and testing purposes. Since

future iterations of this design will include more components on the antenna PCB, the array elements must be spaced further apart to provide more room. While this will introduce grating side lobes, the goal of this thesis is not to eliminate or reduce array sidelobes. Therefore, the standard side lobe level of around -13 dB below the main lobe is considered acceptable for this design [22].

A preliminary diagram of POC1 is shown in Figure 3.7.

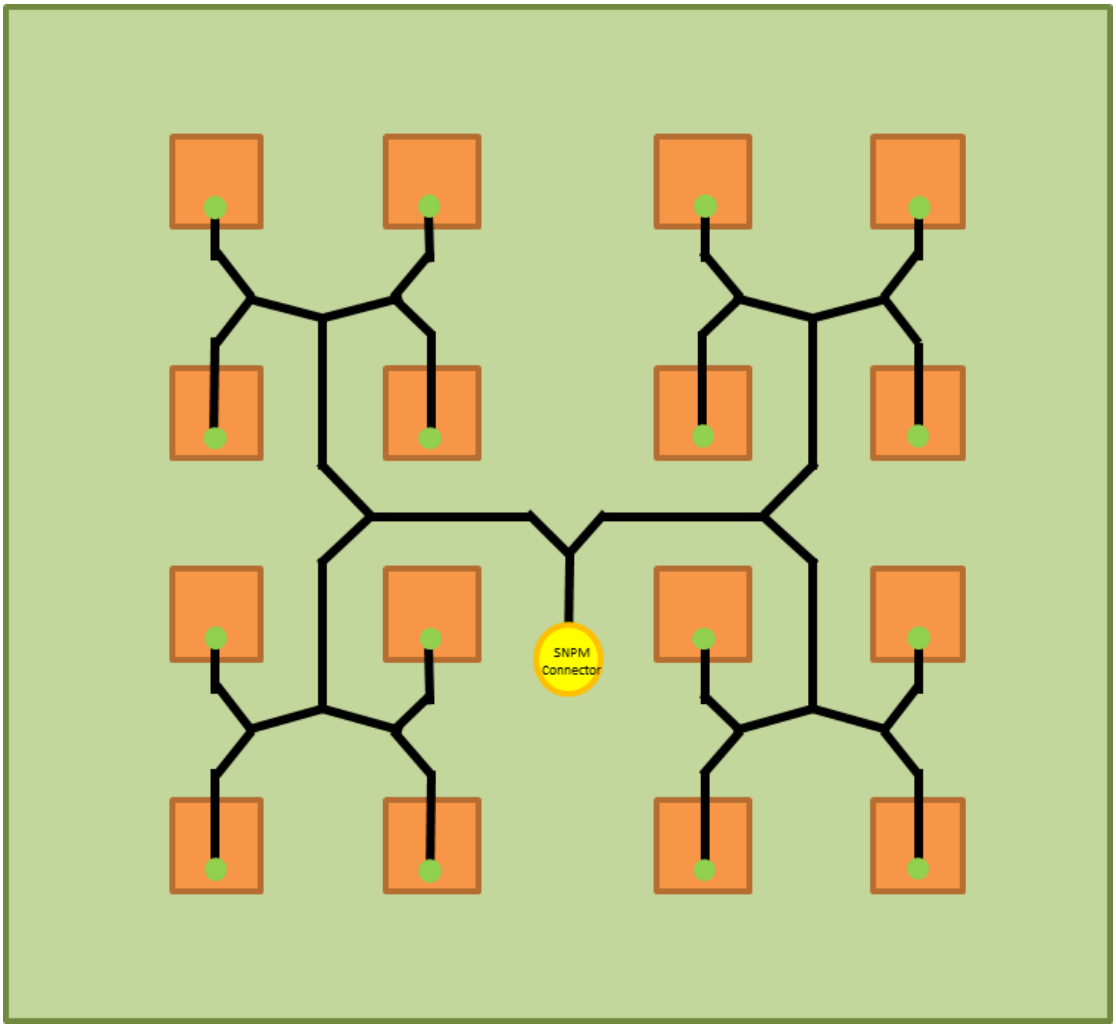

Figure 3.7: System Diagram of POC1.

3.3 Design and Simulation

With the specifications set, the design process of a single square patch antenna can be initiated that will later be scaled up into an array. A method for increasing the bandwidth of a patch antenna through resistive loading will also be presented. A 16-branch microstrip feeding network will connect multiple patch antennas into a 4x4 element antenna array.

3.3.1 Design of Single Patch Antenna

For the selected RO4003 substrate, the following parameters are known:

$$\epsilon_r = 3.55 \quad , \quad h = 0.5\,mm \quad , \quad f_o = 9.45\,GHz$$

The first step is to find the width of a standard patch antenna on the selected substrate at the selected frequency. Equations 3.1-3.6 outline the process for designing a single patch antenna [14] [32].

$$W = \frac{c}{2f_o}\sqrt{\frac{2}{\epsilon_r + 1}} \tag{3.1}$$

The fringing fields at the patch edges along the W sides can be accounted for using the effective dielectric constant instead of the nominal value, giving a more accurate patch size.

$$\frac{W}{h} > 1: \quad \epsilon_{reff} = \frac{\epsilon_r + 1}{2}\frac{\epsilon_r - 1}{2\sqrt{1 + 12\frac{h}{W}}} \tag{3.2}$$

Now the effective length of the square patch is calculated.

$$L_{eff} = \frac{c}{2f_o\sqrt{\epsilon_{reff}}} \tag{3.3}$$

Additional fringing fields along the L sides can be accounted for using the term ΔL which represents some additional length on either side of the patch.

$$\Delta L = 0.412\, h \frac{\left(\epsilon_{reff} + 0.3\right)\left(\frac{W}{h} + 0.264\right)}{\left(\epsilon_{reff} + 0.258\right)\left(\frac{W}{h} + 0.8\right)} \tag{3.4}$$

Now the actual side length of the patch with fringing fields can be determined.

$$L = L_{eff} - 2\Delta L \tag{3.5}$$

$$L = \mathbf{8.35\ mm}\ or\ \mathbf{329\ mil}$$

Equation 6 determines the feed point location from the center of the patch.

$$x_f = \frac{L}{2\sqrt{\epsilon_{reff}}} \tag{3.6}$$

$$x_f = \mathbf{2.74\ mm}\ or\ \mathbf{108\ mil}$$

Figure 3.8 shows a square patch antenna of the calculated size after some fine-tuning of the size and feeding location during simulation.

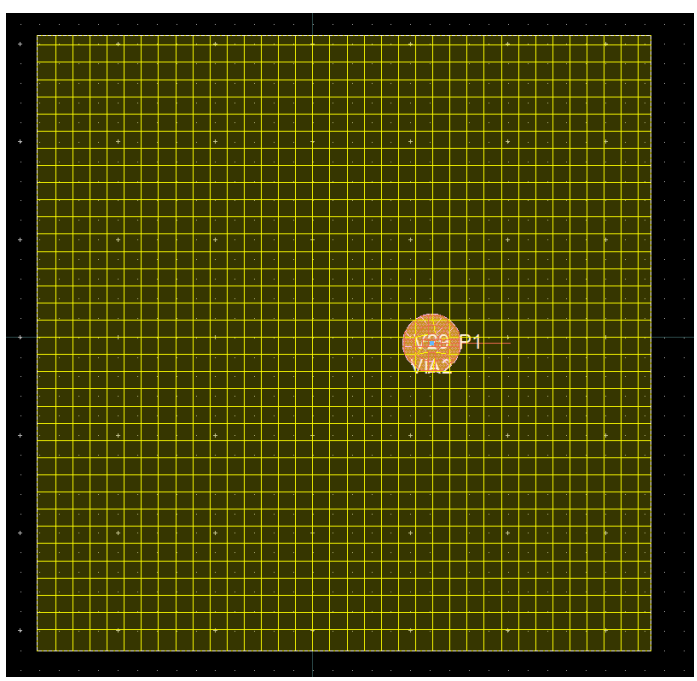

Figure 3.8: Standard Square Patch Antenna.

The return loss of the patch in Figure 3.8 is displayed in Figure 3.9.

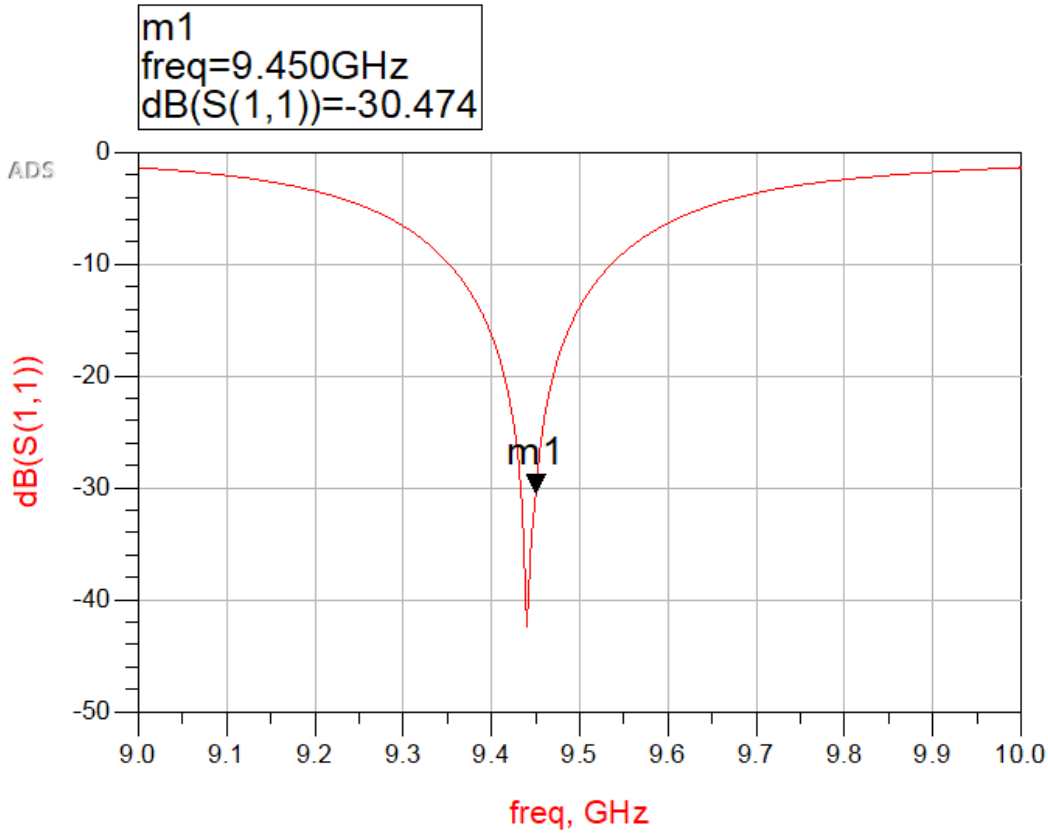

Figure 3.9: Return Loss of Single Square Patch Antenna.

The performance in Figure 3.9 shows a good return loss of -30.5 dB at 9.45 GHz, which indicates the single patch is well matched to the target frequency. One issue is that the impedance bandwidth is very close to the minimum value of 100 MHz. This could cause issues when combined with the feeding network and other patches because any slight variations or mismatches in the feeding network could cause the in-band return loss to go outside specification because it is so thin.

The radiation pattern of the single patch at the center frequency of 9.45 GHz is displayed in Figure 3.10.

Frequency	E_max	Theta_max	Phi_max	Directivity_max	Gain_max	RadiatedPower	InputPower	Efficiency	CutType	CutAngle
9.450E9	0.729	179.000	0.000	6.735	5.502	0.002	0.002	0.753	Phi	0.000

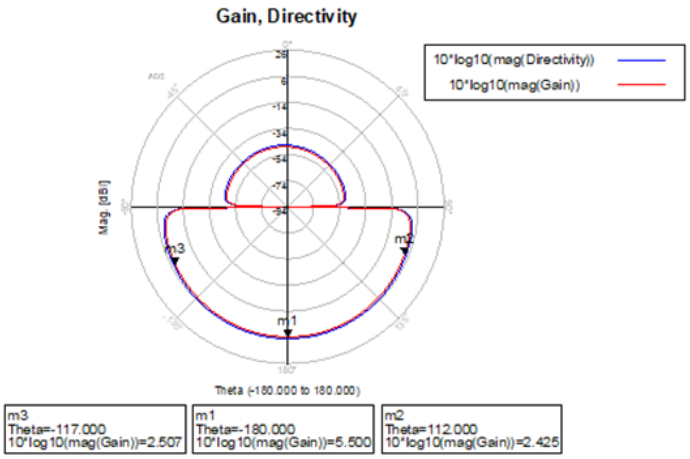

Figure 3.10: Gain and Efficiency of Single Square Patch Antenna.

As seen in Figure 3.10, the single patch antenna has a gain of 5.5 dB, an HPBW of 131° and power efficiency of 75%. So far, the single patch is meeting the required system specifications. However, the bandwidth is very close to the minimum value, so a method of increasing the bandwidth is needed.

3.3.2 Broadbanding of Patch Antenna Through Resistive Loading

One way to increase the impedance bandwidth of a patch antenna is to increase its impedance by attaching a set of resistive loads. This added resistance will have the negative effect of introducing more losses into the system, which will degrade the gain and efficiency of the antenna [33]. This risk is acceptable since the gain and efficiency of the antenna are higher than their minimum values compared to the bandwidth, which is in danger of violating the system specifications.

In this case, the patch antenna can be treated as a series resonator. This means the equations for a series resonator can be used to expand the patch antenna bandwidth [34].

$$Q = \frac{\omega_o}{BW} \tag{3.7}$$

From Equation 3.7, one way to increase the bandwidth while keeping the same center frequency is to reduce the patch quality factor (Q). The Q of the patch can be reduced by loading the patch with a series resistance, as seen by comparing Equations 3.8 and 3.9 [34].

$$Q_{unloaded} = \frac{\omega_o L}{Z_o} \tag{3.8}$$

$$Q_{loaded} = \frac{\omega_o L}{R + Z_o} \tag{3.9}$$

Figure 3.11 shows the square patch antenna with three 0402 sized 50Ω resistors added at an equal distance from the patch center as the input feeding pin.

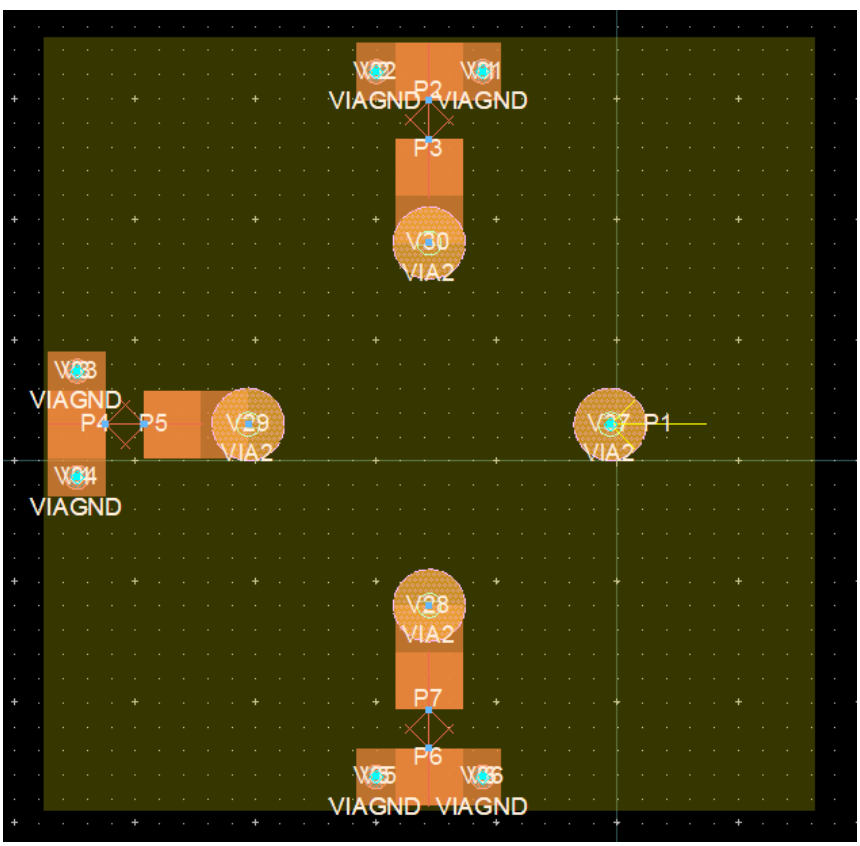

Figure 3.11: Resistively Loaded Single Patch Antenna.

The return loss of the loaded patch in Figure 3.11 is displayed in Figure 3.12, along with a comparison to the unloaded patch seen in Figure 3.8.

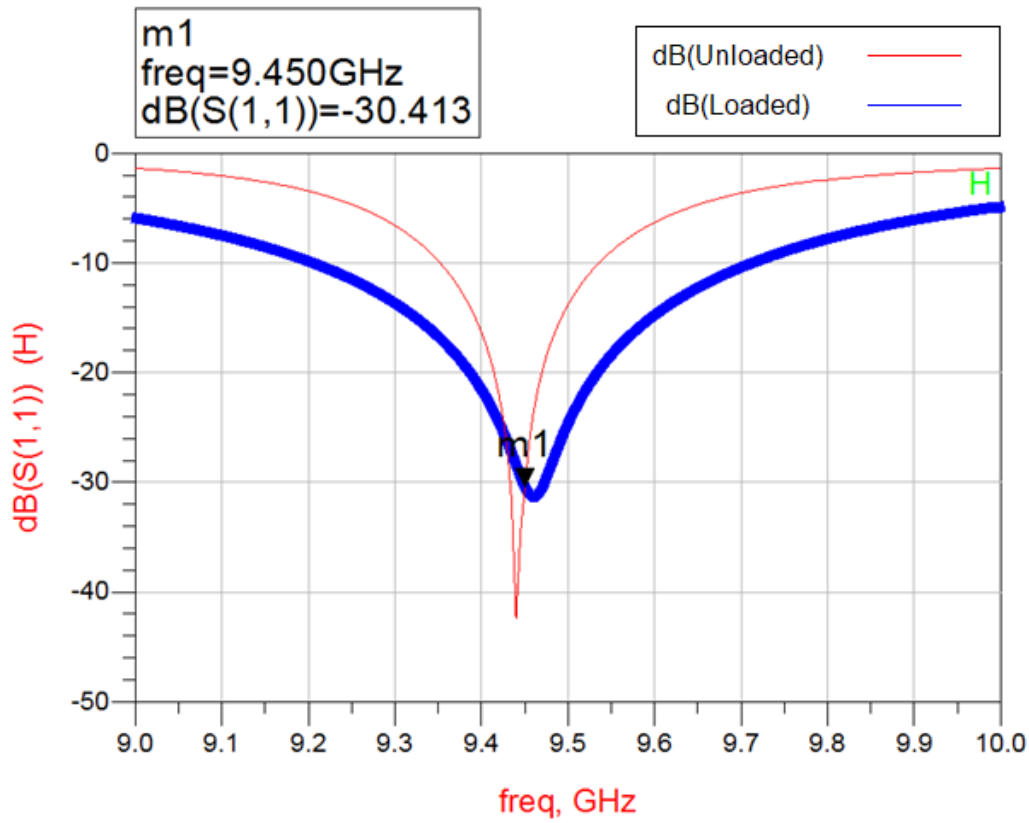

Figure 3.12: Return Loss Comparison of Unloaded and Loaded Patch Antenna.

As seen in Figure 3.12, the impedance bandwidth of the loaded patch antenna has increased significantly over that of the unloaded patch. As discussed in Section 2.1.2, the impedance bandwidth of an antenna is the range of frequencies with less than -10 dB return loss. An increase from around 200 MHz to 500 MHz is achieved while maintaining the same return loss at the center frequency.

The radiation pattern of the single-loaded patch at the center frequency of 9.45 GHz is displayed in Figure 3.13.

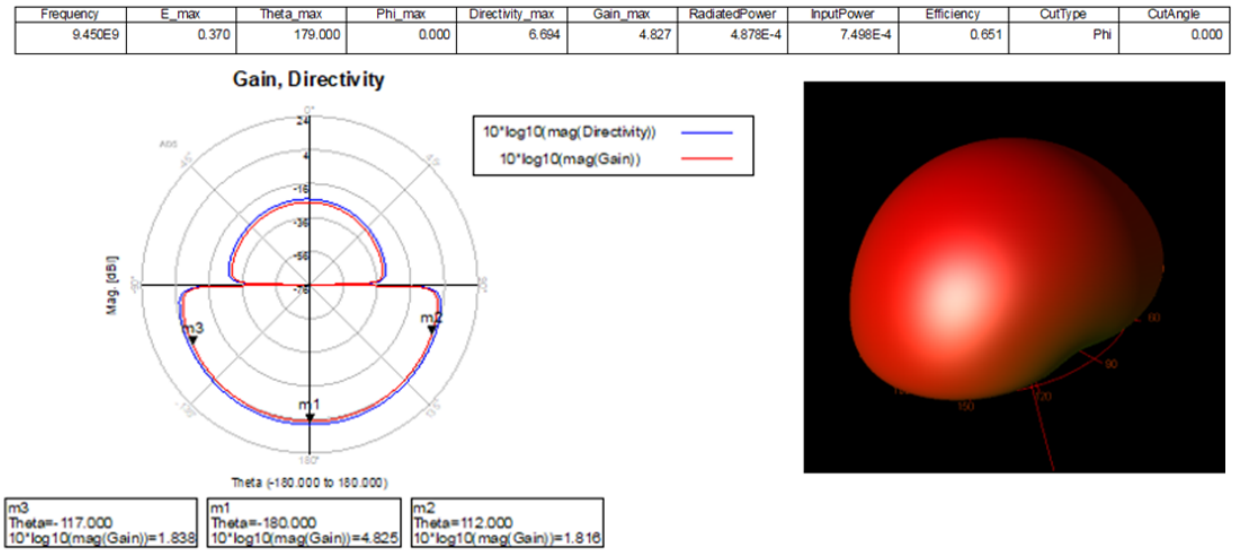

Figure 3.13: Gain and Efficiency of Loaded Square Patch Antenna.

Comparing Figure 3.13 to Figure 3.10, gain and efficiency degraded by around 0.7 dB and 10% as predicted, but the HPBW has stayed the same. These values are still within the system specifications, so the losses are acceptable for the increased bandwidth.

3.3.3 Design of POC1 Feeding Network

Antenna elements will be connected using a 1 to 16 microstrip power divider. This feeding method provides flexibility in element spacing and high bandwidth and will make integrating packaged components easier. The potential disadvantages of this topology are the high insertion loss and large physical size. Ordinarily, feeding lines on the same plane as the antenna can give rise to undesired radiation that interferes with the antenna at high frequencies, increasing mutual coupling and cross-polarization of the array [14]. This interference is mitigated in POC1 by placing the feeding network and antenna array on opposite sides of the PCB.

The feeding network comprises multiple quarter-wave transformers (QWT) arranged in a branching pattern that will split the input power in half multiple times depending on the number of elements in the array. Since each patch antenna is matched to 50Ω and fed using 50Ω transmission lines, they can be considered 50Ω loads. Two patch antennas connected in parallel can then be considered a 25Ω load. If 100Ω lines are used as an intermediary impedance, then a QWT for the first branch can be found.

$$Z_{QWT} = \sqrt{Z_o Z_L} \tag{3.10}$$

$$Z_{QWT1} = \sqrt{25 * 100} = \mathbf{50\ \Omega}$$

When two branches are connected in parallel at 100Ω, they can be considered a 50Ω load. If 100Ω lines are still used as an intermediary impedance, then a QWT for the next branch can be found using Equation 3.10.

$$Z_{QWT2} = \sqrt{50 * 100} = \mathbf{70.7\ \Omega}$$

A 16-element power divider can now be made together by branching 50Ω, 70.7Ω and 100Ω transmission lines. During the simulation, some line readjusting will need to be made in each branch. This is due to reflections occurring at every T-shaped branch, which will add together when combined into a single feed.

The 16-element power divider with the landing pad for the selected SMPM connector is seen in Figure 3.14 after the lines were optimized in simulation.

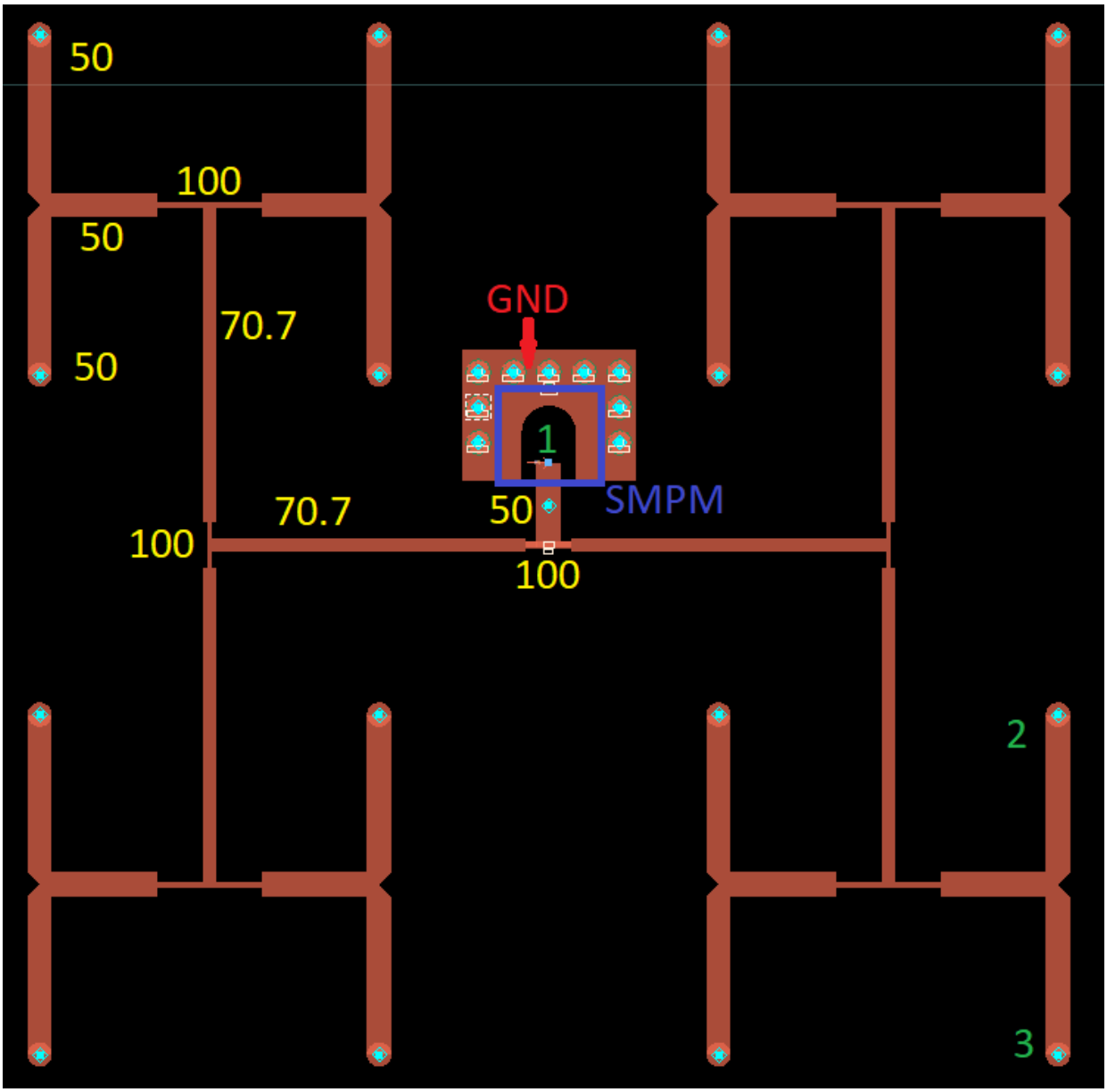

Figure 3.14: POC1 Microstrip Feeding Network.

The parameters that must be optimized on the input are the return loss of each port, isolation between adjacent ports, and the insertion loss from the input to each output. The ports where S-Parameter data was measured are labelled green in Figure

3.14; all other ports are loaded with 50Ω. The S-Parameters of the POC1 feeding network are shown in Figure 3.15.

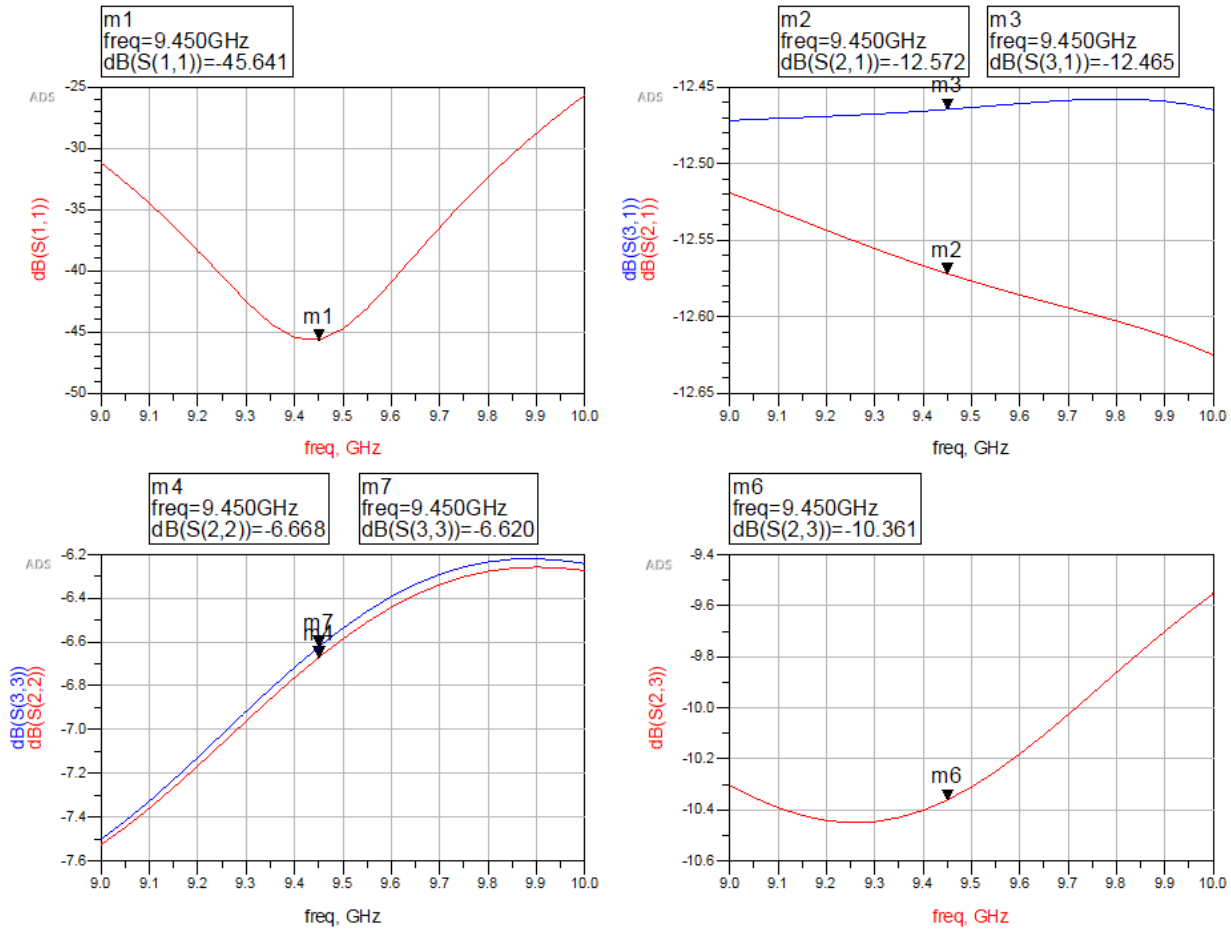

Figure 3.15: Performance of POC1 Feeding Network.

As seen in Figure 3.15, the return loss at the input port is excellent and has a wide bandwidth, making it easy to match the patch antennas. It should be noted that the power splitting in half between two branches is equivalent to a -3 dB drop, and since the input power splits four times, a drop of -12 dB is expected. While Figure 3.15 shows the S21 and S31 to be around -12.5 dB each, the feeding network insertion loss is around -0.5 dB, much lower than the 2 dB allocated in the system specifications. The isolation between

adjacent output ports is very close to the -10 dB threshold but is still within the specifications, so it is acceptable enough to move on. The return loss on the output ports is too high above the -10 dB threshold, which means the outer tips of the feeding network are not correctly matched to 50Ω. The input pin of the patch antenna must be adjusted when assembling and optimizing the full array since the feeding network can not be adjusted at the outputs without interfering with patch spacing and isolation.

3.3.4 Simulation of Full POC1 Antenna Array

Now that the patch antenna and feeding network have been designed and verified, the components can be assembled to form the full 4x4 patch antenna array. To avoid increased sidelobes when tiling multiple POC1 boards together, the distance from the outer patches to the edge of the board is set to exactly half the distance between neighbouring patches. This way, when multiple POC1 boards are tiled together, the distance between the outer patches of each board should be the same as the distance between patches on the same board. Figure 3.16 shows the full 4x4 antenna array after some fine-tuning of the feeding network and patches once connected.

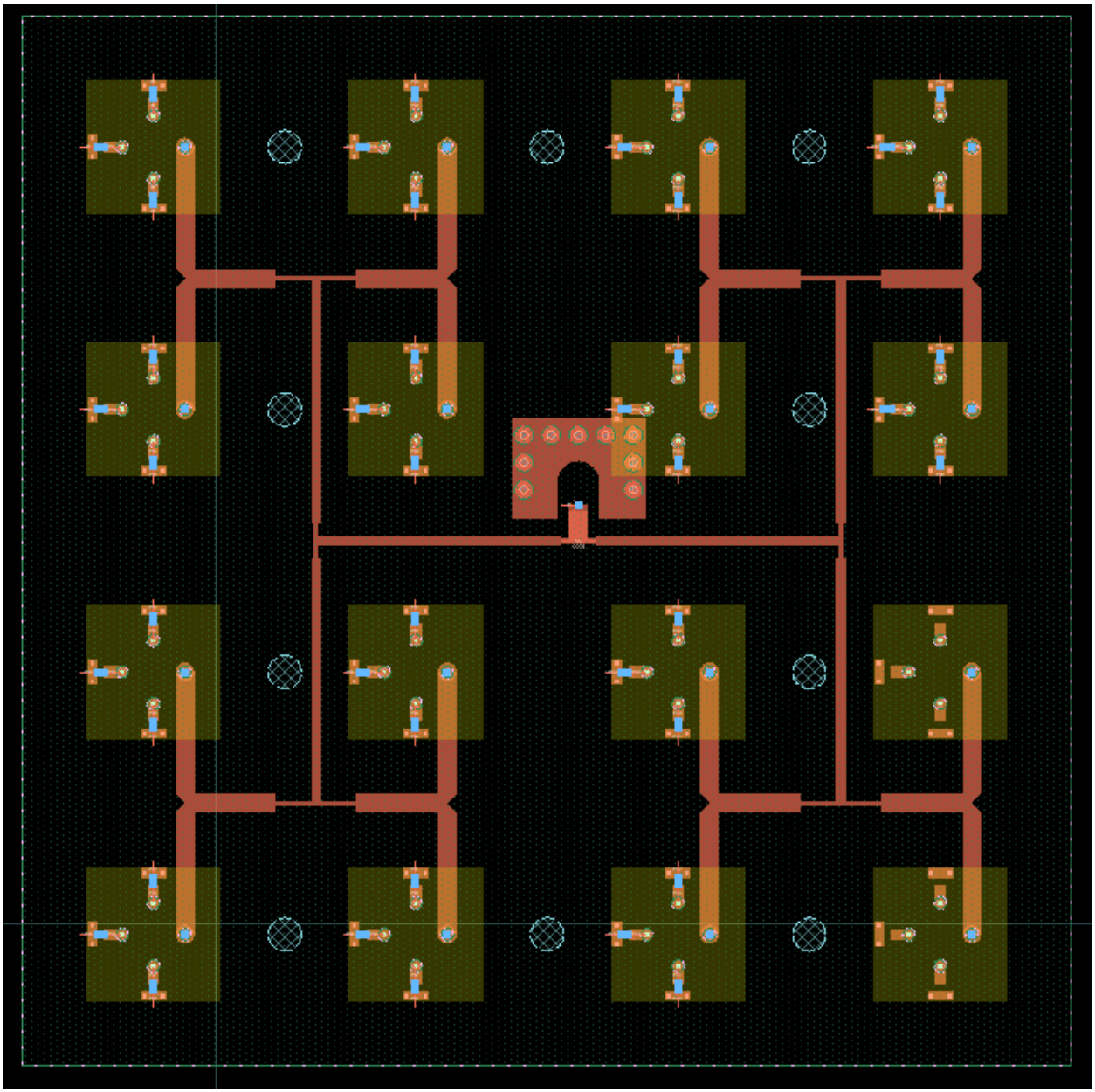

Figure 3.16: Full POC1 Antenna Array (2D View).

In addition to the 2D view shown in Figure 3.16, a 3D top and bottom view of POC1 is shown in Figure 3.17.

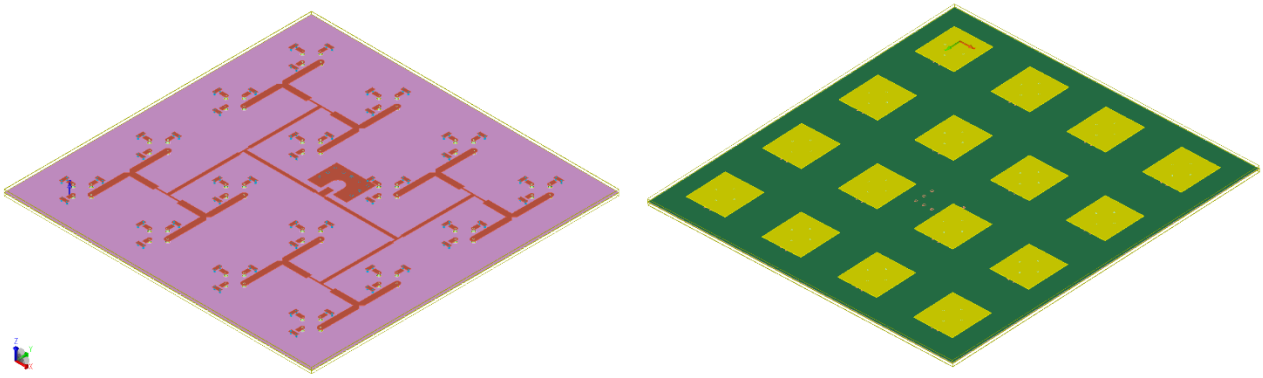

Figure 3.17: Full POC1 Antenna Array (3D View).

Figure 3.18 shows the return loss of the full POC1 antenna array.

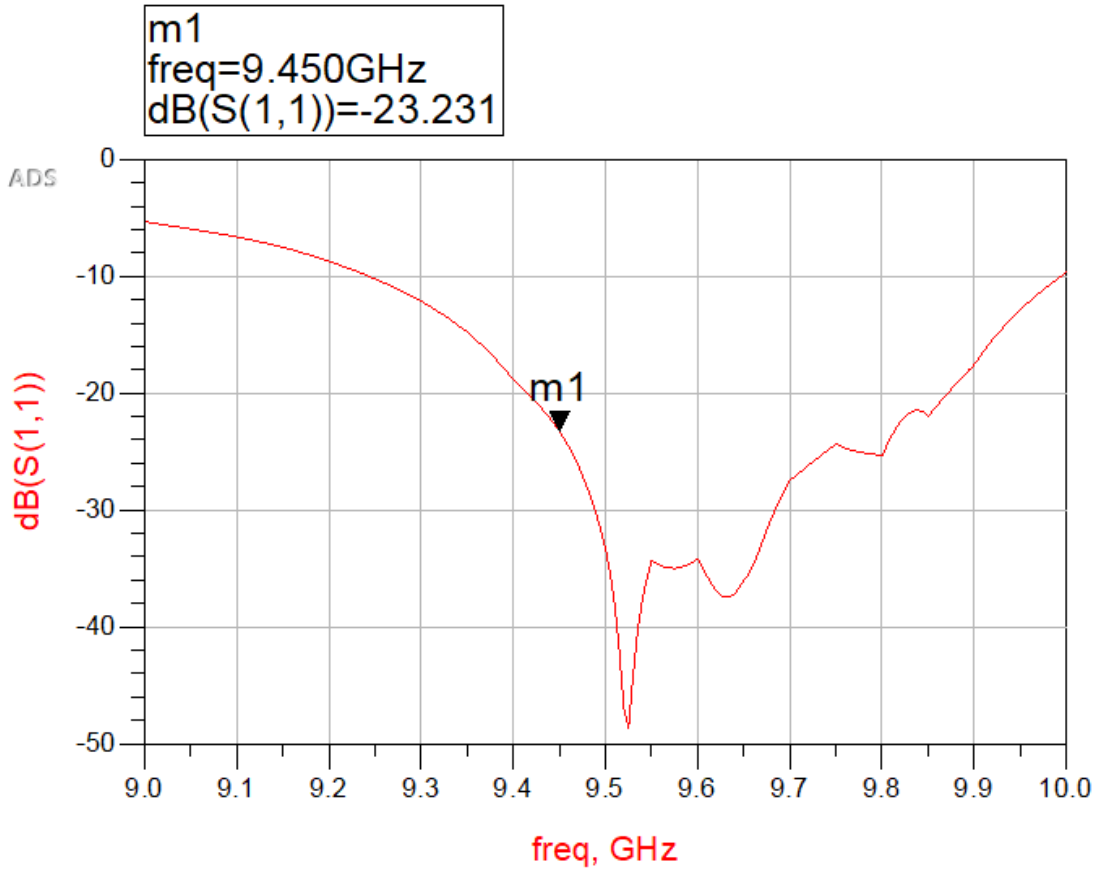

Figure 3.18: Simulated Return Loss of Full POC1 Array.

While the plot in Figure 3.18 indicates the center frequency has shifted to around 9.52 GHz, the return loss is still excellent across the desired band from 9.4 to 9.5 GHz. A bonus is that the overall bandwidth has dramatically increased to around 750 MHz. Figure 3.19 shows the radiation pattern of the full POC1 array.

Frequency	E_max	Theta_max	Phi_max	Directivity_max	Gain_max	RadiatedPower	InputPower	Efficiency	CutType	CutAngle
9.450E9	1.402	179.000	291.000	16.764	14.348	6.910E-4	0.001	0.671	Phi	0.000

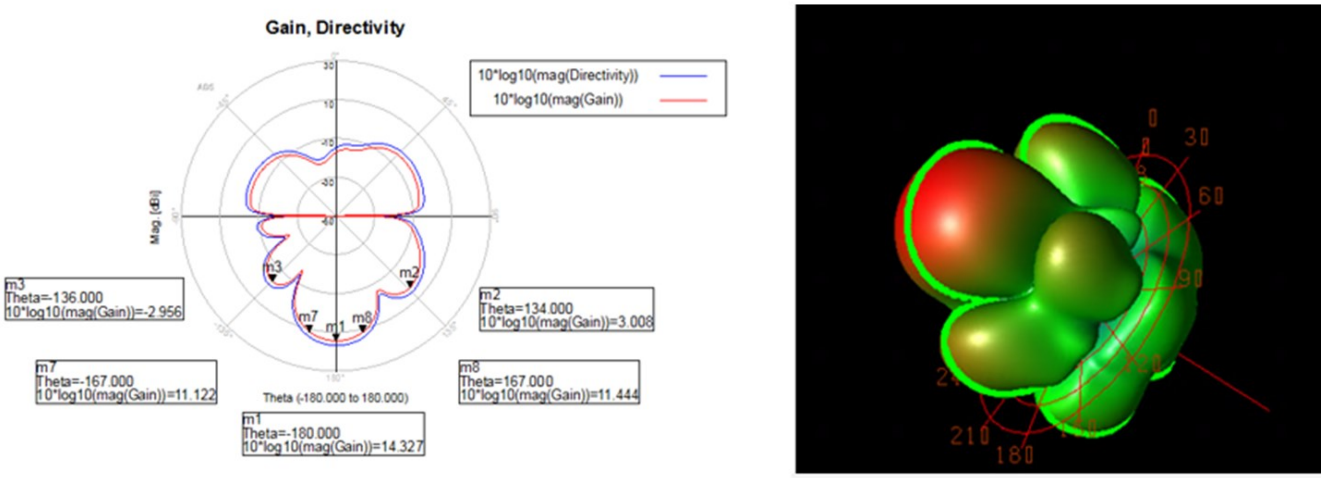

Figure 3.19: Simulated Gain and Efficiency of Full POC1 Array.

Figure 3.19 shows that while the gain and efficiency are lower than desired, they still meet the minimum values of 11 dB and 60%. The HPBW is around 26º, close to the specified value of 30º. Side lobes are at -3 dB and 3 dB giving a distance from the main lobe of -16 dB and -11 dB, respectively; these are close enough to the nominal value of -13 dB below the main lobe.

The simulated values shown in Figures 3.18 and 3.19 indicate that POC1 meets the required system specifications and is ready for fabrication and testing.

3.4 Measurement of POC1

Once the full POC1 antenna array was verified in simulation, it was sent out for fabrication to be later tested in the anechoic chamber at Carleton University. Figure 3.20 shows the fabricated POC1 antenna array.

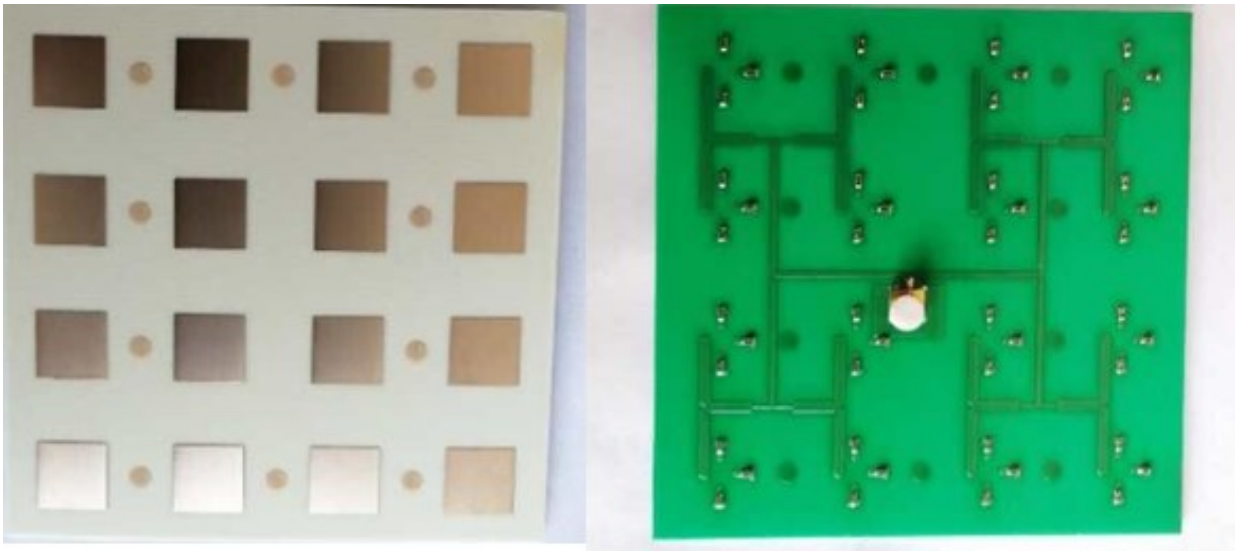

Figure 3.20: Fabricated POC1 Antenna Array.

3.4.1 Measurement of Single POC1 Antenna Array

The single POC1 antenna board shown in Figure 3.20 was tested at Carleton University using the S-Parameter test setup presented in Section 2.6.1 to measure the return loss of the array. The measured return loss of POC1 can be seen and compared to simulation results in Figure 3.21 below.

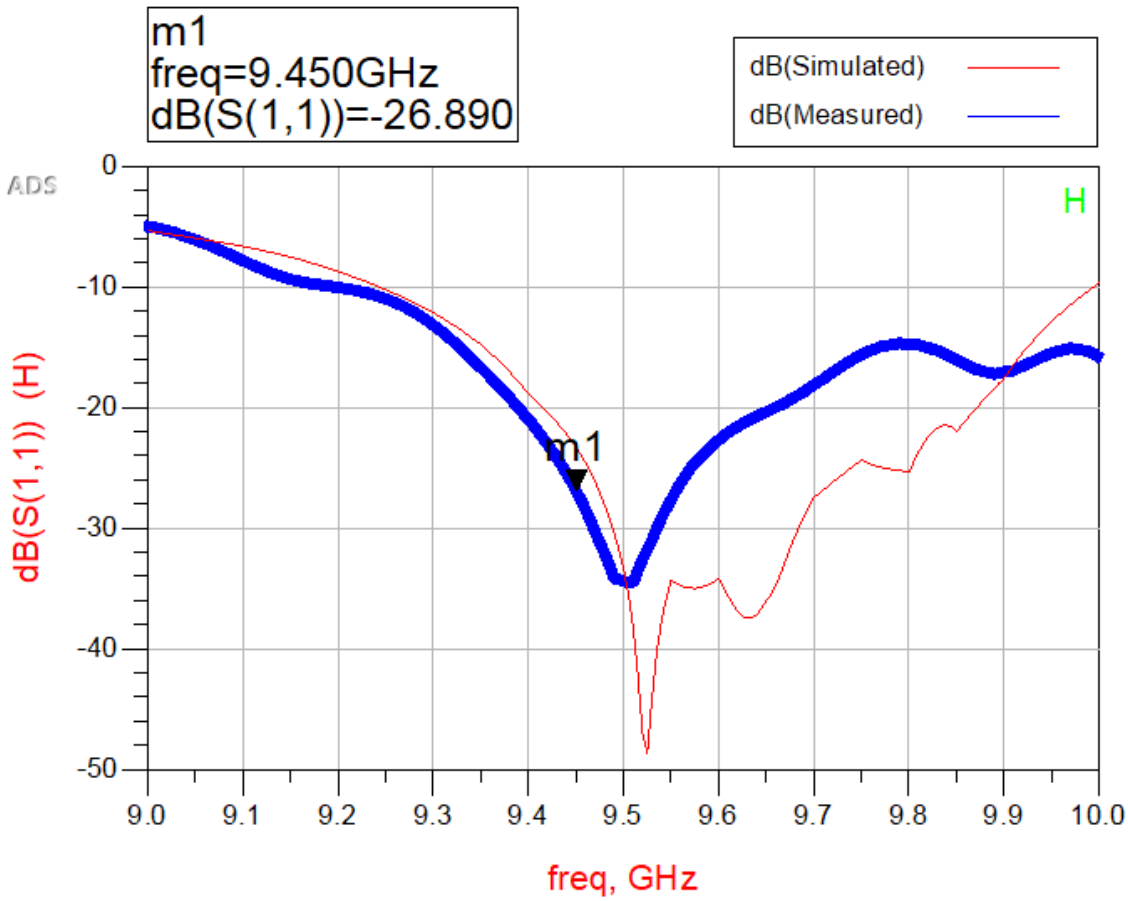

Figure 3.21: Comparison of Simulated and Measured Return Loss of Single POC1.

As seen in Figure 3.21, the measured return loss closely mirrors the simulated response until around 9.5 GHz. It is possible that slight variations in width and thickness of the feeding network could affect the performance of the transmission lines at frequencies above 9.5 GHz. However, this change is acceptable since the measured return loss is still below -10 dB across the same frequency band.

Once the return loss was verified, POC1 was placed in the anechoic chamber at Carleton University to test its radiation pattern using the setup presented in Section 2.6.2. The radiation pattern measured at the center frequency of 9.45 GHz is shown below in Figure 3.22.

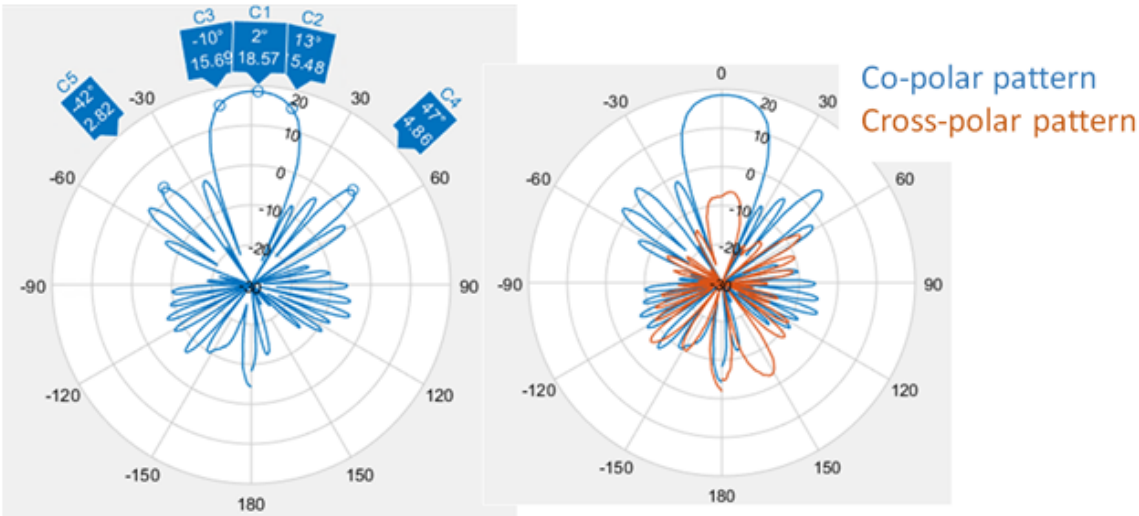

POC1 1x1	Main lobe location & level (Realized Gain)	Sidelobe location & level (left)	Sidelobe location & level (right)	Null location (left)	Null location (right)	Beam width
Co, φ =0°	2°, 18.57dB	-42°, 2.82dB	47°, 4.86dB	-20°	24°	23°

Figure 3.22: Measured Radiation Pattern of POC1 at 9.45 GHz.

Figure 3.22 shows that the gain of the main lobe is around 18.6 dB which is a 4 dB increase over the simulated value. The HPBW is around 23°, close to the simulated value of 26°. Side lobes are at 2.8 dB and 4.9 dB, which increased by 5.8 dB and 1.9 dB over simulation, with the distance to the main lobe being 15.8 dB and 13.7 dB, respectively. Overall, the measured response of the manufactured POC1 antenna array meets the required specifications of 11 dB main lobe gain, around 30° HPBW and side lobes at least 13 dB below the main.

3.4.2 Measurement of Four Tiled POC1 Antenna Arrays:

Once a single POC1 PCB was measured and verified, four POC1 boards were tiled together to form an 8x8 element array and measured in the same manner as the single

POC1 board. The only difference is that a ZC4PD-153-S+ four-way power splitter/combiner was added to provide power to all 4 POC1 boards. Figure 3.23 shows the measured and simulated return loss of four POC1 boards connected using the power splitter.

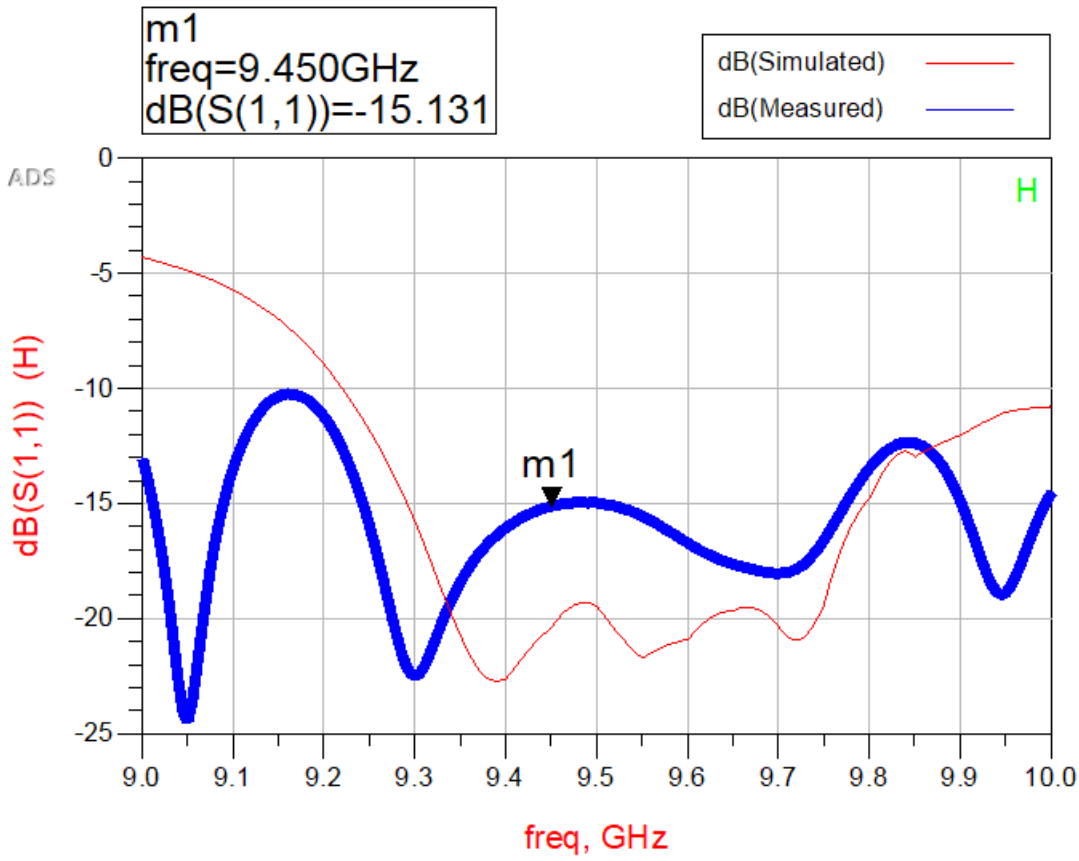

Figure 3.23: Simulated and Measured Return Loss of 4 POC1 Boards.

As seen in Figure 3.23, the simulated and measured return losses match each other well. The most logical source of discrepancy would be the physical performance of the chosen power splitter. Likely, the fabricated POC1 boards are not as well matched to the power splitter as the simulated values were to the splitter S-parameter file.

The radiation pattern measured for 4 POC1 boards at the center frequency of 9.45 GHz is shown below in Figure 3.24.

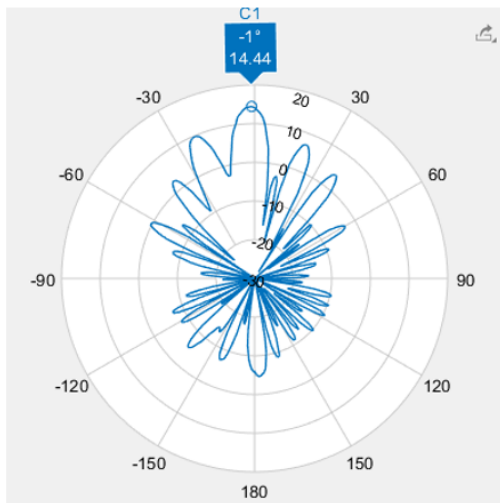

POC1 2x2 array	Main lobe location & level (Realized Gain)	Sidelobe location & level (left)	Sidelobe location & level (right)	Null location (left)	Null location (right)	Beam width
Co, φ =0°	-1°, 14.44dB	-23°, 9.81dB	21°, 6.98dB	-14°	9°	9°

Figure 3.24: Measured Radiation Pattern of 4 POC1 Boards at 9.45 GHz.

From Figure 3.24, the radiation pattern of 4 POC1 boards tiled together is not as clean as the single POC1 due to a side lobe merging with the main lobe on one side. As stated in Section 3.3.4, the distance from outer patches to the board edge is half the distance between inner patches. This was done to avoid increased side lobes when tiling multiple boards. Since the boards are not on the same piece of substrate, they are likely not perfectly in line with each other in the holder. If one of the boards is tilted slightly away from the others, it could result in a lopsided main beam and higher side lobes, as seen in Figure 3.24. It should be noted that the power combiner has an insertion loss of around 0.7 dB at 9.45 GHz [35]. A 6 dB drop is also present due to four-way power splitting. So while Figure 3.24 shows the peak gain to be 14.4 dB, the actual gain would

be closer to 21.1 dB, which is only 2.5 dB higher than a single POC1. Ideally, an array with four times as many elements would see a 6 dB gain increase. The extra 3.5 dB of gain was likely lost to the large sidelobe seen in Figure 3.24.

3.5 Conclusion

A brief system analysis of the desired switchable polarization phased array was presented from which the specifications for POC1 were derived. A 4x4 patch antenna array was designed, simulated, fabricated, and measured using these specifications. This simple linearly polarized array is the first steppingstone toward making a version that has switchable polarization.

The array was designed on a multilayer Rogers Duroid substrate with the antenna array and feeding network on opposite sides of the same PCB package. This resulted in a low-profile design that measures 2.5x2.5 inches. A method for increasing the bandwidth by loading each patch element with series resistors was also successful and increased the bandwidth of a single patch antenna by 300 MHz.

The measured results of the single fabricated antenna array met all the required specifications. A single POC1 board has a clean radiation pattern with a peak gain of 18.6 dB. When four POC1 boards are tiled together to form a larger array, the radiation pattern has a higher gain close to 21.1 dB. However, the radiation pattern is not as clean with large sidelobes and a lopsided main lobe.

The next step in this thesis is to add another layer of complexity to this design by making a circularly polarized antenna array on the same substrate. The design process of this new circularly polarized 4x4 array known as POC2 will be discussed in Chapter 4.

Chapter 4: Circularly Polarized Antenna Array

4.1 Introduction

Proof of Concept 2 (POC2) aims to design, simulate, and test a simple left-hand circularly polarized (LHCP) antenna array on the selected substrate. This development will be used to realize an antenna structure with a switchable polarization state. The purpose of POC2 is similar to POC1. The difference is that POC2 will be used to identify potential challenges with feeding and patch antenna design for circular polarization before adding any packaged components.

Like Chapter 3, this chapter will outline the design process of POC2, starting with the required specifications of the circularly polarized 4x4 patch antenna array. The specifications are used to design a single patch antenna to be used as the building block of a 4x4 antenna array that is to be fabricated and tested in a later stage. The major difference from POC1 is that each patch antenna will need two feeding ports, and the feeding network will need to apply a 90° phase shift to one of those ports to achieve circular polarization [16].

4.2 Specifications

The system-level analysis performed for POC1 in Section 3.2 is also valid for POC2. The only additional specification needed for POC2 is the axel ratio since POC2 is meant to be circularly polarized. The standard axel ratio threshold of 3 dB or lower will be used as the specification [16]. Table 4.1 shows a summary of the system specifications for POC2.

Table 4.1: POC2 System Specifications.

SECTION	TITLE/DESCRIPTION	SPECIFICATION				COMMENTS
1	**Antenna Array Specification**	Unit	Min	Nominal	Max	
1.1	Operating Frequency	GHz	9.4	9.45	9.5	
1.2	Gain of Antenna	dB	11	16		EIRP – Pin
1.3	EIRP	dBm		33		Keep fixed EIRP
1.4	HPBW	deg		30		
1.5	Input IF frequency	GHz		9.45		
1.6	Input IF power Pin	dBm		18		Varying the Pin to achieve fixed EIRP
1.7	Return Loss	dB			-10	
1.8	Side Lobe Level	dB		13		Below main lobe.
1.9	Efficiency	%	60			
1.10	System loss	dB		2		Insertion losses of 1/16 power divider and RF connector
1.11	Axel Ratio	dB			3	
1.12	Polarization type	Left Hand Circular Linear				Towards the direction of propagation.
2	**Environmental Specifications**					
2.1	Operating Temperature	°C	-40	25	85	
3	**Physical Specifications**					
3.1	Dimensions (W x L)	mm		64 x 64		Rogers 4003 20 mil two layers

Similar to POC1, the patch antennas on POC2 will be spaced approximately 0.95λ apart. This was done to maintain uniformity in the substrate dimensions for all iterations of this design, including POC3 and onward. As mentioned in Section 3.2.1, extra space is needed on POC2 to allow for twice as many feeding points in the feeding network. While this will cause larger sidelobes than if the elements were spaced 0.5λ apart, this is a

necessary trade-off for the extra space needed. POC2 also uses the same substrate stackup as POC1, as shown in Figure 3.6 in Section 3.2.1. A preliminary diagram of POC2 is shown in Figure 4.1.

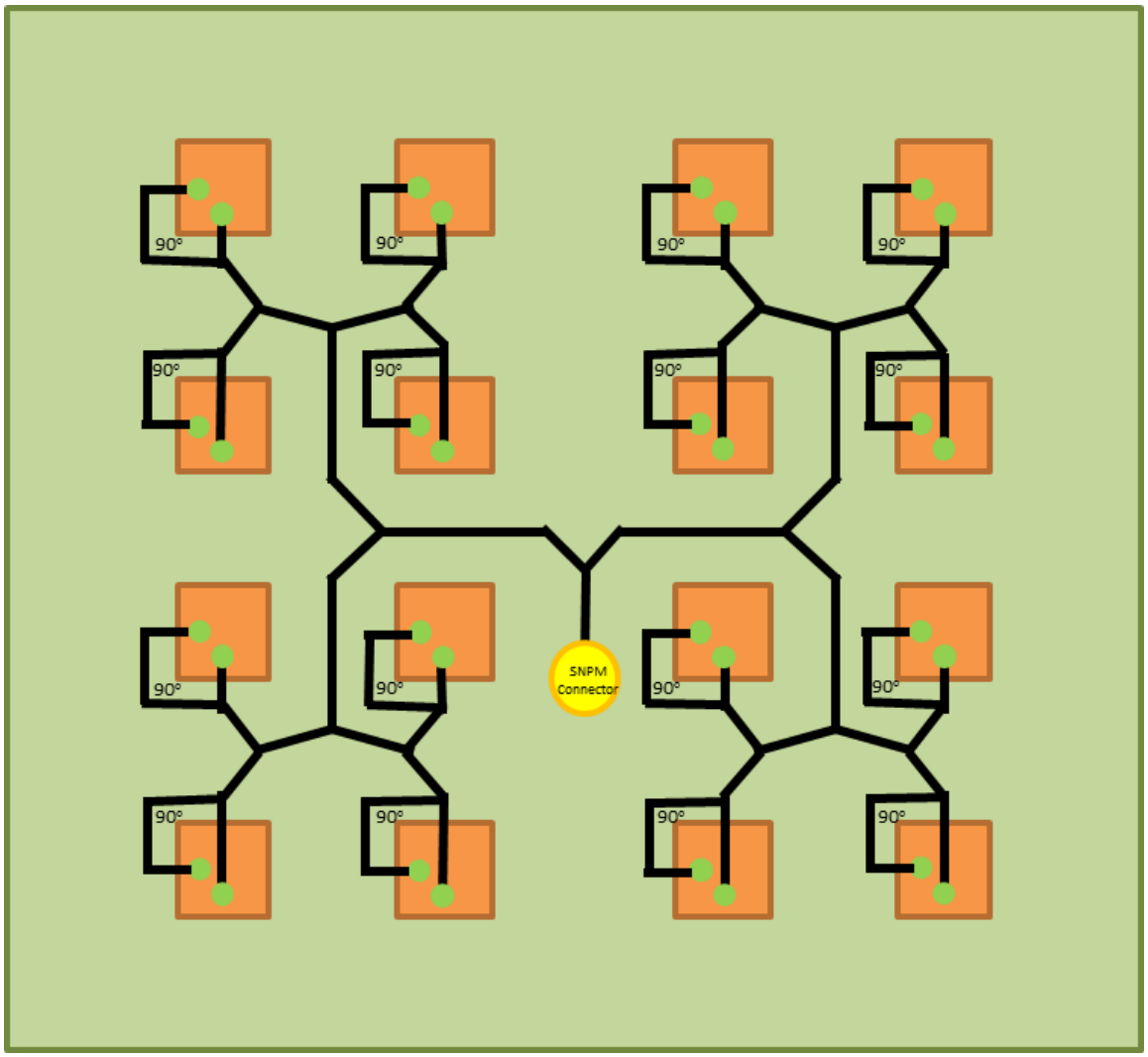

Figure 4.1: System Diagram of POC2.

4.3 Design and Simulation

Noting the specifications in Table 4.1, the design process of a single square patch antenna can be initiated that will later be scaled up into an array. The method for increasing the

patch antenna bandwidth through resistive loading presented in Section 3.3.2 is also used here. Since POC2 calls for circular polarization, each patch antenna must be designed with 2 feeding points with a 90^0 phase shift on one feed point. With twice as many feed points, a 32-branch microstrip feeding network will be needed to connect multiple patch antennas into a 4x4 array.

4.3.1 Design of Single Patch Antenna with Two Feeding Points

The design process for a single patch antenna with resistive loading shown in Sections 3.3.1 and 3.3.2 was repeated for POC2. Figure 4.2 shows the square patch antenna with two 0402 sized 50Ω resistors added at an equal distance from the patch center as the two input feeding pins.

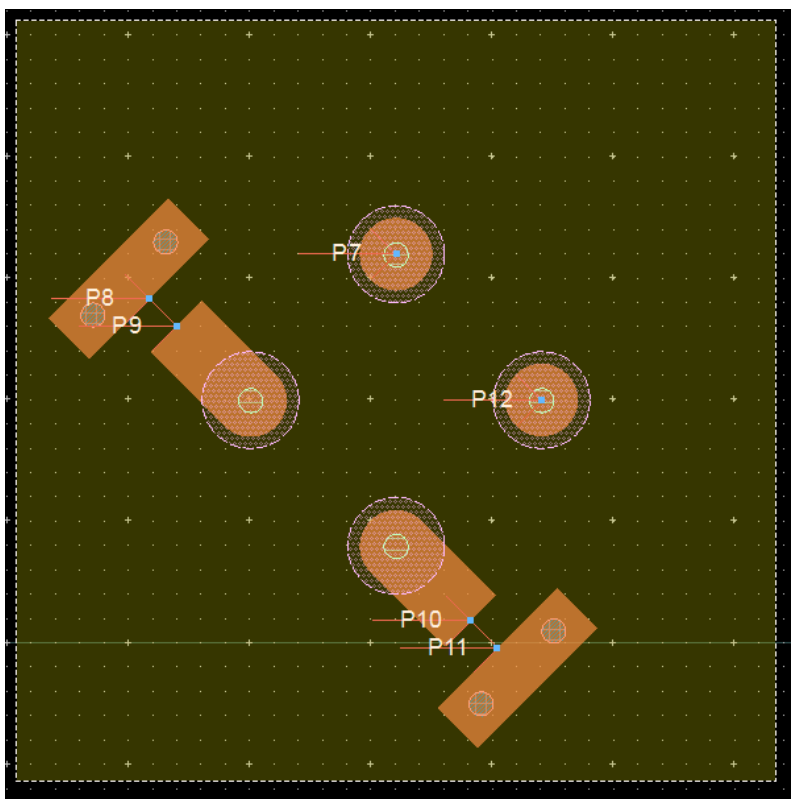

Figure 4.2: Resistively Loaded Two Port Patch Antenna.

The return loss of the loaded patch in Figure 4.2 is displayed in Figure 4.3.

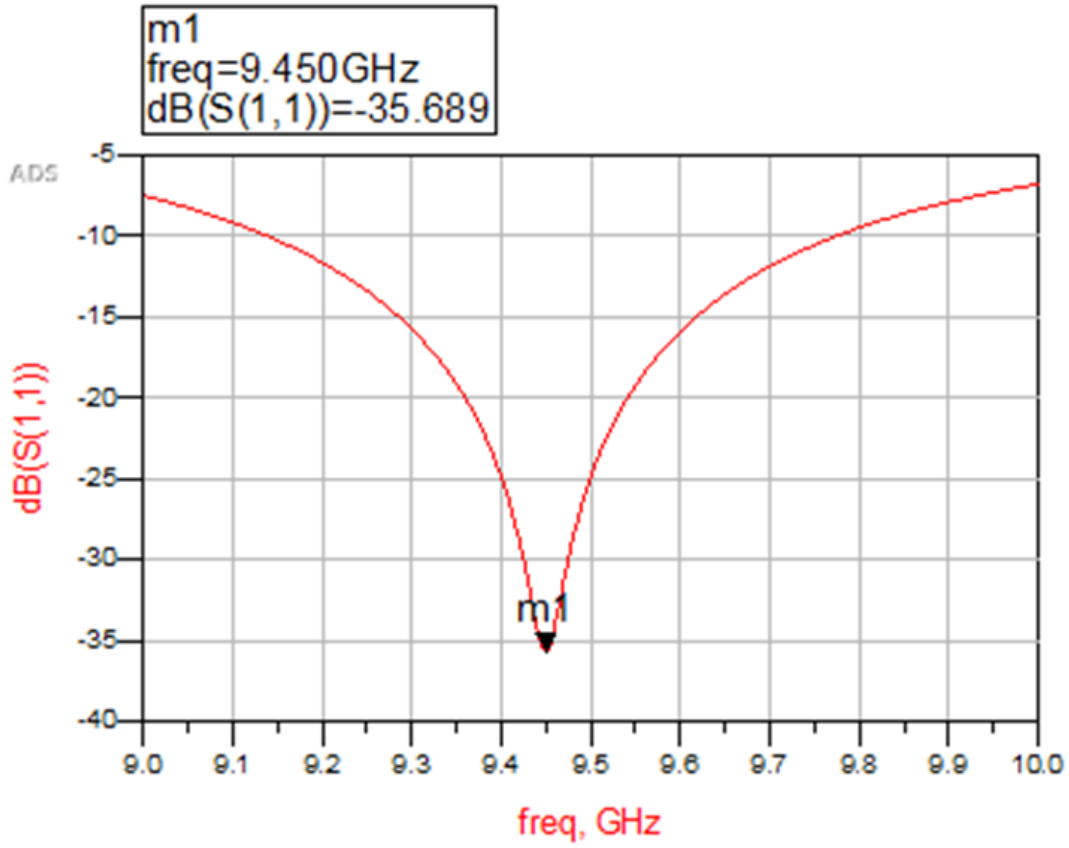

Figure 4.3: Return Loss of Loaded Two Port Patch Antenna.

The performance in Figure 3.9 shows a good return loss of -35.7 dB at 9.45 GHz, which indicates the single patch is well matched to the target frequency. The bandwidth is approximately 600 MHz which is well above the minimum specification. The radiation pattern of the single-loaded patch at the center frequency 9.45 GHz is seen in Figure 4.4.

Frequency	E_max	Theta_max	Phi_max	Directivity_max	Gain_max	RadiatedPower	InputPower	Efficiency	CutType	CutAngle
9.450E9	0.348	179.000	0.000	6.643	2.071	4.386E-4	0.001	0.349	Phi	0.000

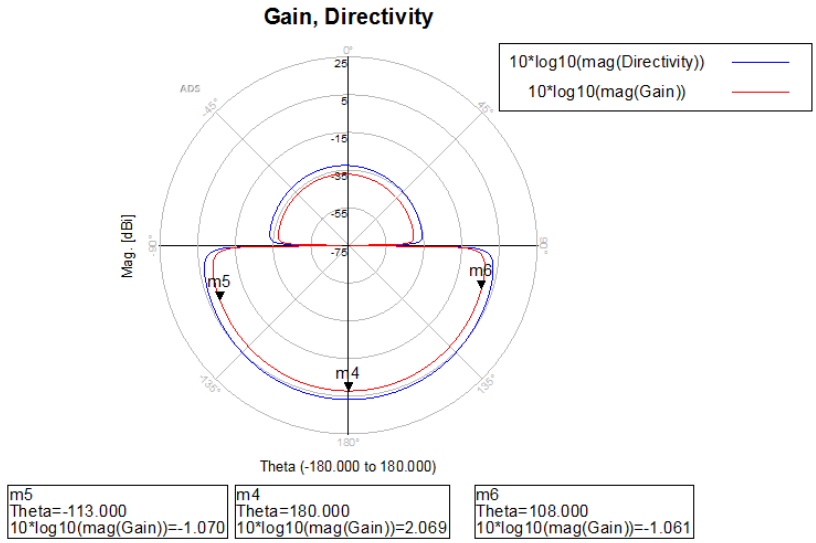

Figure 4.4: Gain and Efficiency of Loaded Square Patch Antenna (POC2).

According to Figure 4.4, gain and efficiency have dropped dramatically to 2.1 dB and 35%. This could present some challenges when assembling the full 4x4 array. For now, an attempt to mitigate this loss will need to be made when designing the feeding network. Resistive loading may need to be re-evaluated in future design stages to avoid this drop in gain and efficiency.

4.3.2 Design of POC2 Feeding Network

Antenna elements will be connected using a 1 to 32 microstrip power divider. The feeding network was designed in the same fashion as POC1, as seen in Section 3.3.3. The feeding network comprises multiple quarter-wave transformers (QWT) arranged in a branching pattern that will split the input power in half multiple times depending on the number of elements in the array. The major difference included in POC2 is that one of

the feeding lines for each patch element will include a corner turn to achieve a 90° phase shift. A 32-element power divider can now be made by branching 50Ω, 70.7Ω and 100Ω transmission lines together. The 32-element power divider with the landing pad for the selected SMPM connector is seen in Figure 4.5.

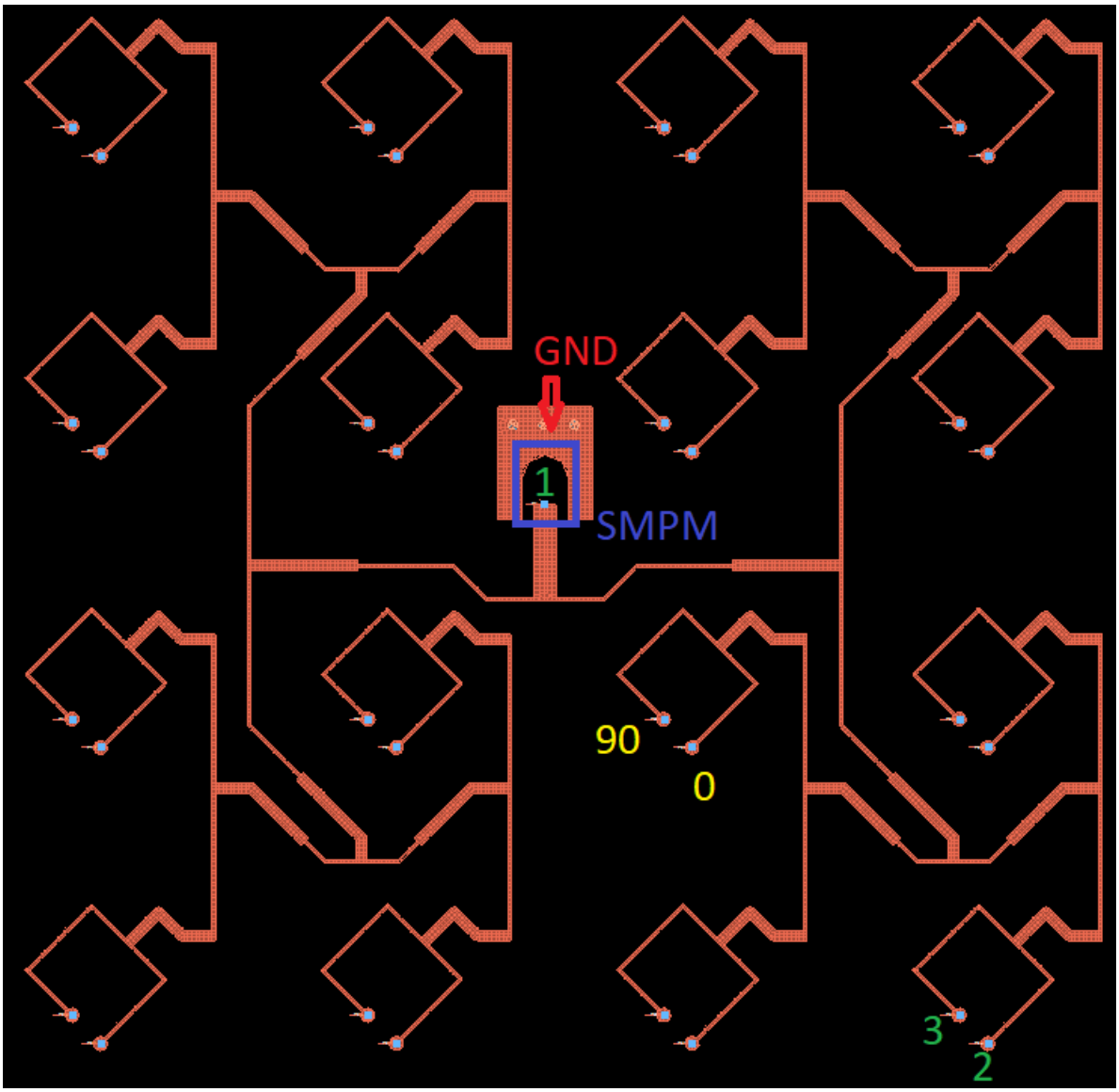

Figure 4.5: POC2 Microstrip Feeding Network.

Like with POC1, the parameters that must be optimized on the input are the return loss of each port, isolation between adjacent ports, and the insertion loss from the input to each output. For POC2, the important factors to watch are the gain and phase balance between two feeding lines on the same patch. The ports where S-Parameter data was measured are labeled green in Figure 4.5; all other ports are loaded with 50Ω. The S-Parameters of the POC2 feeding network are shown in Figure 4.6.

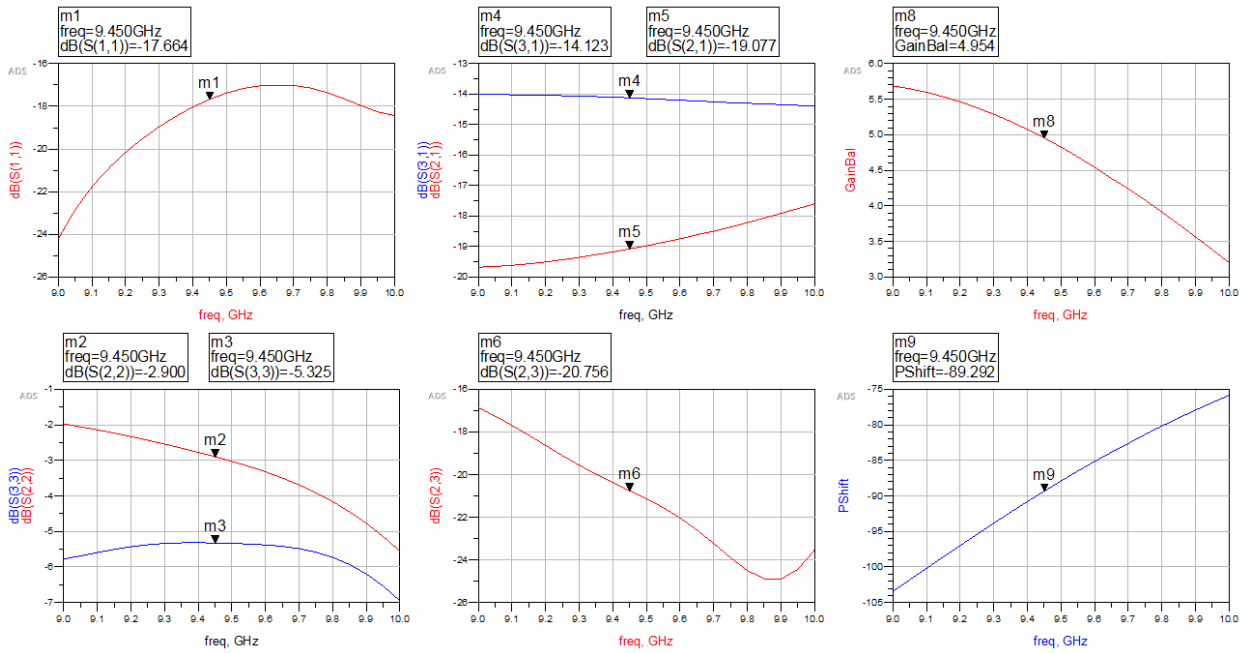

Figure 4.6: Performance of POC2 Feeding Network.

As seen in Figure 4.6, the return loss at the input port is good and has a wide bandwidth, making it easy to match the patch antennas. It should be noted that the power splitting in half between two branches is equivalent to a -3 dB drop, and since the input power splits five times, a drop of -15 dB is expected. So while Figure 4.6 shows the S21 to be -19 dB and S31 to be -14 dB, the feeding network's insertion loss is around -4 dB and -1 dB, respectively. The slight problem is that the insertion loss of one feeding point

is below the -2 dB specification. This higher loss in one path also leads to a gain imbalance of around 5 dB between the two feeding ports. This subpar gain performance is necessary due to the phase balance between the feeding ports needing to be close to 90°; therefore, a trade-off between gain and phase balance had to be made. The isolation between adjacent output ports is well below the -10 dB threshold. The return loss on the output ports is too high above the -10 dB threshold, which means the outer tips of the feeding network are not correctly matched to 50Ω. The input pin of the patch antenna must be adjusted when assembling and optimizing the full array since the feeding network can not be adjusted at the outputs without interfering with patch spacing and isolation.

4.3.3 Simulation of Full POC2 Antenna Array

Now that the patch antenna and feeding network have been designed and verified, the components can be assembled to form the full 4x4 patch antenna array. Figure 4.7 shows the full 4x4 antenna array after some fine-tuning of the feeding network and patches once connected.

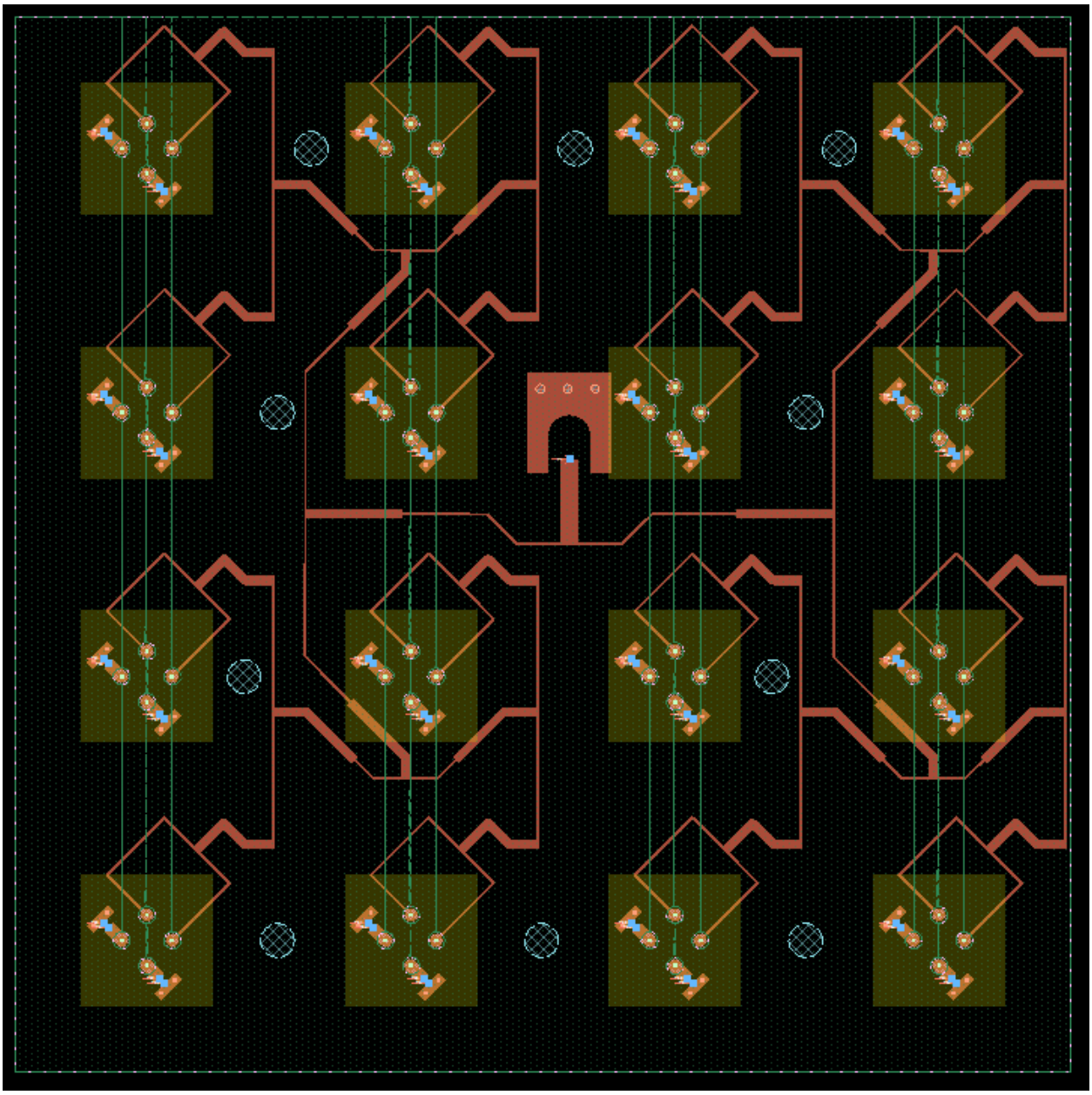

Figure 4.7: Full POC2 Antenna Array (2D View).

In addition to the 2D view shown in Figure 4.7, a 3D top and bottom view of POC2 is shown in Figure 4.8.

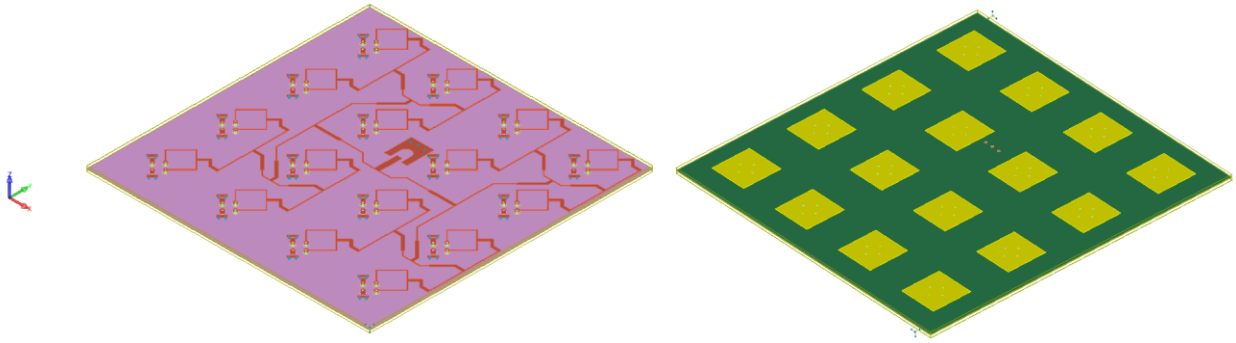

Figure 4.8: Full POC2 Antenna Array (3D View).

Figure 4.9 shows the return loss of the full POC2 antenna array.

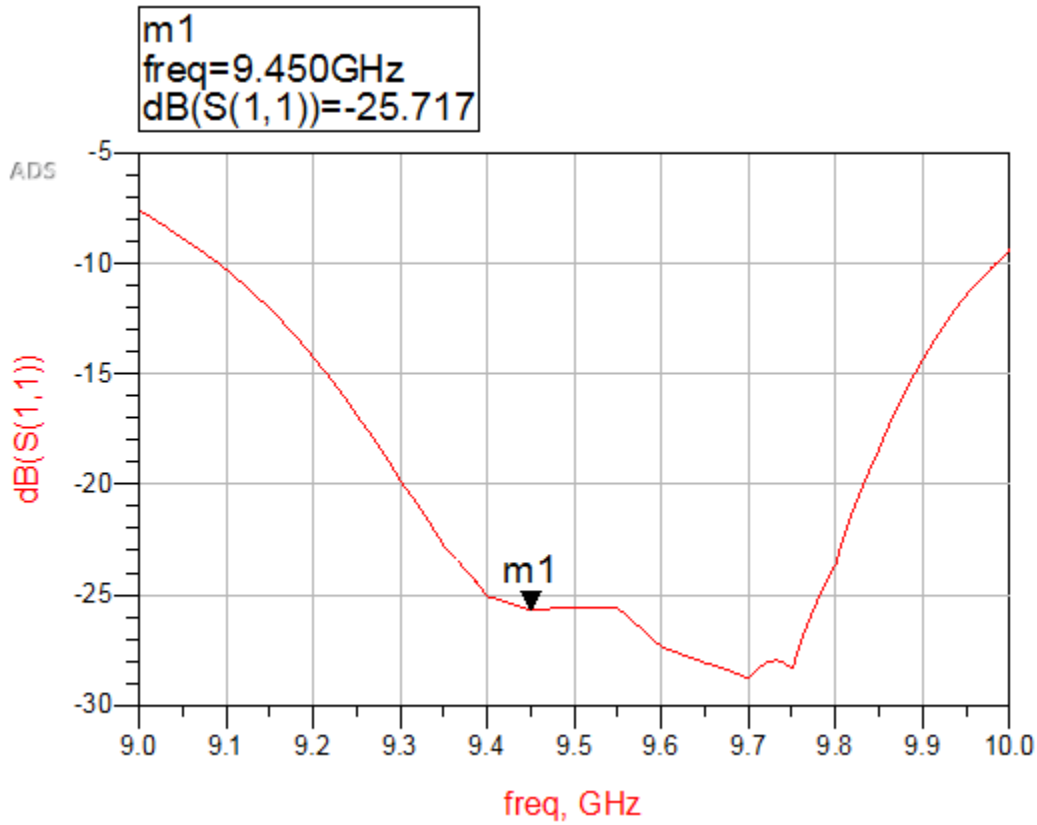

Figure 4.9: Simulated Return Loss of Full POC2 Array.

Figure 4.9 indicates the return loss is still excellent across the desired band from 9.4 to 9.5 GHz. A bonus is that the overall bandwidth has dramatically increased to around 900 MHz. Figure 4.10 shows the radiation pattern of the full POC2 array.

Frequency	E_max	Theta_max	Phi_max	Directivity_max	Gain_max	RadiatedPower	InputPower	Efficiency	CutType	CutAngle
9.450E9	3.134	179.000	65.000	16.901	14.937	0.003	0.005	0.636	Phi	90.000

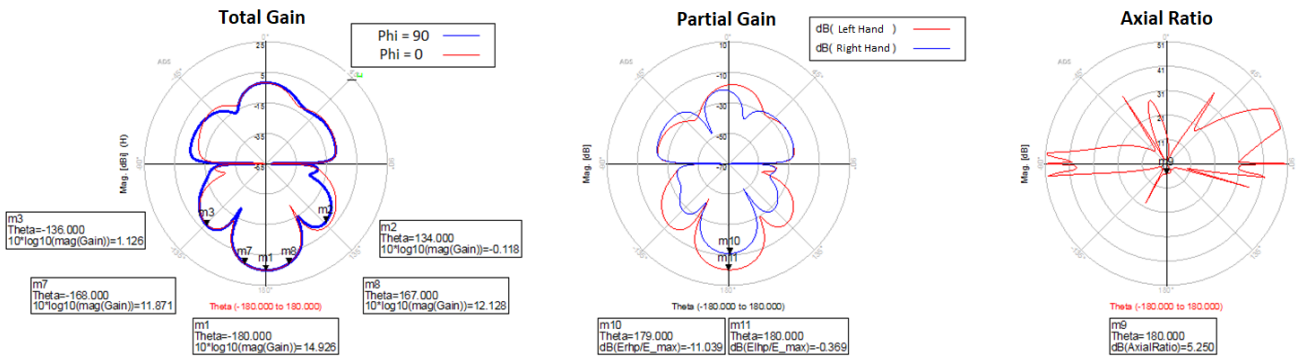

Figure 4.10: Simulated Gain and Efficiency of Full POC2 Array.

Figure 4.10 shows that the peak gain of both the 0º and 90º cuts is 15 dB and the efficiency is 63.6 %, which both meet the minimum values of 11 dB and 60%. Figure 4.10 also shows that the partial gain in the left- and right-hand planes indicate POC2 is LHCP as desired. Even though the gain and efficiency are good, the axial ratio is above the 3 dB specification. The feeding network designed in Section 4.3.2 showed a 5 dB gain imbalance between the feed points, explaining a 5 dB axial ratio. The axial ratio seems odd considering that the axial ratio represents the deviation between the 0º and 90º cuts of the radiation pattern. According to Figure 4.10, the two cuts are almost identical, with the gain of both peaking around 15 dB with an HPBW of 25º, which would mean the axial ratio should be lower. The whole POC2 array was imported into HFSS to replot the gain and axel ratio to reconcile this discrepancy. Figures 4.11 and 4.12 show the HFSS axial ratio and gain plots.

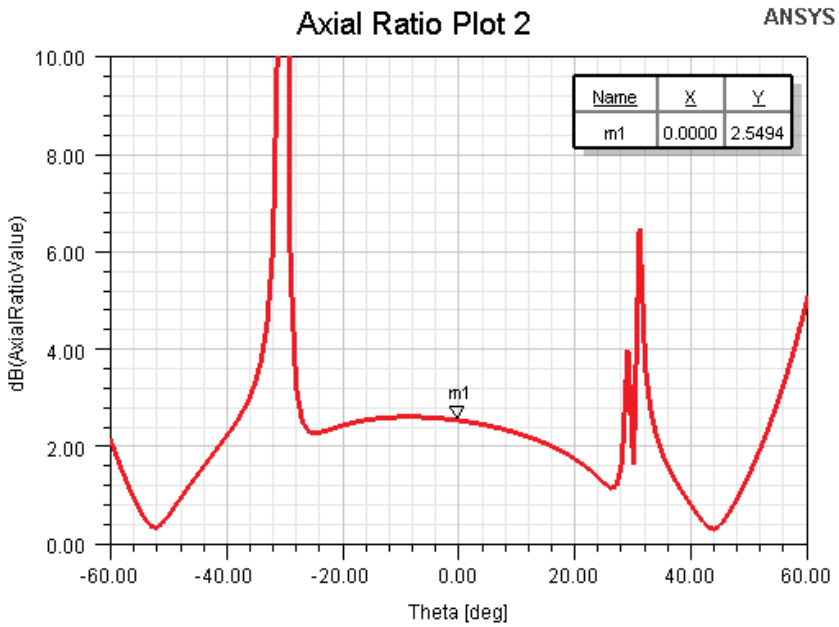

Figure 4.11: HFSS Axial Ratio Plot.

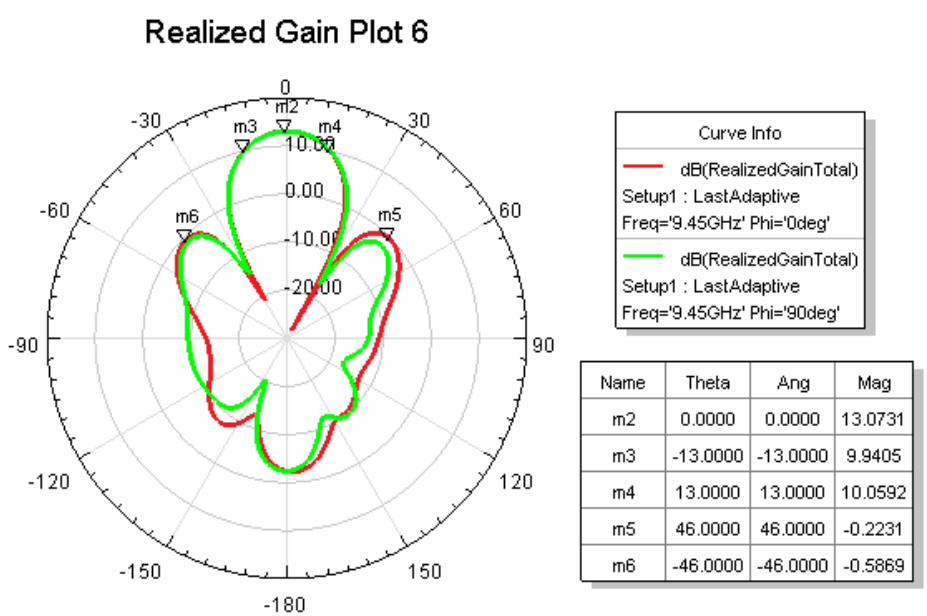

Figure 4.12: HFSS Gain Plot.

A few conclusions can be drawn by comparing the ADS plots shown in Figure 4.10 to the HFSS plots in Figures 4.11 and 4.12. The gain of the ADS plot showed a peak

gain of 15 dB for both cuts, while HFSS showed 13 dB. This is not a big concern since both values meet the 11 dB minimum. What is of interest is that the axial ratio in HFSS shows an axial ratio of 2.5 dB, which meets the 3 dB specification and is more consistent with the similarity of the two gain cuts. The HPBW is around 26°, close to the specified value of 30°. Side lobes are at -0.2 dB and -0.5 dB giving a distance from the main lobe of -13 dB and -13.5 dB, respectively; these are close enough to the nominal value of -13 dB below the main lobe. The simulated values shown in Figures 4.11 and 4.12 indicate that POC2 meets the required system specifications and is ready for fabrication and testing.

4.4 Measurement of POC2

Once the full POC2 antenna array was verified in simulation, it was sent out for fabrication to be later tested in the anechoic chamber at Carleton University. Figure 4.13 shows the fabricated POC2 antenna array.

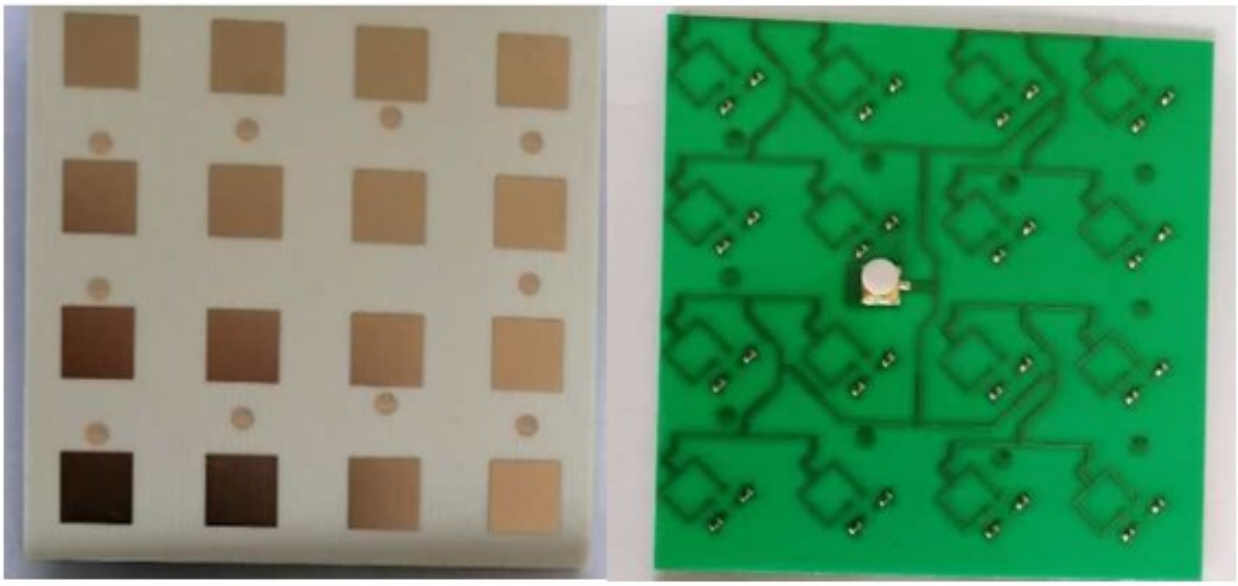

Figure 4.13: Fabricated POC2 Antenna Array.

4.4.1 Measurement of Single POC2 Antenna Array

The single POC2 antenna board shown in Figure 4.13 was tested at Carleton University using the S-Parameter test setup presented in Section 2.6.1 to measure the return loss of the array. The measured return loss of POC2 can be seen and compared to simulation results in Figure 4.14 below.

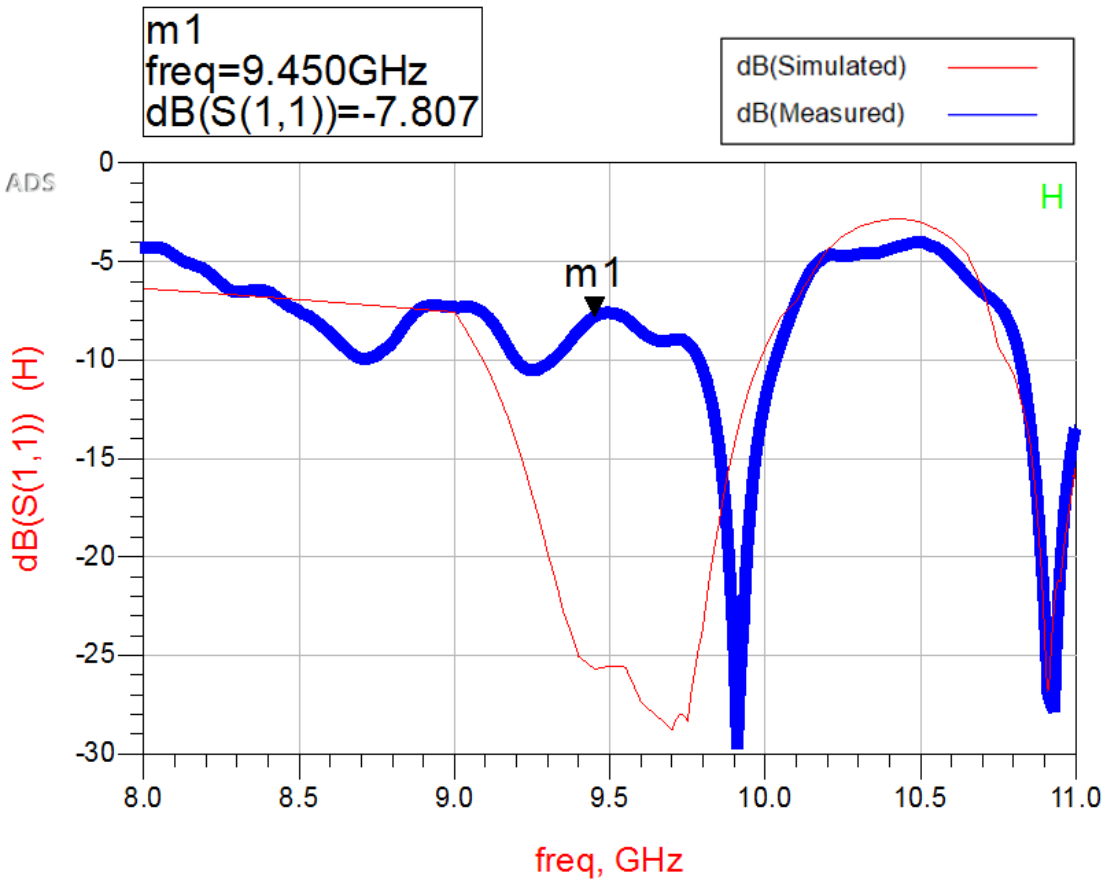

Figure 4.14: Comparison of Simulated and Measured Return Loss of Single POC2.

As seen in Figure 4.14, the measured return loss closely mirrors the simulated response from 8 GHz to 9 GHz and again from 10 GHz to11 GHz. Unfortunately, the most significant discrepancy is between 9 and 10 GHz, where the target band is located. A possible explanation is that unwanted resonance was created in the feeding network

and not captured by the simulator around the desired center frequency. The full POC2 array was once again re-simulated in HFSS to try and capture any problems in the target band. Figure 4.15 shows a comparison of the return loss simulated in ADS and HFSS along with the measured data.

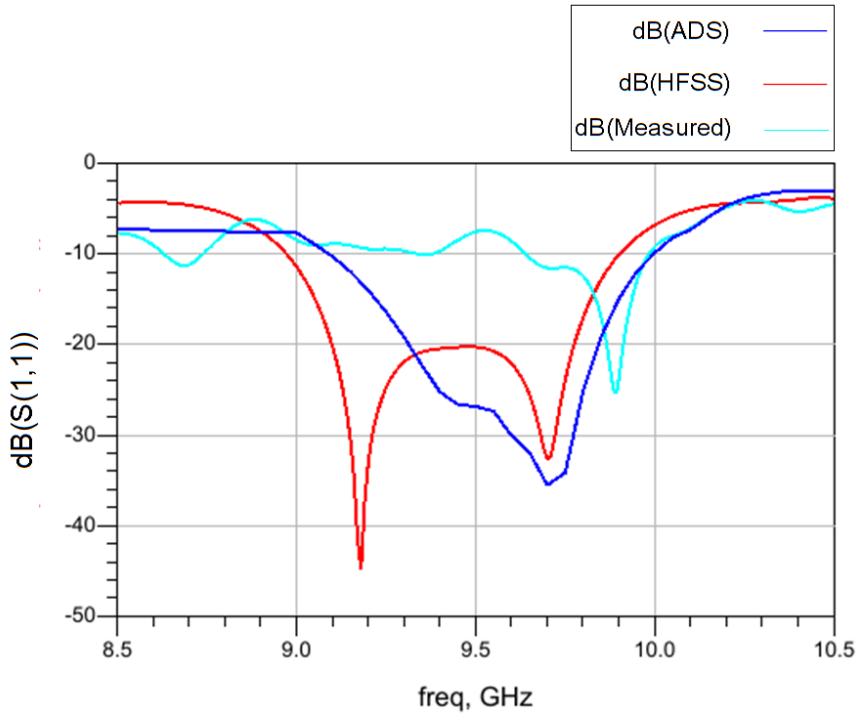

Figure 4.15: POC2 Return Loss Comparison Between ADS, HFSS and Measured.

The HFSS return loss in Figure 4.15 follows the same pattern as Figure 4.14. All three data sets agree with one another below 9 GHz and above 10 GHz. There is a slight discrepancy between ADS and HFSS between 9 and 9.3 GHz, which is likely due to the difference in algorithms used by each. However, the two simulators show very similar responses in the target band. POC1 was simulated using ADS which matched the measured results well. This means that the discrepancy between simulated and measured results for POC2 are due to a flaw in the design rather than the simulators.

Once the return loss was measured, POC2 was placed in the anechoic chamber at Carleton University to test its radiation pattern using the setup presented in Section 2.6.2. The radiation pattern measured at the center frequency of 9.45 GHz is shown below in Figure 4.16.

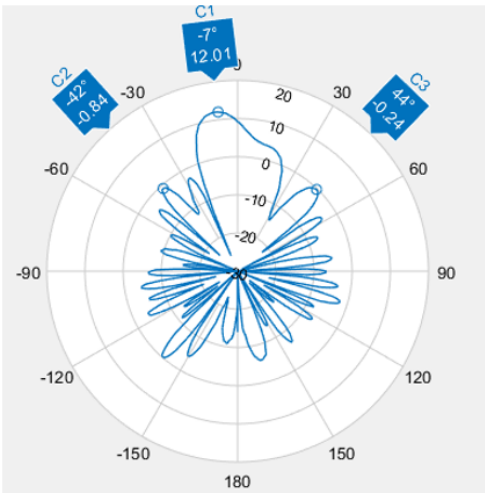

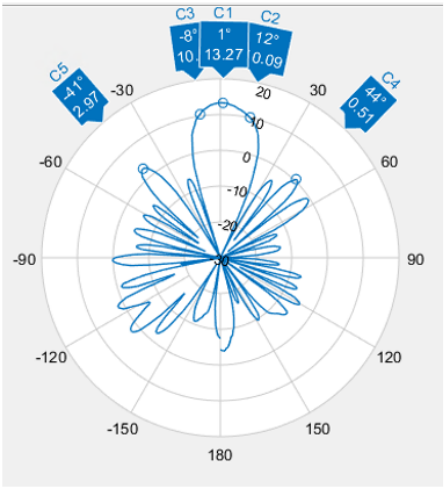

POC2 1x1	Main lobe location & level (Realized Gain)	Sidelobe location & level (left)	Sidelobe location & level (right)	Null location (left)	Null location (right)	Beam width
Co Y	-8°, 12.07dB	-42°, -0.84dB	44°, -0.24dB	-23°	31°	16°
Co X	1°, 13.27dB	-41°, 2.97dB	44°, -0.51dB	-18°	26°	20°

Figure 4.16: Measured Radiation Pattern of POC2 at 9.45 GHz.

Figure 4.16 shows that the gain of the main lobe is around 13 dB in one plane and 12 dB in the other, which closely matches the simulated value. The axial ratio is the difference between the peaks is around 1.3 dB, which is a slight improvement over the simulated value of 2.5 dB. The HPBW is around 20°, close to the simulated value of 26°. Side lobes are at -0.8, -0.2, 0.5 and 3 dB. Three of the sidelobes closely match the simulation and meet the specification of 13 dB below the main lobe. However, the fourth sidelobe does not meet the specification, being only 10 dB below the main lobe. Overall,

the measured response of the manufactured POC2 antenna array meets most of the required specifications, with one sidelobe being too big and the HPBW being too narrow.

4.4.2 Measurement of Four Tiled POC2 Antenna Arrays

The single POC2 antenna board shown in Figure 4.13 was tested at Carleton University using the S-Parameter test setup presented in Section 2.6.1 to measure the return loss of the array. The measured return loss of POC2 can be seen and compared to simulation results in Figure 4.17 below.

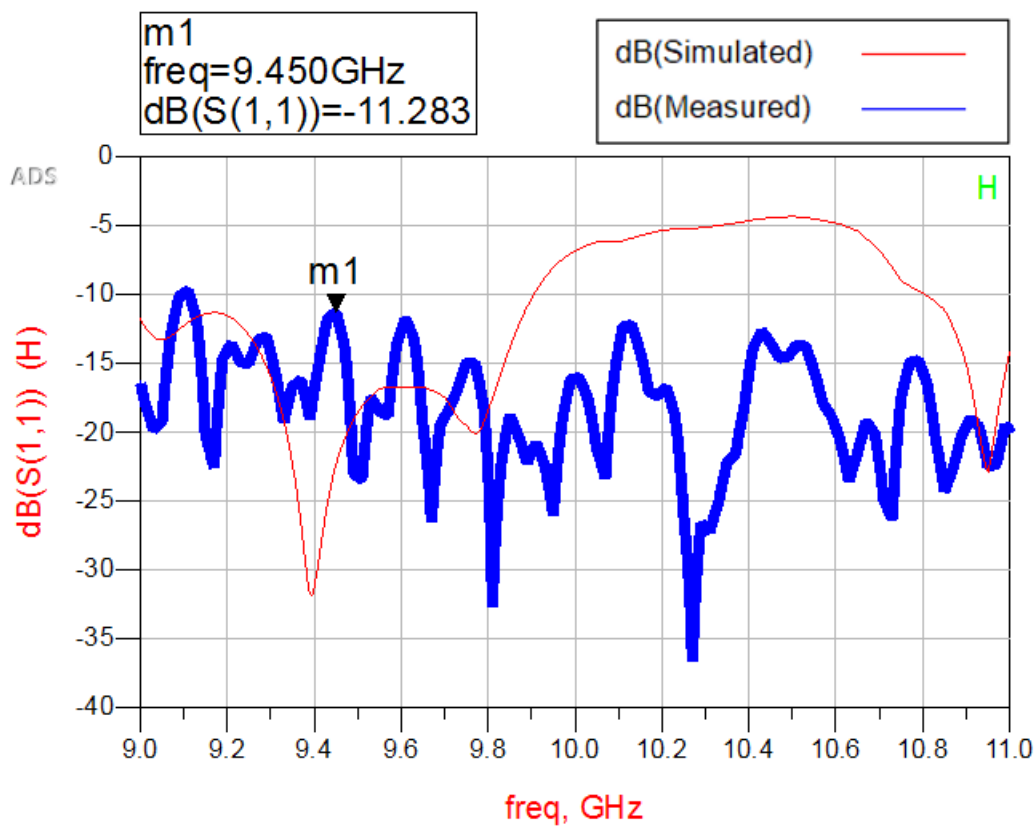

Figure 4.17: Simulated and Measured Return Loss of 4 POC2 Boards.

As seen in Figure 4.17, the simulated and measured return losses do not match each other well. Likely, the fabricated POC2 boards are not as well matched to the power

splitter as the simulated values were to the splitter S-parameter file. This would explain why the measured return loss appears to be so noisy over the frequency span.

The radiation pattern measured for 4 POC2 boards at the center frequency of 9.45 GHz is shown below in Figure 4.18.

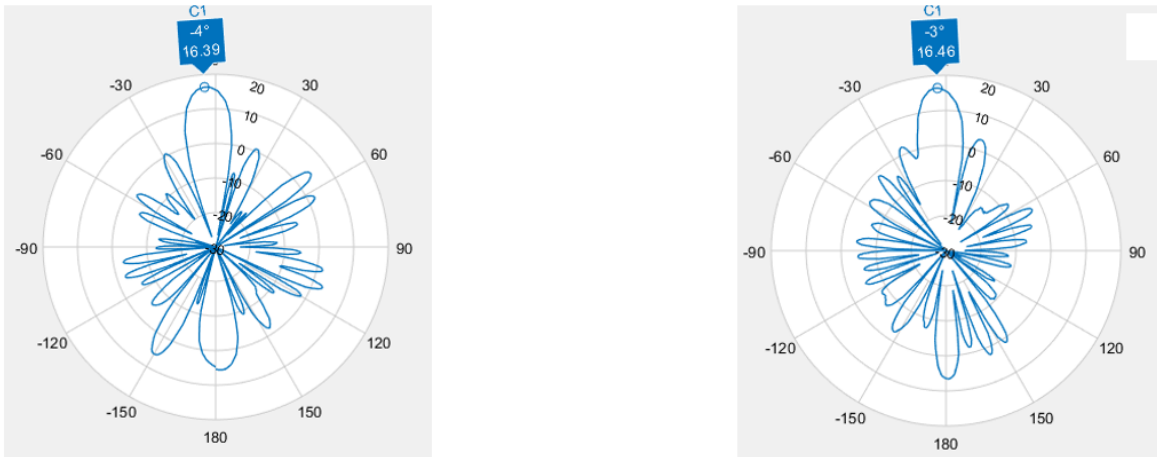

POC2 2x2	Main lobe location & level (Realized Gain)	Sidelobe location & level (left)	Sidelobe location & level (right)	Null location (left)	Null location (right)	Beam width
Co X	-4°, 16.39dB	-29°, 0.64dB	14°, -7.93dB	-20°	11°	13°
Co Y	-3°, 16.46dB	-24°, 2.1dB	17°, 3.17dB	-17°	11°	12°

Figure 4.18: Measured Radiation Pattern of 4 POC2 Boards at 9.45 GHz.

As seen in Figure 4.18, the radiation pattern of 4 POC2 boards tiled together has higher side and back lobes than the single POC2 radiation pattern seen in Figure 4.16. This is most likely because the four boards are not made on the same piece of the substrate, and they are likely not perfectly in line with each other in the holder. If one of the boards is tilted slightly away from the others, it could result in a lopsided main beam and higher side and back lobes, as seen in Figure 4.18. It should be noted that the power combiner has an insertion loss of around 0.7 dB at 9.45 GHz [35]. So while Figure 4.18

shows the peak gain to be around 16.4 dB, the actual gain would be closer to 17.2 dB which is around 5.2 dB greater than a single POC2 board.

4.5 Conclusion

A 4x4 patch antenna array was designed, simulated, fabricated, and measured using the specifications derived for POC1 in the previous chapter. This simple left-hand circularly polarized array is another steppingstone toward making a switchable polarization array.

The array was designed on a multilayer Rogers Duroid substrate with the antenna array and feeding network on opposite sides of the same PCB package. Just like POC1, the design of POC2 was low-profile enough to fit on a 2.5x2.5 inch PCB. The method for increasing the patch bandwidth through resistive loading was repeated as well.

The measured results of the single fabricated antenna array met most of the required specifications. A single POC2 board produced a slightly lopsided radiation pattern with a peak gain of 13.3 dB and an axial ratio of 1.3 dB. When four POC2 boards are tiled together, they produce a lopsided main beam around 17.2 dB with high sidelobes and even higher back lobe. Two potential problems were discovered that need to be addressed in the next stage of this thesis. Power leakage between multiple pins in the single patch will need to be addressed, and a need for a feeding mechanism that has better performance in terms of gain and phase imbalance.

The next step is to add yet another layer of complexity to this design by introducing a single switch that will make an antenna array on the same substrate with two different polarizations. The design process of this two-mode switchable polarized 4x4 array known as POC3 will be discussed in Chapter 5.

Chapter 5: Switchable Polarization Antenna Array

5.1 Introduction

Proof of Concept 3 (POC3) aims to design, simulate, and test two different switchable polarized antenna arrays. One version will switch between LHCP and RHCP, while the other will switch between vertical and horizontal linear polarization. POC3 utilizes information learned during the development of POC1 and POC2 about the substrate, feeding and patch antenna design with additional packaged components. These additional components will allow for a single array to switch between two polarizations in both transmit and receive mode. For instance, the array board with two linear polarizations could transmit data in vertical mode then switch to receive in horizontal mode.

This chapter will outline the design process of POC3, starting with the required specifications of the switchable polarized 4x4 patch antenna array. The specifications are used to design a single patch antenna that is to be used as the building block of a 4x4 antenna array that will be fabricated and tested later. Integration of packaged components, including a hybrid coupler and SPDT switch will also be discussed.

5.2 Specifications

The system-level analysis performed for POC1 and POC2 in Section 3.2 is also valid for POC3. Table 5.1 shows a summary of the system specifications for POC3.

Table 5.1: POC3 System Specifications.

SECTION	TITLE/DESCRIPTION	SPECIFICATION				COMMENTS
1	**Antenna Array Specification**	Unit	Min	Nominal	Max	
1.1	Operating Frequency	GHz	9.4	9.45	9.5	
1.2	Gain of Antenna	dB	11	16		EIRP – Pin
1.3	EIRP	dBm		33		Keep fixed EIRP
1.4	HPBW	deg		30		
1.5	Input IF frequency	GHz		9.45		
1.6	Input IF power Pin	dBm		18		Varying the Pin to achieve fixed EIRP
1.7	Return Loss	dB			-10	
1.8	Side Lobe Level	dB		13		Below main lobe.
1.9	Efficiency	%	60			
1.10	System loss	dB		2		Insertion losses of 1/16 power divider and RF connector
1.11	Axial Ratio	dB			3	
1.12	Polarization type	LHCP & RHCP				Version 1
		Vertical & Horizontal Linear				Version 2
2	**Environmental Specifications**					
2.1	Operating Temperature	°C	-40	25	85	
3	**Physical Specifications**					
3.1	Dimensions (W x L)	mm		64 x 64		Rogers 4003 20 mil two layers

5.2.1 Substrate Revision and Practical Considerations

At the request of the PCB foundry, the substrate stackup had to be slightly altered for POC3 due to inventory issues. The PCB foundry required POC3 to be designed using Rogers Duroid 4350 instead of the 4003 used previously. The new RO4350 substrate has

an ε_r of 3.66 and a tanδ of 0.0037 at 10 GHz, slightly higher than RO4003 [31]. Since the design requires a PCB with patch antennas on one side and RF circuitry on the other, multiple substrate pieces will need to be stacked. Rogers 4450 prepreg was used to glue multiple pieces of 4350 together. This material was also stipulated by the PCB foundry used to fabricate POC3. For POC3, some extra alterations were made to accommodate the addition of packaged components needed for polarization switching. In POC1 and POC2, the pieces of RO4003 used for the patch antennas and the feeding network were both 20 mils thick. Since POC3 requires additional components on the feeding network side, the substrate thickness on that side was reduced to 10 mils. This way, transmission lines in the feeding network can be made thinner while keeping the same impedance. An extra metal layer was added to be used as a power plane for added switching circuitry. Figure 5.1 shows the new substrate stackup for POC3.

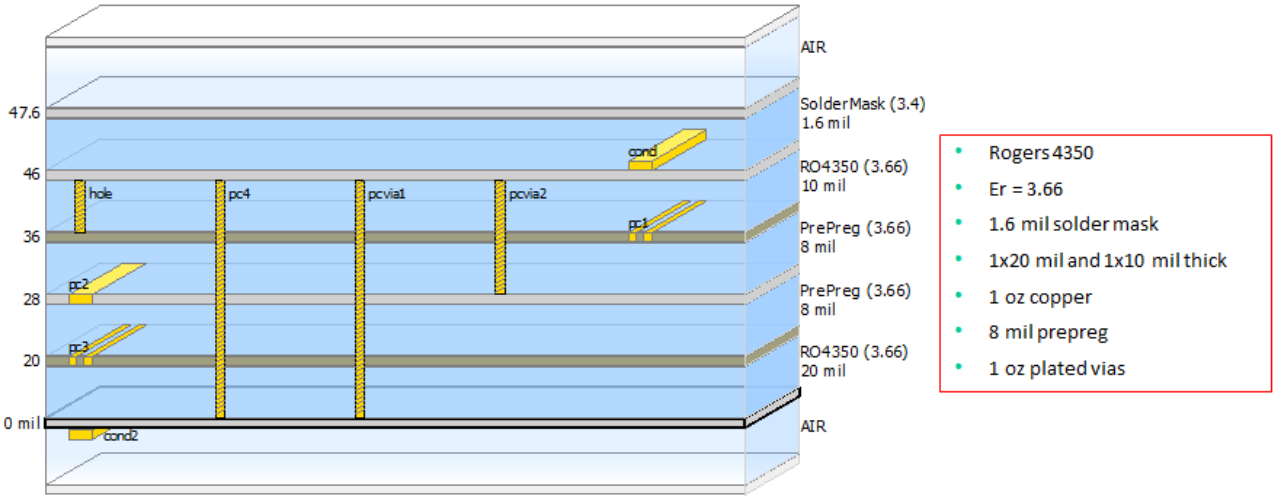

Figure 5.1: POC3 Substrate Stackup.

Like POC1 and POC2, the patch antennas on POC3 will be spaced approximately 0.95λ apart. This was done to maintain uniformity in the dimensions of the substrate for

all iterations of this design, including POC3 and onward. As mentioned in Section 3.2.1, extra space is needed on POC3 to allow for packaged components needed to achieve switchable polarization. While this will cause larger sidelobes than if the elements were spaced 0.5λ apart, this is a necessary trade-off for the extra space needed. A preliminary diagram of POC3 is shown in Figure 5.2.

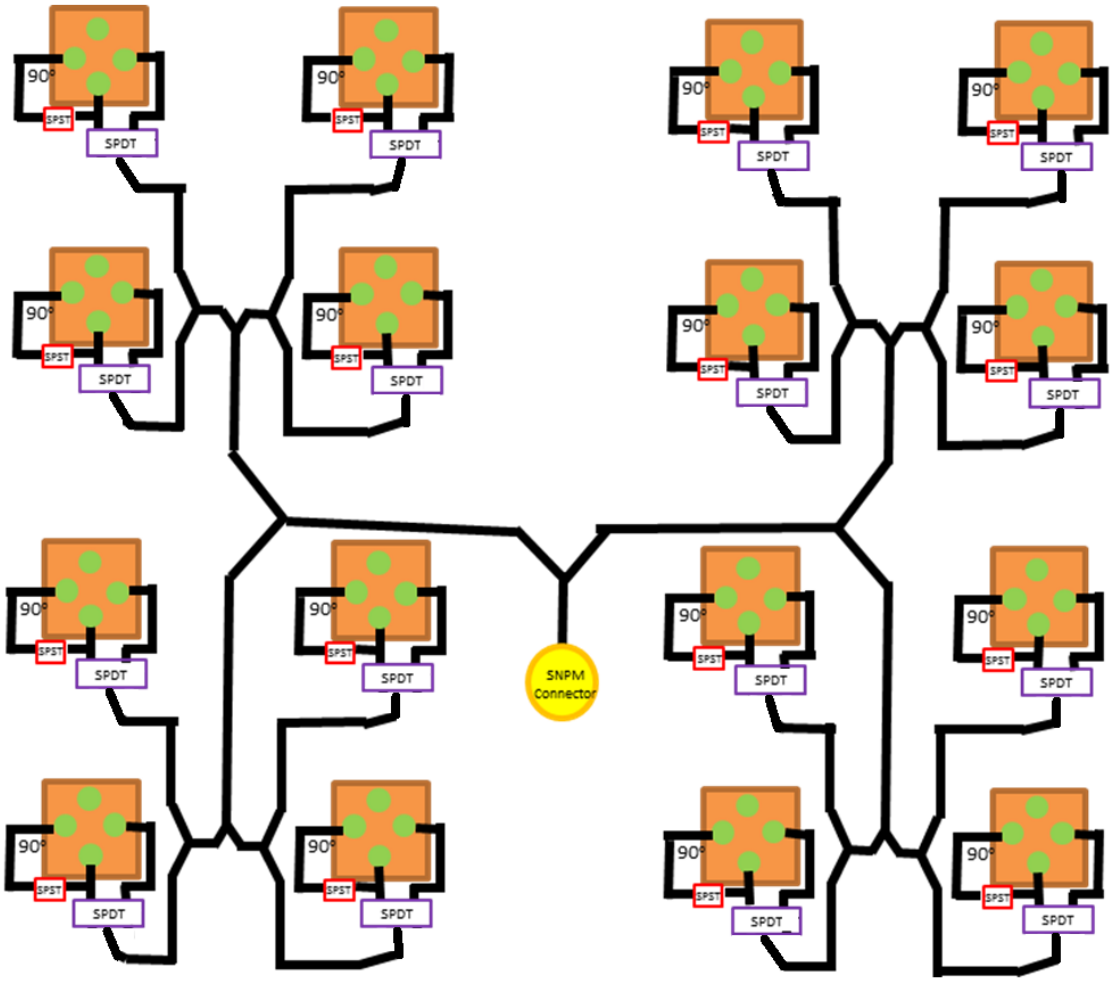

Figure 5.2: Initial System Diagram of POC3.

As seen in Figure 5.2, one method for achieving switchable polarization is connect switches to each patch element. This way power can travel to and from the right-side port of each patch through the right path of an SDPT to achieve horizontal linear

polarization. The left path of the SPDT can be used to achieve vertical linear polarization through the bottom port of the patch when the SPST switch is turned off. When the SPST is turned on, the power from the SDPT is split between the left-side and bottom ports of the patch to get left-hand circular polarization. For POC3, the design shown in Figure 5.2 is split into two separate designs. One design will switch between two circular polarizations and the other between two linear polarizations. This was done to verify both polarization types before combing them on a single PCB.

5.3 Design and Simulation

With the specifications set, the design process of a single square patch antenna can be initiated that will later be scaled up into an array. A comparison between loaded and unloaded patches with two inputs will be discussed. A method for reducing the size of a 90° hybrid coupler through capacitive loading will also be presented. A microstrip feeding network altered from the feeding network for POC1 will connect the packaged SPDTs to the SMPM connector. As mentioned previously, there are two variations of POC3. The design of a switchable circular and switchable linear polarization array will be presented.

5.3.1 Redesign of Single Patch Antenna

The resistive loading used to increase the bandwidth of a single patch in POC1 presented a problem when used on a patch with two input ports. With four total vias on the patch, the power leakage through opposite pins increased, which degraded both the gain and efficiency. Figure 5.3 shows a two-input patch with resistive loading used in POC2.

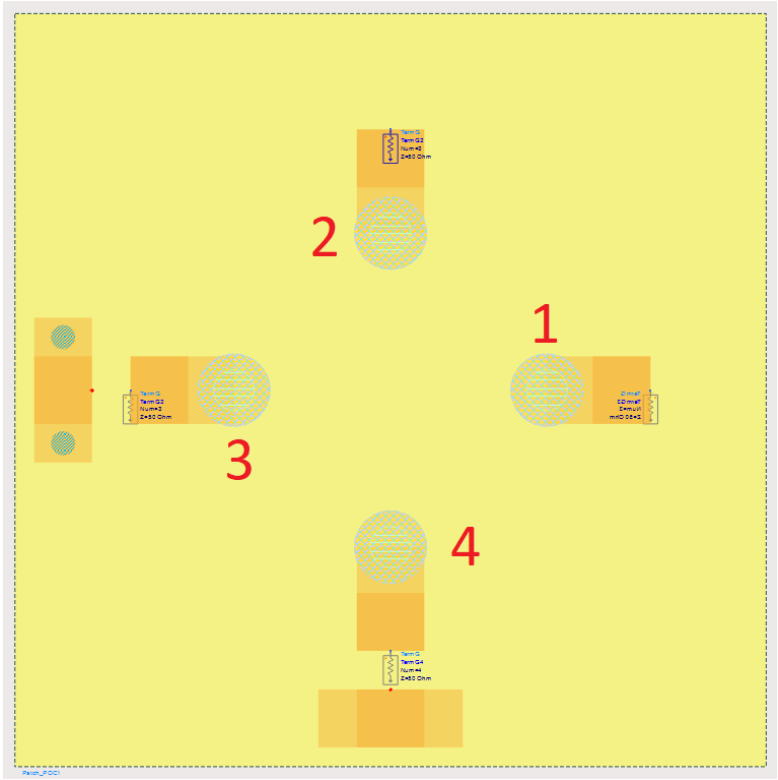

Figure 5.3: 4-Pin Square Patch Antenna with Load Resistors.

The return loss and isolation of each pin in the patch shown in Figure 5.3 are displayed in Figure 5.4.

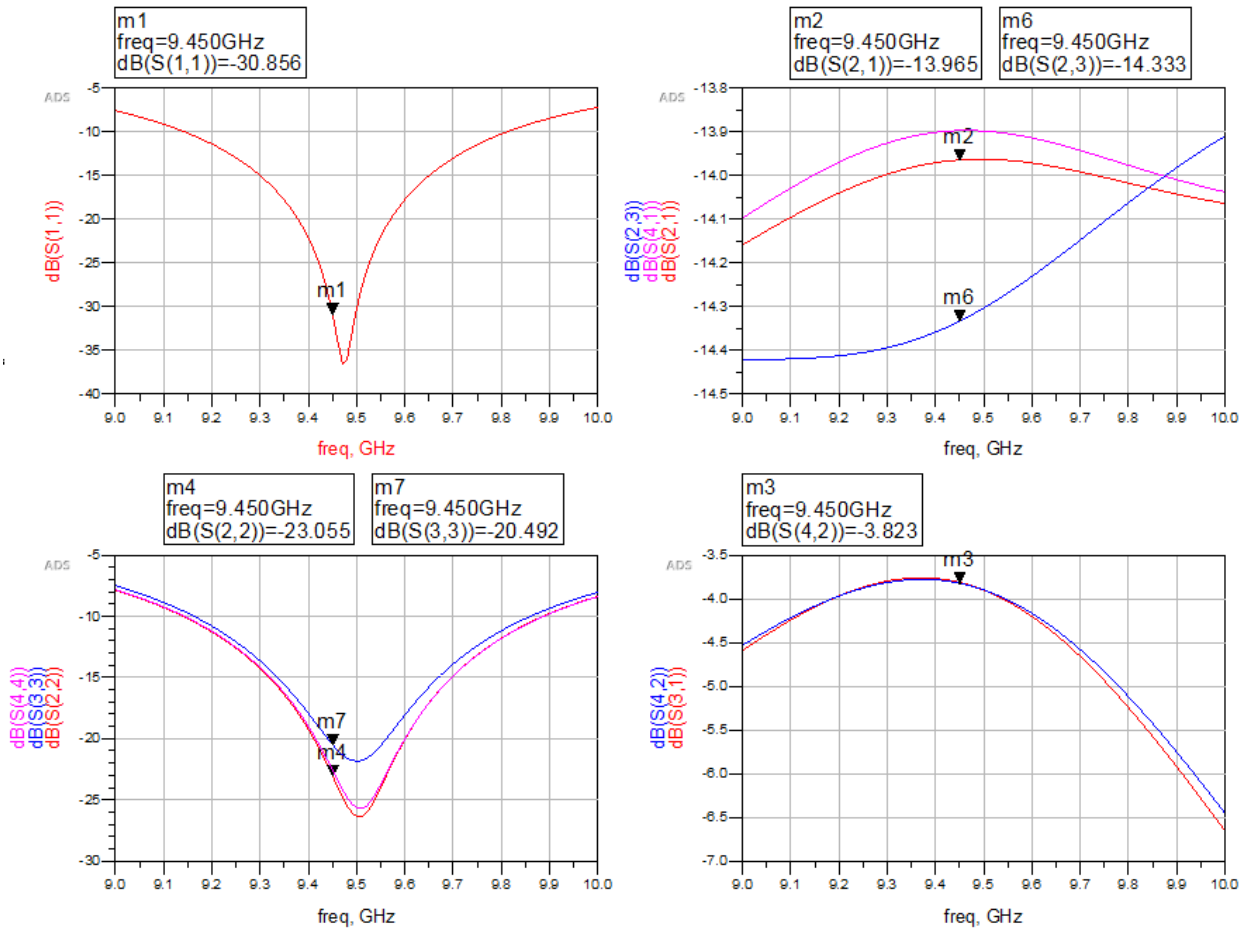

Figure 5.4: Return Loss and Isolation of 4-Pin Patch Antenna.

Figure 5.4 shows a good return loss on all four pins, and the isolation between adjacent pins such as pins 1 and 2 is also sound. However, the isolation between opposite pins, meaning pins 1-3, and pins 2-4 is terrible. This indicates that power is lost through these opposite pins, affecting the gain and efficiency of the two-input patch. The radiation pattern of the single patch at the center frequency of 9.45 GHz is displayed in Figure 5.5.

Frequency	E_max	Theta_max	Phi_max	Directivity_max	Gain_max	RadiatedPower	InputPower	Efficiency	CutType	CutAngle
9.450E9	0.348	179.000	0.000	6.643	2.071	4.386E-4	0.001	0.349	Phi	0.000

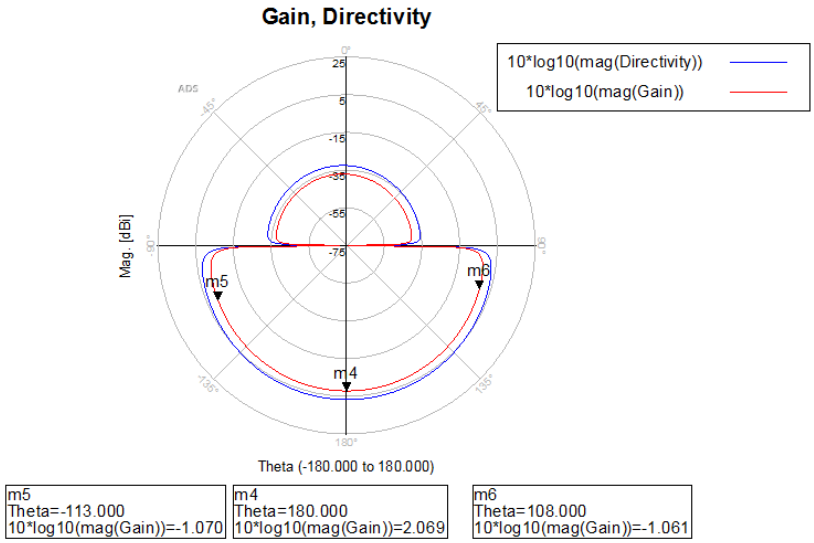

Figure 5.5: Gain and Efficiency of 4-Pin Patch Antenna.

As seen in Figure 5.5, the gain and efficiency have degraded to 2 dB and 35% due to the power leakage in the opposite pins. Because POC3 introduces packaged components that will all have additional losses, the single patch performance degradation cannot be tolerated. Figure 5.6 shows a two-port single patch antenna with the resistive loads removed.

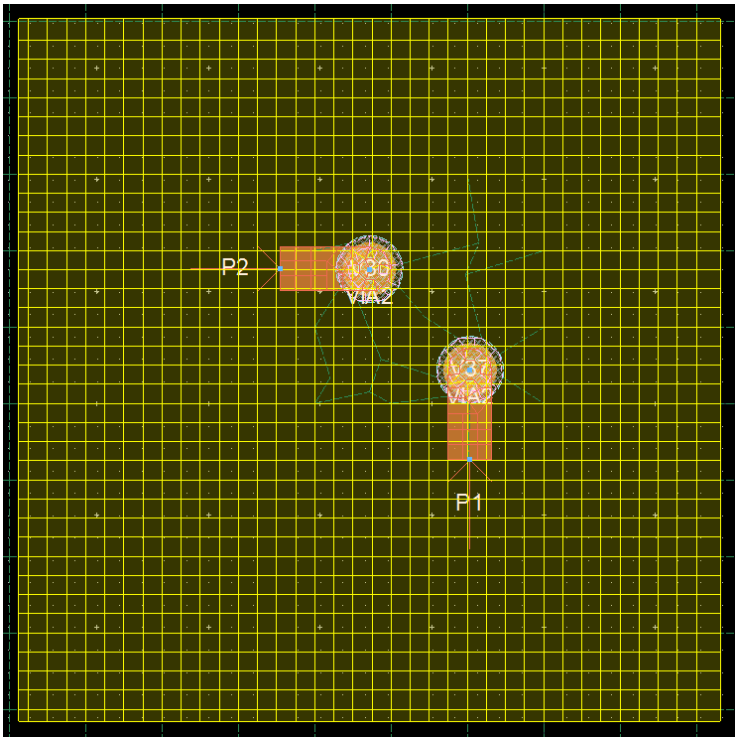

Figure 5.6: Single Two-Port Patch Antenna Unloaded.

The return loss and isolation of each pin in the patch shown in Figure 5.6 are displayed in Figure 5.7.

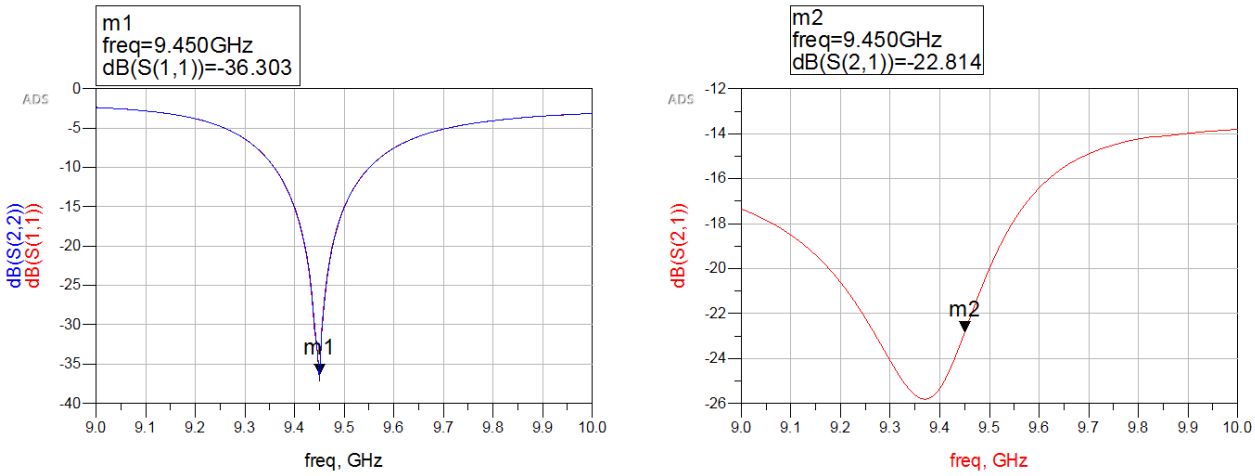

Figure 5.7: Return Loss and Isolation of Unloaded Two-Port Patch Antenna.

Figure 5.4 shows a good return loss on both input ports, and the isolation between them is also sound. This indicates that less power is lost through the pins on the patch, which should improve the gain and efficiency of the two-input patch. The radiation pattern of the single unloaded patch at the center frequency of 9.45 GHz is displayed in Figure 5.8.

Frequency	E_max	Theta_max	Phi_max	Directivity_max	Gain_max	RadiatedPower	InputPower	Efficiency	CutType	CutAngle
9.450E9	0.656	179.000	0.000	6.654	4.600	0.002	0.002	0.623	Phi	0.000

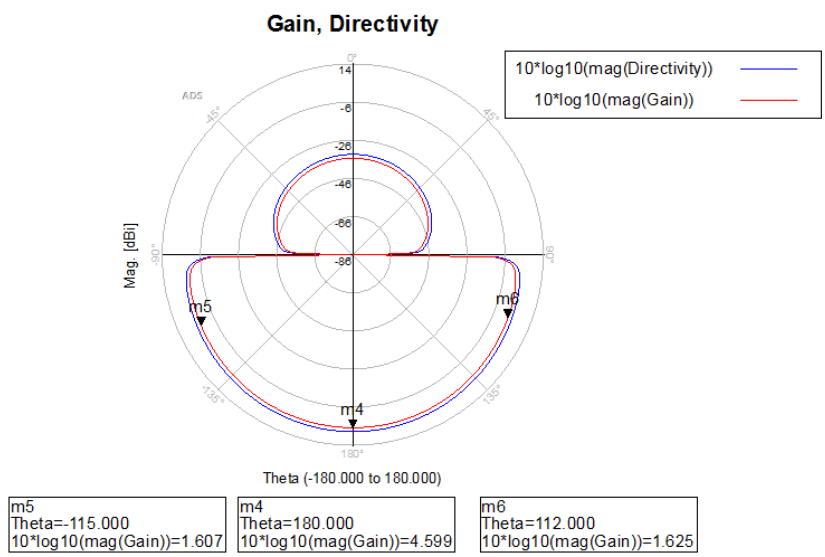

Figure 5.8: Gain and Efficiency of Two-Port Patch Antenna.

As seen in Figure 5.8, the gain and efficiency have improved to 4.6 dB and 62% due to the reduction in power leakage in the ports.

5.3.2 Miniaturized 90º Hybrid Coupler Design

To achieve either left- or right-hand circular polarization (LHCP or RHCP), half the signal power delivered to each patch antenna must be split between the two input ports with a 90º phase difference between the two. Power splitting can be done using a 90º

hybrid coupler, which comprises two sets of coupled ports with a 90° phase shift and high isolation between them. This will remedy a problem observed in POC2 where a trade-off had to be made between gain and phase imbalance. This method has the added benefit of using standard transmission lines and can be fabricated directly on the substrate instead of using another packaged IC.

Figure 2.10 in Section 2.5 shows that a 90° coupler requires two lines at $Z_o/\sqrt{2}$ while the rest are at Z_o. To match the coupler to the patch antenna and SPDT, Z_o must be 50Ω, and the two unique lines must be 35.35Ω. Following these guidelines, a coupler is made on the substrate and added to the patch antenna to evaluate the size limitations, as shown below in Figure 5.9.

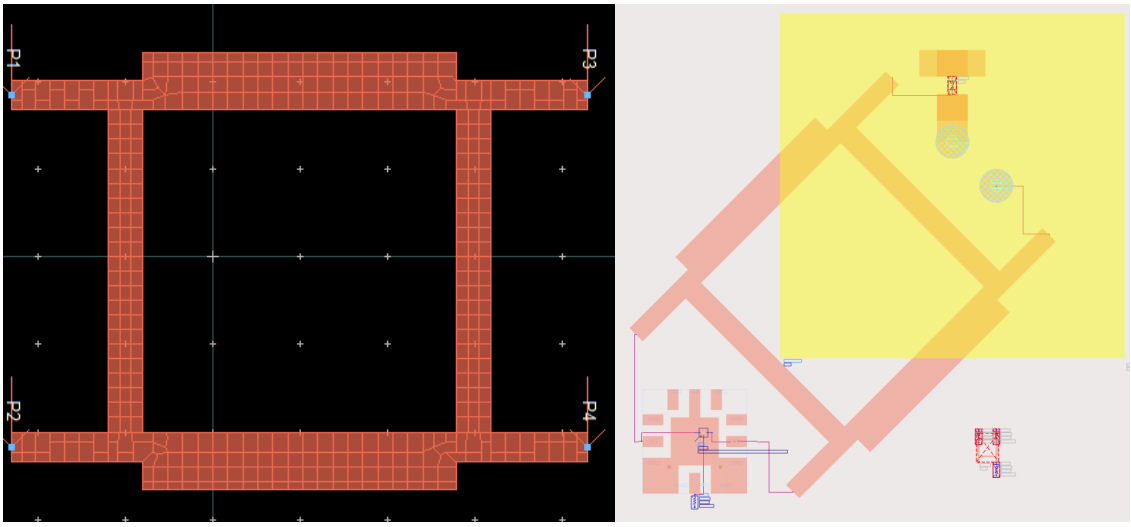

(a) (b)

Figure 5.9: (a) 90° Hybrid Coupler on AESA Substrate. (b) Coupler Size compared to Single Patch Antenna.

The parameters that must be optimized on the input are the return loss of each port, isolation between input and isolated ports, and the insertion loss from the input to

each output. The critical output parameters are the isolation, gain balance and phase difference between the output ports. The S-Parameters of the coupler shown in Figure 5.9a are displayed below in Figure 5.10.

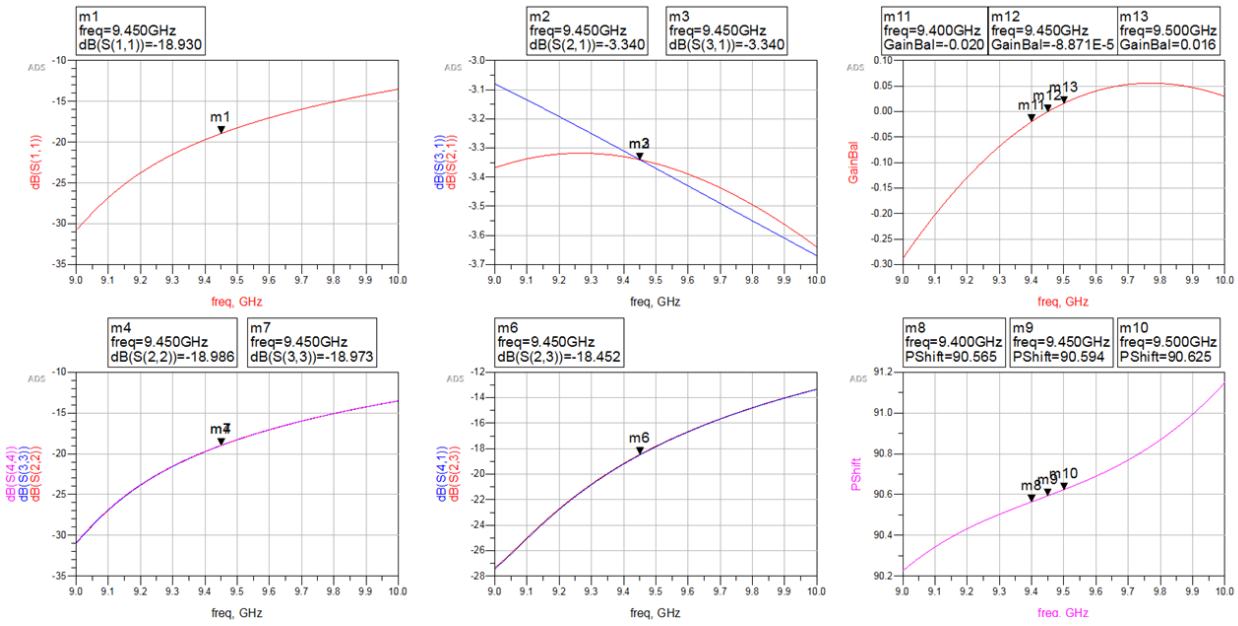

Figure 5.10: Performance of Substrate Coupler.

While Figure 5.10 shows the coupler performance, Figure 5.9b shows it is very big compared to a single patch antenna. If the coupler is to fit on the PCB alongside the feeding network and switches, it will need to be miniaturized. One way of reducing the coupler size is to replace each standard transmission line with lower ground coplanar waveguide (LG-CWP) transmission lines [36]. A comparison between these two types of transmission lines is shown below in Figure 5.11.

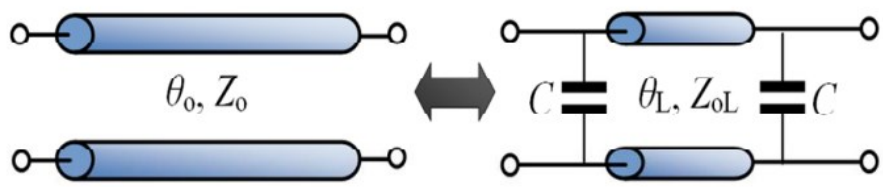

Figure 5.11: Standard vs. LG-CPW Transmission Lines [36].

Placing capacitive loads on either side of a standard transmission line reduces the signal's effective phase velocity, reducing the physical length while keeping the electrical length the same. This is one method for miniaturizing the transmission line. The capacitive loading will be implemented using open-circuit stubs instead of lumped components because stubs are tunable to any capacitance, unlike lumped components [36]. The reduced length θ_L, reduced line impedance Z_{oL}, and capacitive load C can be found by comparing the ABCD parameters of an unloaded and loaded line.

$$\begin{bmatrix} cos\beta\theta_o & jZ_o sin\beta\theta_o \\ jY_o sin\beta\theta_o & cos\beta\theta_o \end{bmatrix} = \begin{bmatrix} 1 & 0 \\ j\omega C & 1 \end{bmatrix} * \begin{bmatrix} cos\beta\theta_L & jZ_{oL} sin\beta\theta_L \\ jY_{oL} sin\beta\theta_L & cos\beta\theta_L \end{bmatrix} * \begin{bmatrix} 1 & 0 \\ j\omega C & 1 \end{bmatrix}$$

$$\begin{bmatrix} cos\beta\theta_o & jZ_o sin\beta\theta_o \\ jY_o sin\beta\theta_o & cos\beta\theta_o \end{bmatrix} = \begin{bmatrix} cos\beta\theta_L & jZ_{oL} sin\beta\theta_L \\ j\omega C cos\beta\theta_L + jY_{oL} sin\beta\theta_L & cos\beta\theta_L - \omega C Z_{oL} sin\beta\theta_L \end{bmatrix} * \begin{bmatrix} 1 & 0 \\ j\omega C & 1 \end{bmatrix}$$

$$\begin{bmatrix} cos\beta\theta_o & jZ_o sin\beta\theta_o \\ jY_o sin\beta\theta_o & cos\beta\theta_o \end{bmatrix} = \begin{bmatrix} cos\beta\theta_L - \omega C Z_{oL} sin\beta\theta_L & jZ_{oL} sin\beta\theta_L \\ j(2\omega C cos\beta\theta_L + Y_{oL} sin\beta\theta_L - \omega^2 C^2 Z_{oL} sin\beta\theta_L) & cos\beta\theta_L - \omega C Z_{oL} sin\beta\theta_L \end{bmatrix}$$

This matrix comparison can convert any standard transmission line into an LG-CPW line by inserting the unloaded length θ_o and desired reduced length θ_L. A standard 90° coupler uses quarter wavelength transmission lines which simplifies the equation. The reduced length will be set to an eighth of a wavelength or half the standard length to simplify the equation further.

$$\begin{bmatrix} 0 & jZ_o \\ jY_o & 0 \end{bmatrix} = \begin{bmatrix} \frac{1}{\sqrt{2}} - \frac{\omega C Z_{oL}}{\sqrt{2}} & \frac{jZ_{oL}}{\sqrt{2}} \\ j(\sqrt{2}\omega C + \frac{Y_{oL}}{\sqrt{2}} - \frac{\omega^2 C^2 Z_{oL}}{\sqrt{2}}) & \frac{1}{\sqrt{2}} - \frac{\omega C Z_{oL}}{\sqrt{2}} \end{bmatrix}$$

The reduced line impedance ZoL and capacitive load C can be found by comparing this matrix equation's A and B portions.

B: $$jZ_o = \frac{jZ_{oL}}{\sqrt{2}} \quad \rightarrow \quad Z_{oL} = \sqrt{2} * Z_o \qquad \textbf{(5.1)}$$

A: $$0 = \frac{1}{\sqrt{2}} - \frac{\omega C Z_{oL}}{\sqrt{2}} \quad \rightarrow \quad C = \frac{1}{\omega Z_{oL}} \qquad \textbf{(5.2)}$$

From Figure 5.9a, the standard coupler needs both 50Ω and 35.35Ω transmission lines, which can be altered to reduce their physical length using Equations 5.1 and 5.2.

50Ω: $$Z_{oL} = \sqrt{2} * 50 = 70.7\Omega$$

$$C = \frac{1}{70.7 * 2\pi * 9.45\ GHz} = 0.24pF$$

35.35Ω: $$Z_{oL} = \sqrt{2} * 35.35 = 50\Omega$$

$$C = \frac{1}{50 * 2\pi * 9.45\ GHz} = 0.34pF$$

Four reduced-size transmission lines are connected in a square pattern to make the center of the coupler with the capacitive loads of each line meeting at the four corners. Since two reduced lines of different impedance are connected at each corner, they must

share a capacitive load. A capacitance of 0.29pF was chosen, which is the midpoint between the load values obtained for the 50Ω and 70.7Ω lines. This value will approximately satisfy both lines at each corner, although some fine-tuning is needed during simulation. Instead of loading the coupler lines with straight stubs, mitered stubs of equivalent capacitance can shrink the structure further. Figure 5.12 shows the reduced size coupler compared to the standard coupler.

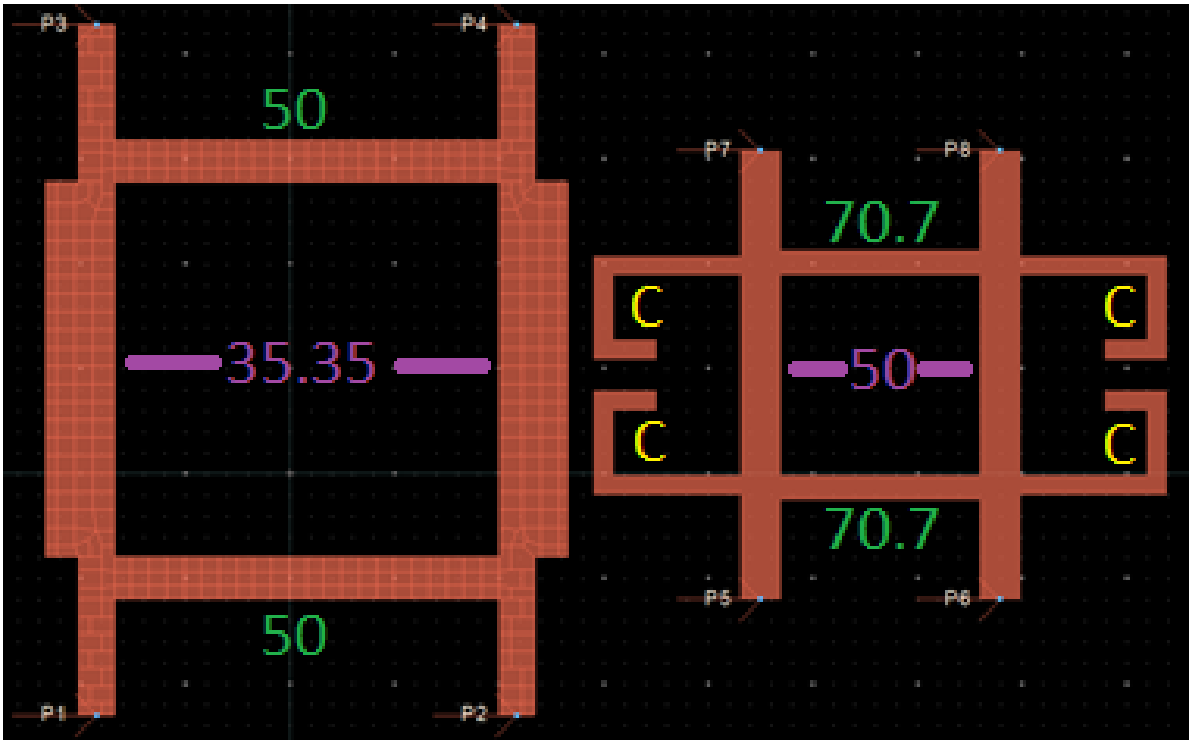

Figure 5.12: Comparison Between Standard and Reduced Size Couplers.

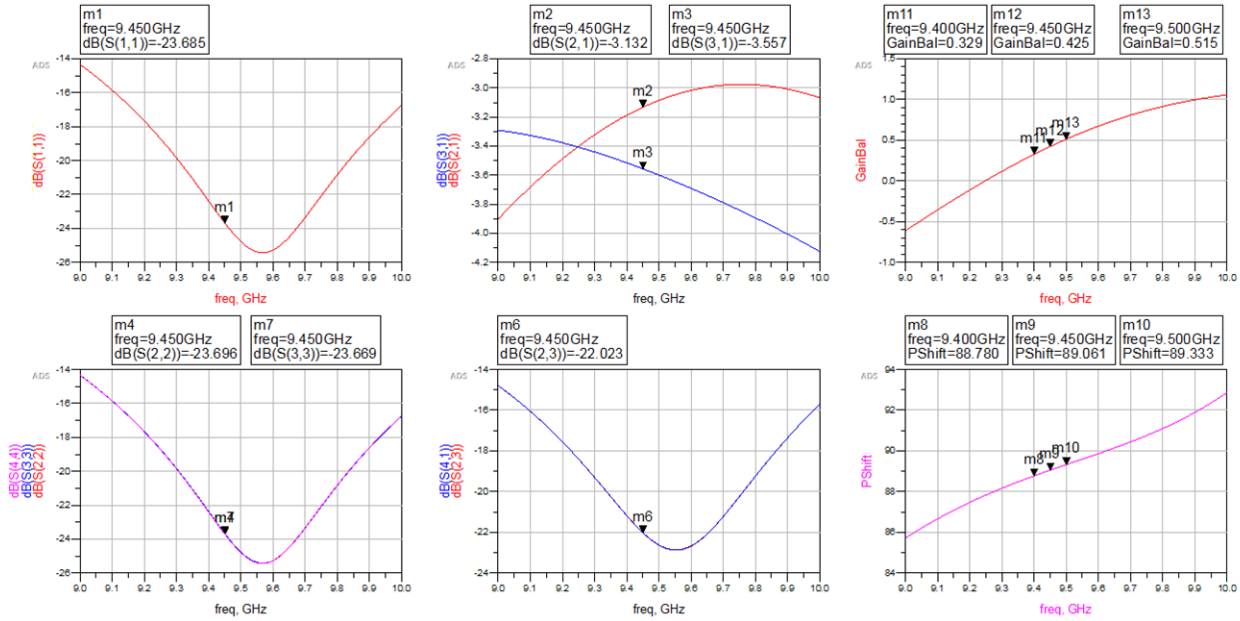

Figure 5.13: Performance of Reduced Size Coupler.

When comparing the performance of the two couplers as given in Figures 5.10 and 5.13, marked improvements of 4.7dB and 3.5dB were observed in the reduced size coupler's return loss and isolation performance. However, this improvement came at the expense of a marginal 0.4dB deterioration of the gain balance between the output ports. Overall, this method reduced the central area of the coupler to around 135x120 mils, a sound reduction from a conventional coupler of 230x215 mils [9].

5.3.3 Design of POC3 Feeding Network

Antenna elements will be connected using a 1 to 16 microstrip power divider. The feeding network was designed in the same fashion as POC1, as seen in Section 3.3.3. The feeding network comprises multiple quarter-wave transformers (QWT) arranged in a branching pattern that will split the input power in half multiple times depending on the number of elements in the array. The significant difference included in POC3 is that each

of the outermost feeding lines connected to the patches in POC1 have been cut short to make room for the coupler and switches. The 16-element power divider with the landing pad for the selected SMPM connector is seen in Figure 5.14.

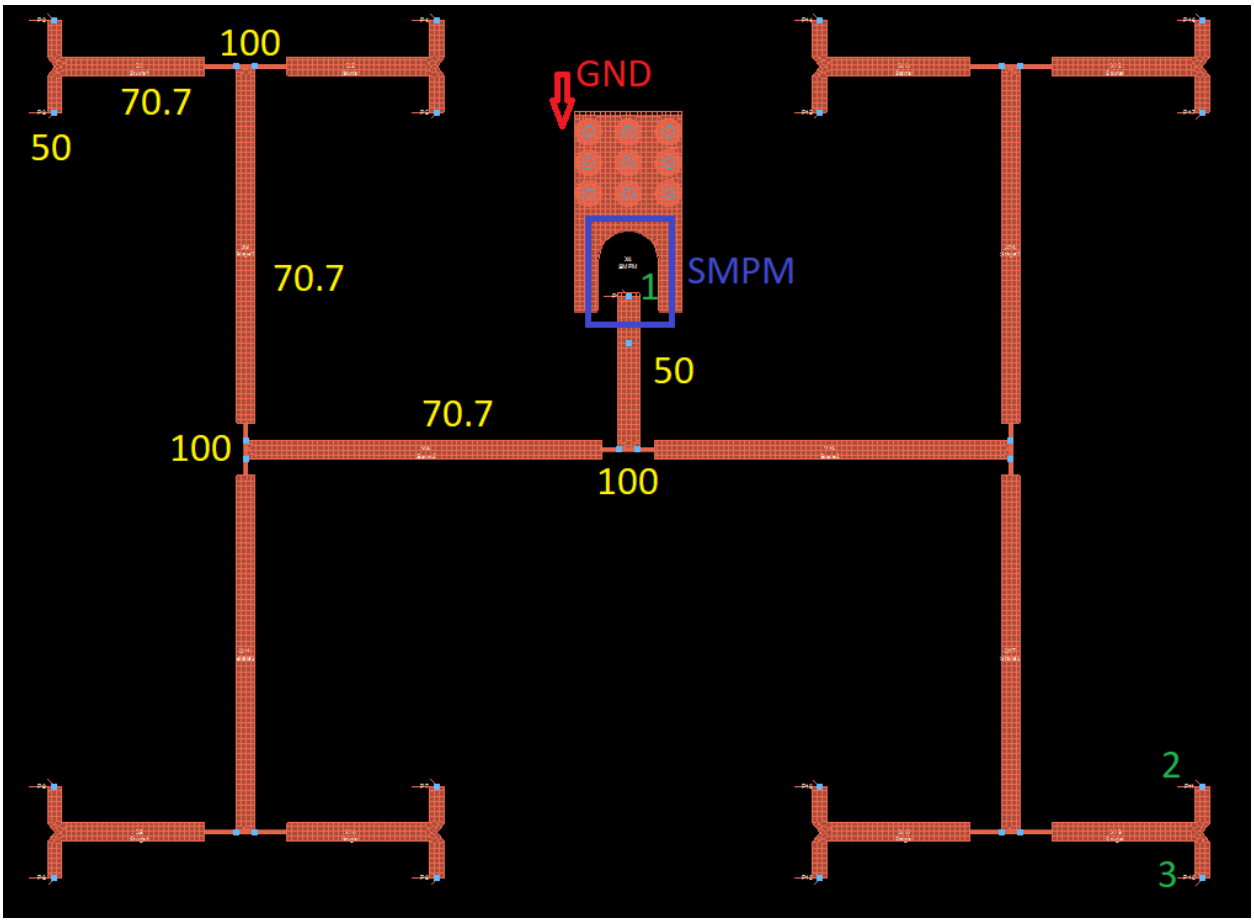

Figure 5.14: POC3 Microstrip Feeding Network.

The parameters that must be optimized on the input are the return loss of each port, isolation between adjacent ports, and the insertion loss from the input to each output. The ports where S-Parameter data was measured are labelled green in Figure 5.14; all other ports are loaded with 50Ω. The S-Parameters of the POC3 feeding network are shown in Figure 5.15.

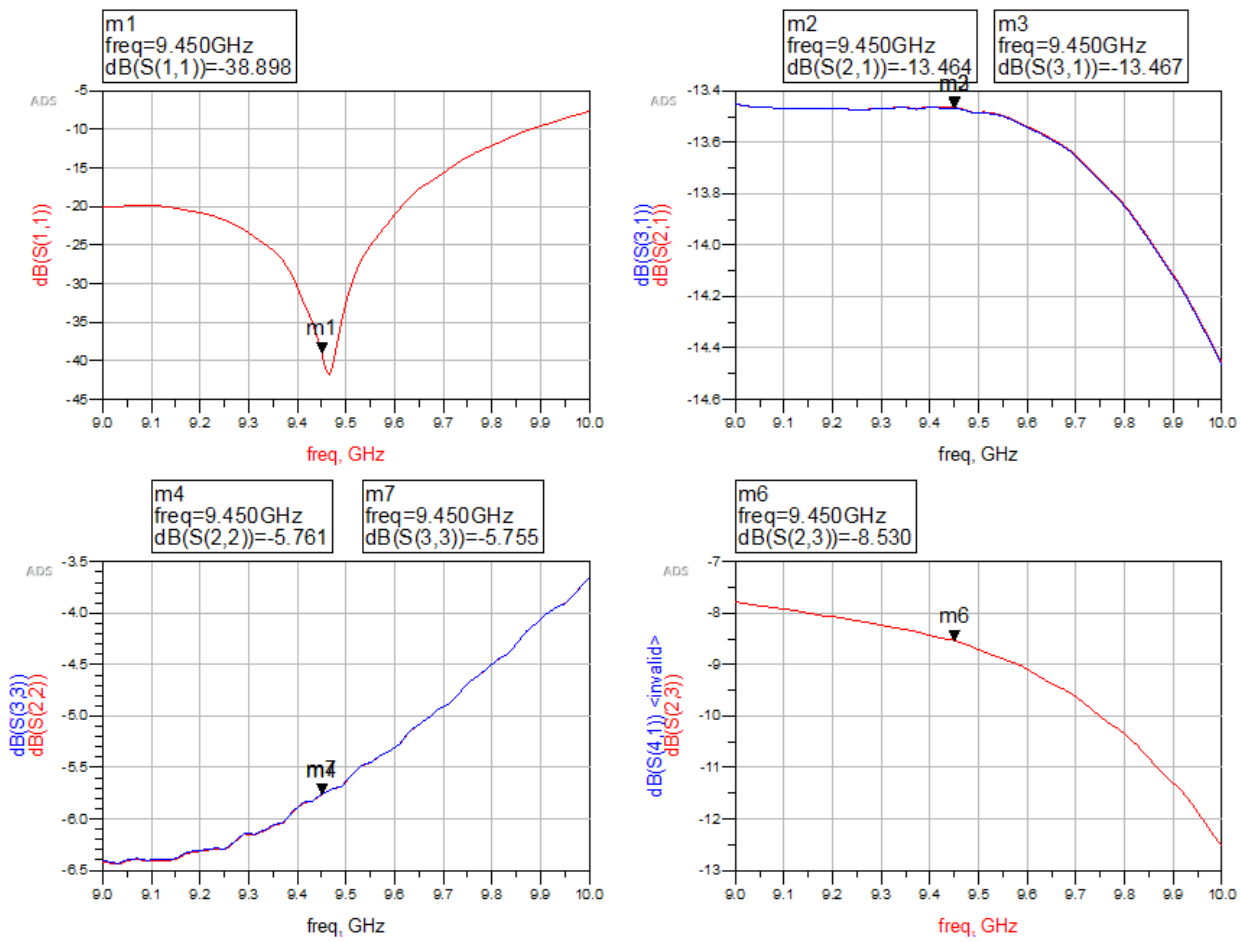

Figure 5.15: Performance of POC3 Feeding Network.

As seen in Figure 5.15, the return loss at the input port is excellent and has a wide bandwidth, making it easy to match the patch antennas. It should be noted that the power splitting in half between two branches is equivalent to a -3 dB drop, and since the input power splits four times, a drop of -12 dB is expected. While Figure 5.15 shows the S21 and S31 to be around -13.5 dB each, the feeding network insertion loss is around -0.5 dB, much lower than the 2 dB allocated in the system specifications. The isolation between adjacent output ports is very close to the -10 dB threshold, so it is acceptable enough to move on. The return loss on the output ports is too high above the -10 dB threshold,

which means the outer tips of the feeding network are not correctly matched to 50Ω. The input pin of the patch antenna must be adjusted when assembling and optimizing the full array since the feeding network cannot be adjusted at the outputs without interfering with patch spacing and isolation.

5.3.4 Simulation of Full POC3 Circular Array

Now that the patch antenna, coupler and feeding network have been designed and verified, the only component needed to assemble the full 4x4 patch antenna array is an SPDT. A PE42520C-Z switch was chosen for its good S-parameter performance between 9 and 10 GHz [37]. However, the S-parameter performance was given in the datasheet for the switch under ideal conditions. To get a better idea of how the switch would perform when integrated on the selected substrate, a footprint was made with metal traces and via grounds, as seen in Figure 5.16.

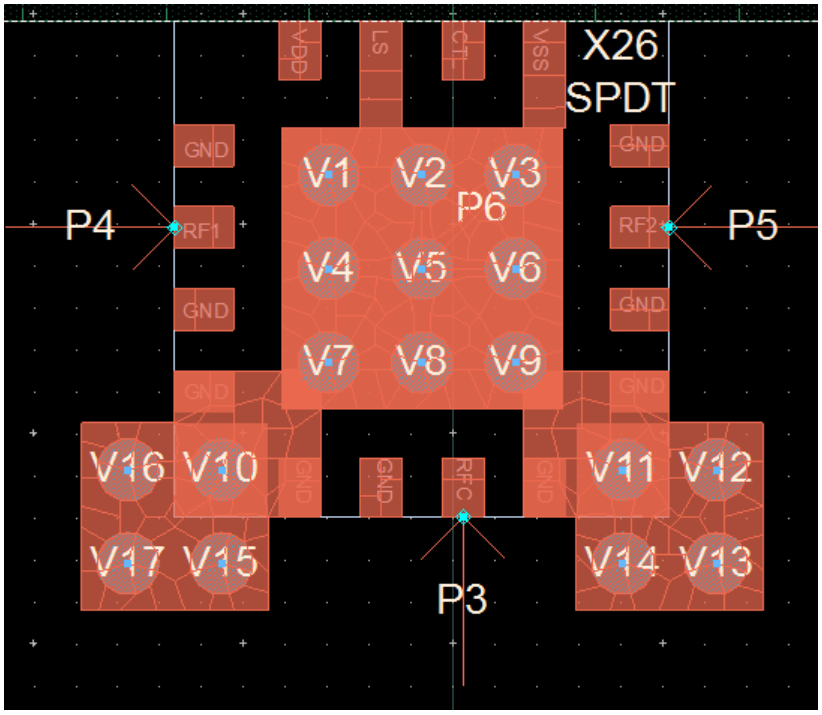

Figure 5.16: SPDT Footprint with Via Grounds.

Figure 5.17 shows the S-parameters of the switch when integrated with the footprint and via grounds.

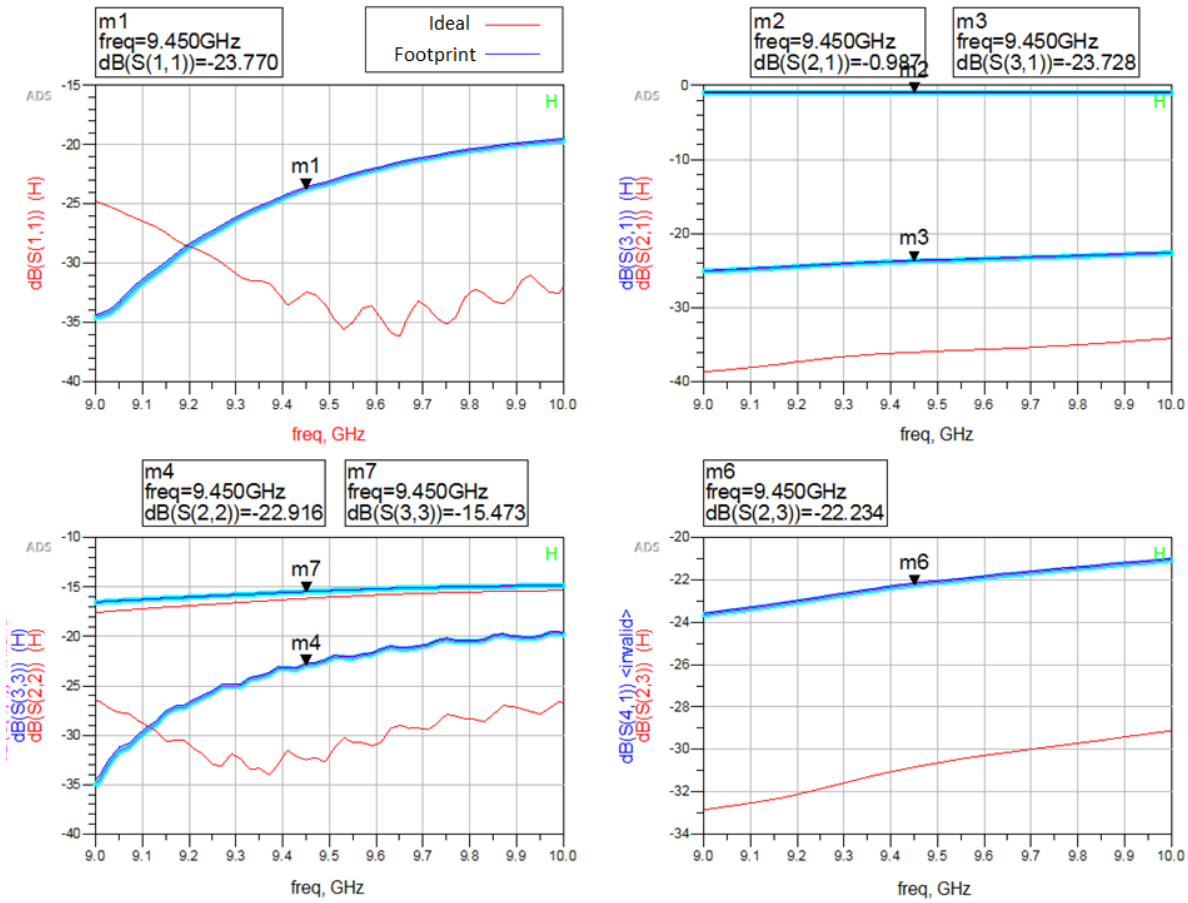

Figure 5.17: SDPT S-Parameters on Physical Footprint.

As seen in Figure 5.17, the S-parameters of the SPDT on the footprint are not as good as the ideal but are still good. The return loss on all three ports and the isolation between output ports are well below -10 dB. The insertion loss is around -1 dB for the open path and -24 for the closed path. The SPDT also requires DC signals for both its power and switching voltage. According to the datasheet, the VDD of the switch is 3.3 V, and the switching voltage is 3.3 V for the RF1 path and 0 V for the RF2 path of the

switch. A pair of 22 pF decoupling capacitors are also needed on each DC line. The DC signals will be provided to the switches via the power plane added to the substrate stackup for POC3, as seen in Figure 5.1.

Figure 5.18 shows the full switchable 4x4 circular antenna array after the patches, coupler, switches and feeding network are matched together.

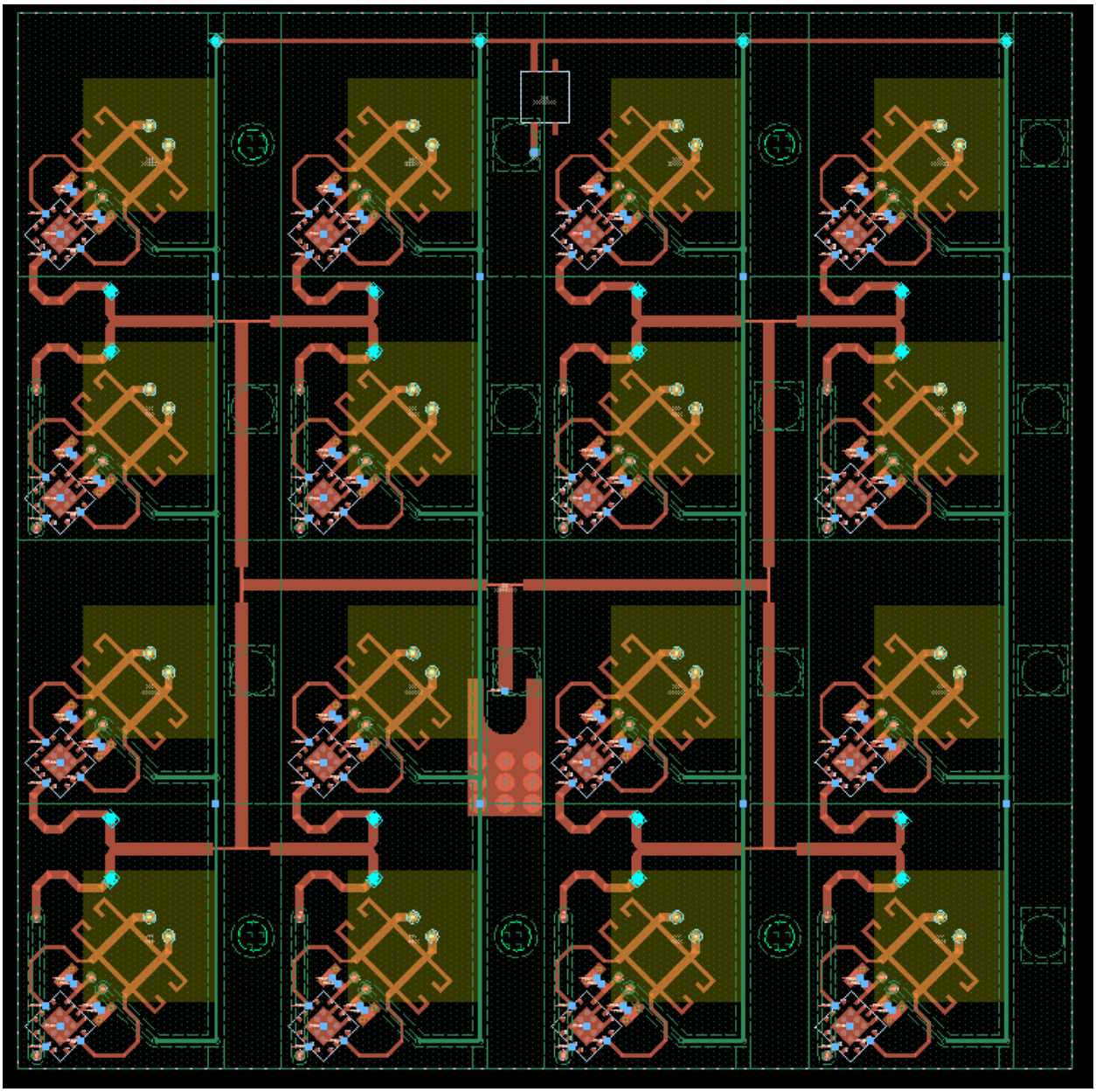

Figure 5.18: Full POC3 Circular Antenna Array (2D View).

In addition to the 2D view shown in Figure 5.18, a 3D top and bottom view of POC3 is shown in Figure 5.19.

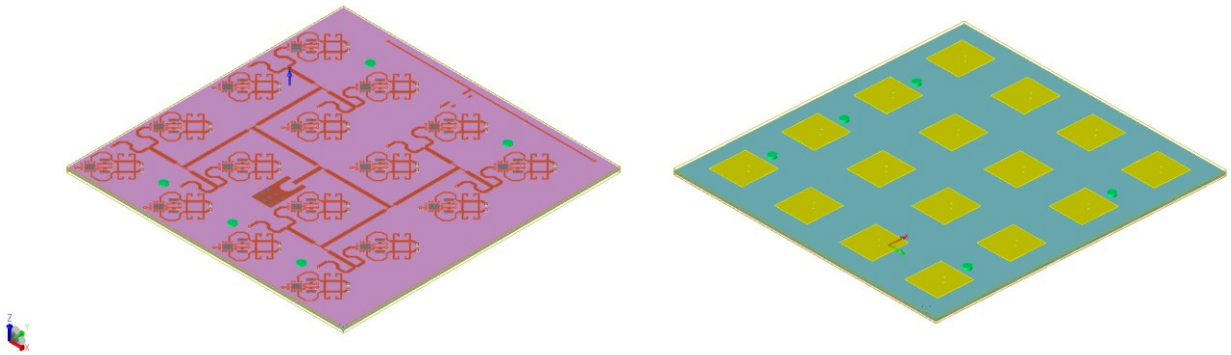

Figure 5.19: Full POC3 Circular Antenna Array (3D View).

Figure 5.20 shows the return loss of the full POC3 antenna array for both paths of the SPDT.

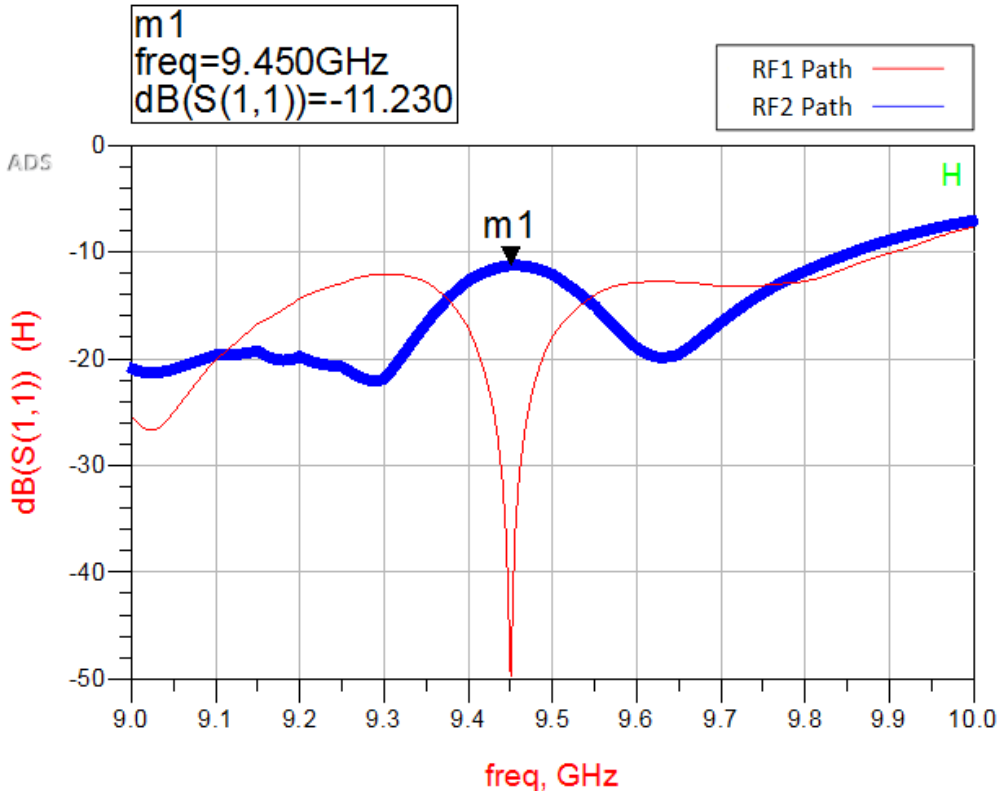

Figure 5.20: Simulated Return Loss of Full POC3 Circular Array.

Figure 5.20 indicates a good return loss across the desired band from 9.4 to 9.5 GHz for both paths of the SPDT. Figure 5.21 shows the radiation pattern of the full POC3 circular array for the RF1 path of the SPDT.

Frequency	E_max	Theta_max	Phi_max	Directivity_max	Gain_max	RadiatedPower	InputPower	Efficiency	CutType	CutAngle
9.450E9	8.333	0.000	180.000	17.178	15.072	0.022	0.036	0.616	Phi	90.000

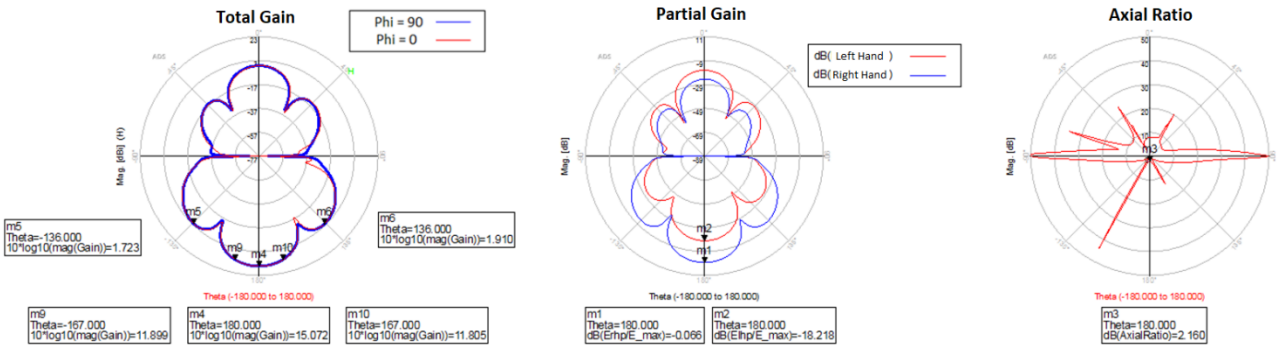

Figure 5.21: Simulated Gain and Efficiency of Full POC3 Array (RF1 Path).

Figure 5.21 shows that the peak gain of both the 0º and 90º cuts is 15 dB and the efficiency is 61.6 %, which both meet the minimum values of 11 dB and 60%. Figure 5.21 also shows that the partial gain in the left and right-hand planes indicate the RF1 path of POC3 is RHCP as desired. The HPBW is around 26º, which is close to the desired 30º. The axial ratio is 2.2 dB, which is below the 3 dB specification. Figure 5.22 shows the radiation pattern of the full POC3 circular array for the RF2 path of the SPDT.

Frequency	E_max	Theta_max	Phi_max	Directivity_max	Gain_max	RadiatedPower	InputPower	Efficiency	CutType	CutAngle
9.450E9	8.343	0.000	267.000	17.181	15.090	0.022	0.036	0.618	Phi	90.000

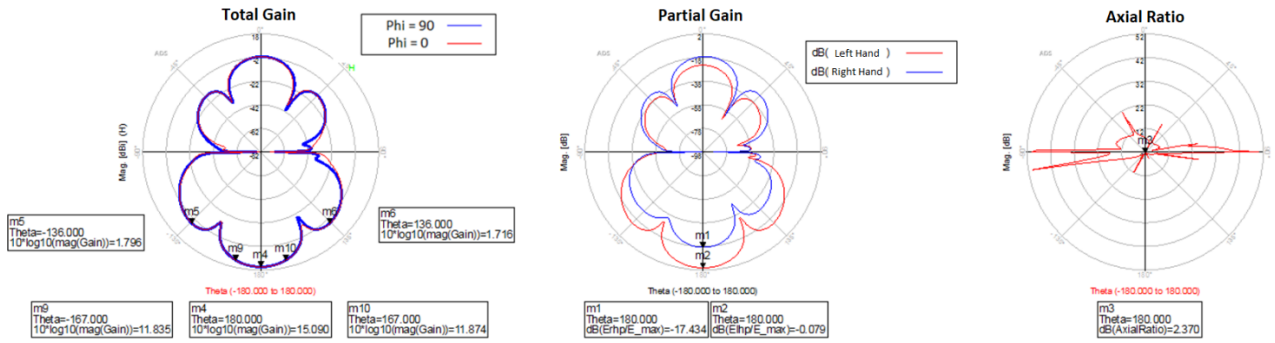

Figure 5.22: Simulated Gain and Efficiency of Full POC3 Array (RF2 Path).

Figure 5.22 shows that the peak gain of both the 0° and 90° cuts is 15 dB and the efficiency is 61.8 %, which both meet the minimum values of 11 dB and 60%. Figure 5.22 also shows that the partial gain in the left and right-hand planes indicate the RF2 path of POC3 is LHCP as desired. The HPBW is around 26°, which is close to the desired 30°. The axial ratio is 2.4 dB, which is below the 3 dB specification. The simulated values shown in Figures 5.21 and 5.22 indicate that the circular switchable array of POC3 meets the required system specifications and is ready for fabrication and testing.

5.3.5 Simulation of Full POC3 Linear Array

Like the switchable circular array design shown in Section 5.3.5, another version of POC3 was made but with switchable linear polarization. The process is the same as the previous, but the hybrid coupler is excluded and the SPDT is connected directly to the patch antennas. The feeding network was also made smaller, but the design and performance are similar to the 4x4 feeding network. Due to COVID-19 and the increase

in the cost of materials, the linear switchable antenna was made using a 2x2 element array to reduce the cost of manufacturing.

Figure 5.23 shows the full switchable 2x2 linear antenna array after the patches, switches, and feeding networks are matched.

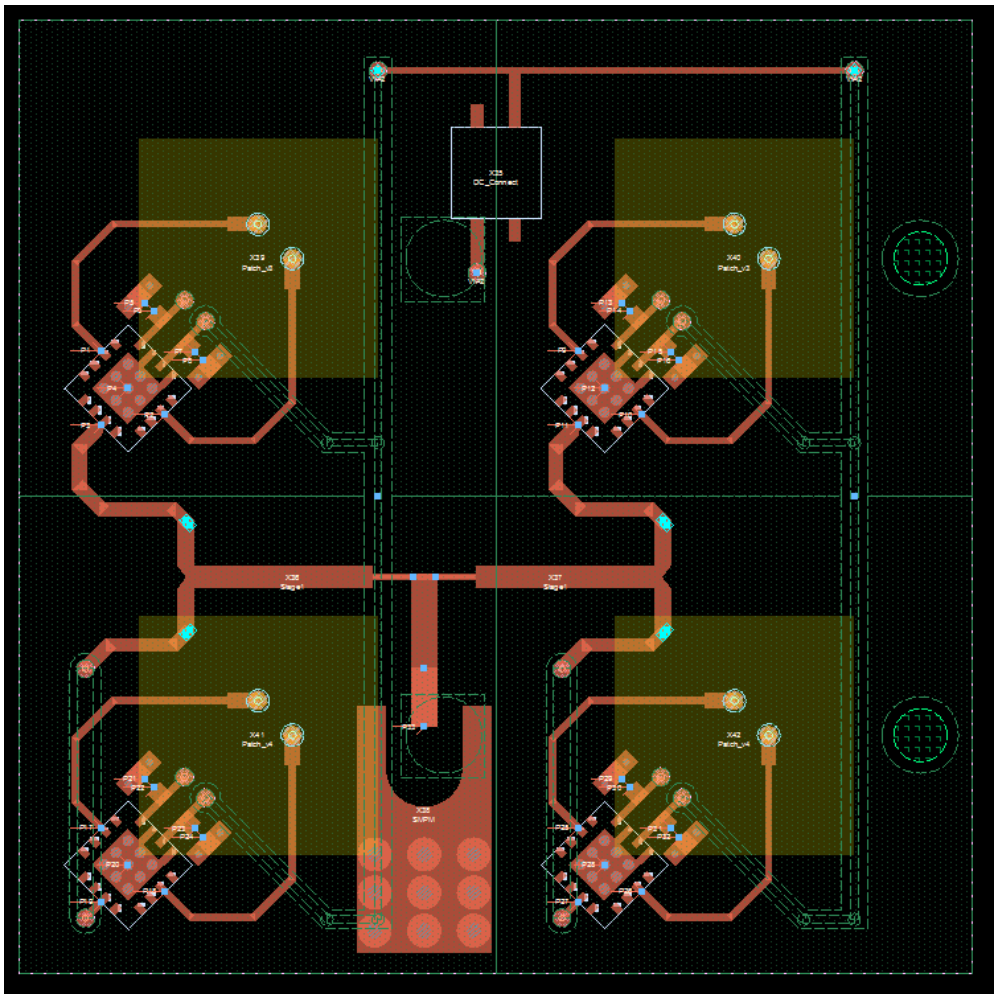

Figure 5.23: Full POC3 Linear Antenna Array (2D View).

In addition to the 2D view shown in Figure 5.23, a 3D top and bottom view of the linear POC3 is shown in Figure 5.24.

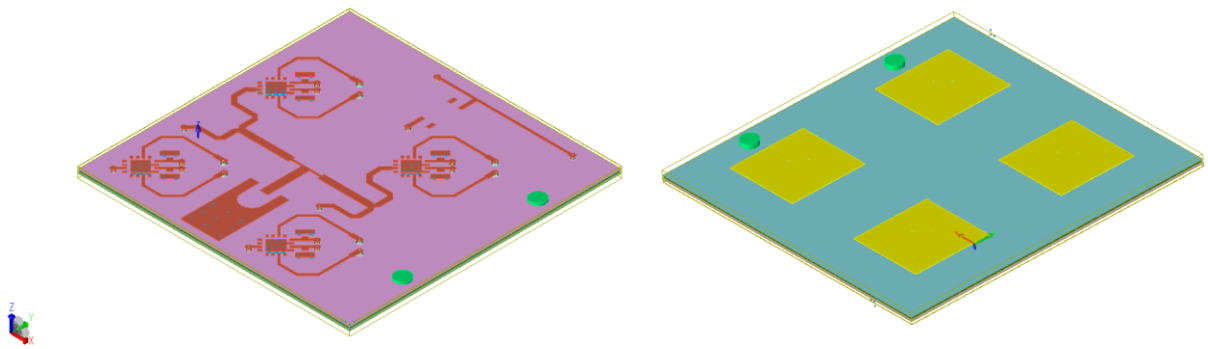

Figure 5.24: Full POC3 Linear Antenna Array (3D View)

Figure 5.25 shows the return loss of the full linear POC3 antenna array for both paths of the SPDT.

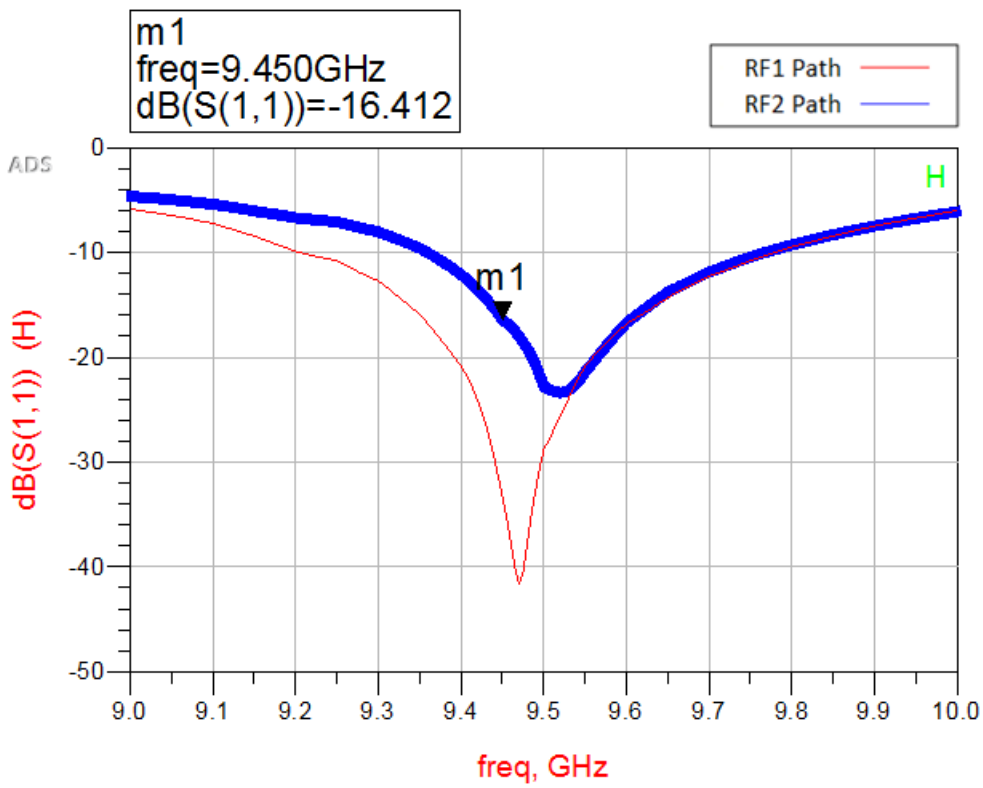

Figure 5.25: Simulated Return Loss of Full POC3 Linear Array.

Figure 5.25 indicates a good return loss across the desired band from 9.4 to 9.5 GHz for both paths of the SPDT. While the RF1 path has better matching and broader bandwidth, the RF2 path is still within the specifications across the target band. Figure 5.26 shows the radiation pattern of the full POC3 linear array for the RF1 path of the SPDT.

Frequency	E_max	Theta_max	Phi_max	Directivity_max	Gain_max	RadiatedPower	InputPower	Efficiency	CutType	CutAngle
9.450E9	2.368	0.000	281.000	11.492	9.904	0.007	0.010	0.694	Phi	0.000

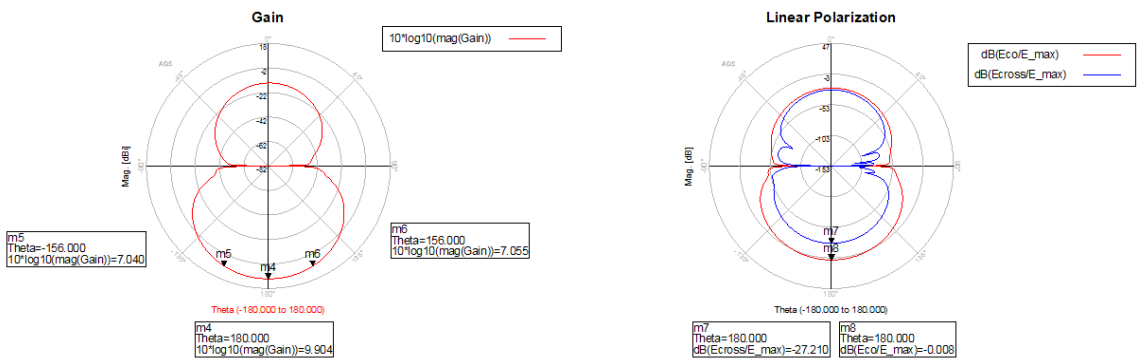

Figure 5.26: Simulated Gain and Efficiency of Full POC3 Linear Array (RF1 Path).

Figure 5.26 shows that the peak gain is around 9.9 dB and the efficiency is 69.4 %. Figure 5.26 also shows a good distinction between the co-pol and cross-pol elements, indicating good linear polarization. The HPBW is around 48°, which is much higher than the desired 30°. Also, Figure 5.26 does not show any sidelobes, which may result from fewer elements in the array, causing the main and sidelobes to appear as one prominent lobe in the simulator. This phenomenon will need to be examined when the linear array is measured.

Figure 5.27 shows the radiation pattern of the full POC3 linear array for the RF2 path of the SPDT.

Frequency	E_max	Theta_max	Phi_max	Directivity_max	Gain_max	RadiatedPower	InputPower	Efficiency	CutType	CutAngle
9.450E9	2.367	179.000	5.000	11.494	9.890	0.007	0.010	0.691	Phi	0.000

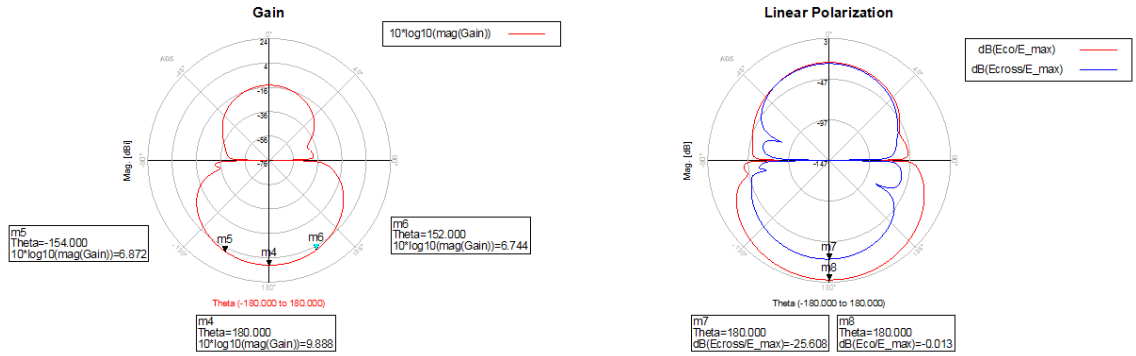

Figure 5.27: Simulated Gain and Efficiency of Full POC3 Linear Array (RF2 Path).

Figure 5.27 shows that the peak gain is around 9.9 dB and the efficiency is 69 %. Figure 5.27 also shows a good distinction between the co-pol and cross-pol elements, indicating good linear polarization. The HPBW is around 54^{o,} which is much higher than the desired 30°. Like with the RF1 path, this is likely because the main lobe and side lobes have combined in the simulator, but this will have to be verified in measurement.

5.4 Measurement of POC3

Due to global supply chain difficulties and related production delays, the fabricated POC3 antenna arrays were not measurement ready at the time of writing. Once received, the plan is to test them using the same method as POC1 and POC2 outlined in Section 2.6. The results can then be compared to the simulations, and any discrepancies will need to be investigated. Once this is done, the measurement results can be published later.

5.5 Conclusion

Two different switchable polarization patch antenna arrays, one linear and one circular, were designed and simulated using the specifications derived in the system analysis in Chapter 3.

The arrays were designed on a multilayer Rogers Duroid substrate with the antenna array and feeding network on opposite sides of the same package. Switchable polarization was achieved by integrating a commercial SPDT and 90° hybrid coupler onto the antenna PCB. A method for miniaturizing the hybrid coupler by capacitive loading was also successful. This method resulted in a compact hybrid coupler with a central area of 135x120 mils, down from a conventional coupler area of 230x215 mils in reference [9]. This integration effort resulted in the 4x4 switchable circular array fitting on a low-profile 2.5x2.5 inch PCB and the 2x2 switchable linear array on a 1.25x1.25 inch PCB.

Several next steps can be taken to improve this design, like adding more packaged components such as a beamformer to the array and developing a custom switching network to achieve more polarization states on a single board. These potential improvements will be discussed in Chapter 6.

Chapter 6: Conclusion

6.1 Summary

The research presented in this thesis was conducted with the desire to provide Canada with new technologies to be used for both commercial and military purposes. This would be useful for many applications such as surveillance of Canada's arctic borders and support for nuclear and mining industries. This goal was to be achieved by developing a switchable polarization 4x4 AESA array integrated with packaged components on a low-profile PCB by utilizing both sides of the board. This was accomplished in stages, starting with developing a simple 4x4 linearly polarized array (POC1) on a multilayer Rogers Duroid PCB. The next stage was to repeat the process for a simple 4x4 circular polarized array (POC2) on the same PCB stackup. After that, two different switchable polarization arrays (POC3) were designed, one linear and one circular using packaged components integrated on the PCB.

A system-level analysis was performed using commercial parts that could potentially be used at some design stage. This system analysis was used to determine the specifications for each design stage in this thesis.

POC1 used these specifications to design, simulate, fabricate and measure a 4x4 linearly polarized patch antenna array. POC1 was designed on a multilayer Rogers Duroid substrate with the antenna array and feeding network on opposite sides of the same package. A method for increasing the bandwidth by loading each patch element with series resistors was also successful. The measured results of the fabricated antenna array met all the required specifications.

POC2 was similar to POC1, with the critical difference being the development of a 4x4 circularly polarized patch antenna array on the same multilayer PCB. The measured results of the fabricated antenna array met most of the required specifications. Some problems like power leakage between multiple pins in the single patch and a need for a feeding mechanism with better performance in terms of gain and phase imbalance were discovered. These potential problems were addressed in the following design stage.

POC3 saw the design of two switchable polarization arrays, one linear and one circular. Due to manufacturer limitations, the PCB stackup had to be slightly altered. The patch arrays and feeding networks from POC1 and POC2 were slightly altered to include an SPDT and hybrid coupler to achieve polarization switching. A method for miniaturizing a hybrid coupler through capacitive loading was also presented.

6.2 Thesis Contributions

The following achievements were made as a result of the research outlined in this thesis:

- System-level analysis of full RF chain for proposed switchable polarization AESA array to derive the specifications of each sub-component.
- Design of a custom 3D antenna holder that allows for testing of multilayer PCB antenna arrays that utilize both sides of the board.
- Design and simulation of two different switchable polarization AESA arrays integrated with packaged components on a multilayer PCB. Once realized, this polarization diversity can be used to improve standard AESA systems with greater detection and tracking capabilities.

- Design and simulation of a miniaturized 90º hybrid coupler through capacitive loading. This can significantly improve other RF designs since this process allows for couplers and other transmission-line based components to be miniaturized and better integrated with other packaged components.
- Some of the work done for POC1 and POC2 contributed to designing a new dual-differential feeding mechanism for patch antennas. This feeding method allows for six different polarization states from the same patch antenna. This design can also switch radiation patterns from a single main beam to a four-lobe multi-beam setup. These contributions were part of two publications [38] and [39].

6.3 Future Work and Recommendations

The research done for this thesis shows promise; however, some improvements such as the following can be made.

- Firstly, the fabricated POC3 antenna arrays will need to be measured and verified. After that, any discrepancies between simulated and measured values will need to be explored.
- Another stage called POC4 would integrate even more RF circuits such as beamformers onto the antenna array PCBs already designed. This would provide the switchable polarization arrays with beam steering capabilities through phase shifters.

- POC3 and the proposed POC4 would be done initially using multiple commercial parts that would later be replaced by a single custom circuit capable of performing all the needed functions in one package.
- Designs can be used for low or high-power applications depending on the power limitations of the circuitry involved. Higher power arrays will need high-power circuit processes like gallium nitride (GaN).
- Use of dual differential feeding mechanism to allow more polarization states and radiation patterns on a single board. This new setup could also open the door for adaptive polarization detection on the differential feeding lines. This will require the design of a custom switching network that can be made compact and integrated onto the antenna PCB [38] [39].
- Improve the performance of the antenna array PCB by incorporating metamaterials such as split-ring resonators or electromagnetic bandgaps. These metamaterials could be used to reduce sidelobes and mutual coupling between array elements [39].

References

[1] R. Patterson et al." Elec. Comp. for Use in Extreme Temp. Aerospace Apps," 12th CMSE , Feb. 2008.

[2] M. Wijesundara, "Silicon Carbide Microsystems for Harsh Env.," ISBN: 978-1-4419-7120-3, 2011.

[3] Y. Mancuso, "Components and Technologies for T/R Modules," IEEE Aerospace and Electronics Systems, Vol. 25, No. 10, pp. 39-43, Oct. 2010.

[4] J. F. Valenzuela-valdes, M. A. Garcia-fernandez, A. M. Martinezgonzalez and D. Sanchez-Hernandez, "The Role of Polarization Diversity for MIMO Systems Under Rayleigh-Fading Environments," IEEE Antennas Wirel Propag. Lett., vol. 5, pp. 534-536, 2006

[5] Liang Dong, Hosung Choo, R. W. Heath and Hao Ling, "Simulation of MIMO channel capacity with antenna polarization diversity," IEEE Trans. Wireless Commun.s, vol. 4, no. 4, pp. 1869-1873, July 2005

[6] W. Lin, H. Wong and R. W. Ziolkowski, "Circularly Polarized Antenna With Reconfigurable Broadside and Conical Beams Facilitated by a Mode Switchable Feed Network," IEEE Trans. Antennas Propag, vol. 66, no. 2, pp. 996-1001, Feb. 2018.

[7] S. S. Yang, K. Luk, H. Lai, A. Kishk and K. Lee, "A dual-polarized antenna with pattern diversity," IEEE Antennas and Propagation Magazine, vol. 50, no. 6, pp. 71-79, Dec. 2008.

[8] “Polarization in radar systems,” *Natural Resources Canada*, 13-Nov-2014. [Online]. Available: https://www.nrcan.gc.ca/maps-tools-and-publications/satellite-imagery-and-air-photos/satellite-imagery-products/educational-resources/tutorial-radar-polarimetry/polarization-radar-systems/9567. [Accessed: 16-Feb-2022].

[9]Y. Ushijima, E. Nishiyama and M. Aikawa, "Circular polarization switchable microstrip antenna with SPDT switching circuit," *2010 IEEE Antennas and Propagation Society International Symposium*, 2010, pp. 1-4, doi: 10.1109/APS.2010.5560951.

[10] S. Feng, E. Nishiyama and M. Aikawa, "Linear polarization switchable slot ring array antenna with SPDT switch circuit," *2009 Asia Pacific Microwave Conference*, 2009, pp. 2794-2797, doi: 10.1109/APMC.2009.5385374.

[11] S. Yao, X. Liu, S. V. Georgakopoulos and R. Schamp, "Polarization switchable origami helical antenna," *2016 IEEE International Symposium on Antennas and Propagation (APSURSI)*, 2016, pp. 1667-1668, doi: 10.1109/APS.2016.7696540.

[12] Aixin Chen, Weiwei Jiang, Zhizhang Chen, Jiaheng Wang, "Overview on Multipattern and Multipolarization Antennas for Aerospace and Terrestrial Applications", International Journal of Antennas and Propagation, vol. 2013, Article ID 102925, 11 pages, 2013. https://doi.org/10.1155/2013/102925

[13] R.R. Tummala, "Moore's law meets its match (system-on-package), IEEE Spectrum, Vol. 43, pp. 44-49.

[14] R. Garg, P. Bhartia, I. Bahl, and A. Ittipiboon, *Microstrip Antenna Design Handbook*. Boston, MA: Artech House, 2001.

[15] Chaudhuri, Sumantra & Mishra, Mohit & Kshetrimayum, Rakhesh & Sonkar, Ramesh & Bhattacharjee, Somen & Saha, Bhaskar. (2020). High port-to-port isolation dual circularly polarised microstrip patch antenna with multifunction DGS. IEE Proceedings - Microwaves Antennas and Propagation. 14. 10.1049/iet-map.2020.0094.

[16] Gao, S.S., Luo, Q., Zhu, F. *Circularly Polarized Antennas.* (John Wiley & Sons, New Jersey, USA, 2013)

[17] "Antenna gain : Directivity, efficiency and gain conversion," *ElProCus*, 11-Sep-2019. [Online]. Available: https://www.elprocus.com/antenna-gain-directivity-efficiency and-its-conversion/. [Accessed: 18-Mar-2022].

[18] B. Syrett, Class Lecture, Topic: "6.0 Matching Circuits." ELEC 4502, Department of Electronics, Carleton University, Ottawa, ON., 2016.

[19] A. D. Yaghjian and S. R. Best, "Impedance, bandwidth, and Q of antennas," in *IEEE Transactions on Antennas and Propagation*, vol. 53, no. 4, pp. 1298-1324, April 2005, doi: 10.1109/TAP.2005.844443.

[20] Robert Mailloux, *Phased Array Antenna Handbook, Third Edition*, Artech, 2017.

[21] K. Benson, “Phased array beamforming ICS simplify antenna design,” *Analog Dialogue*, Jan-2019. [Online]. Available: https://www.analog.com/media/en/analog-dialogue/volume-53/number-1/phased-array-beamforming-ics-simplify-antenna-design.pdf. [Accessed: 19-Apr-2022].

[22] A. Bole, A. Wall, and A. Norris, “The Radar System – Technical Principals,” in Radar and ARPA Manual. Oxford, U.K.: Butterworth-Heinemann, 2014, pp. 29–137

[23] A. Petosa, Class Lecture, Topic: "6. Antenna Arrays." ELEC 5607, Department of Electronics, Carleton University, Ottawa, ON., 2019.

[24] M. N. O. Sadiku, *Elements of Electromagnetics, 6th Edition*. New York: Oxford University Press, 2015.

[25] “Intro to antenna polarization,” *JEM Engineering Blog*, 21-Mar-2022. [Online]. Available: https://jemengineering.com/blog-intro-to-antenna-polarization/#:~:text=The%20polarization%20of%20an%20antenna,is%20received%20by%20an%20antenna. [Accessed: 16-Apr-2022].

[26] A. Sattu et al.,"Small-and Large-Signal Performance of III-Nitride RF Switches With Hybrid Fast/Slow Gate Design," IEEE Microwave and Wireless Comp. Letters, Vol. 21, No. 6, pp. 305-307, Jun. 2011

[27] D. M. Pozar, *Microwave Engineering, 4th Edition*. New York: John Wiley & Sons, ., 2012.

[28] Griesmer, F., 2014. *Modelling a Branch Line Coupler*. [Online] COMSOL Multiphysics. Available at: <https://www.comsol.com/blogs/modeling-branch-line-coupler/> [Accessed 8 October 2021].

[29] Y.C. Hsu, I. Haroun, D.C. Chang, R. E. Amaya and K. Hettak, "A low-cost small-size 60 GHz quadrature coupler for IPD-based SiP radio systems," 2014APMC Conf., pp.831-833, Japan, Sept. 2014.

[30] Analog Devices, “Materials8 GHz to 16 GHz, 4-Channel, X Band and Ku Band Beamformer,” ADAR1000 datasheet, Jun. 2018 [Revised Mar. 2019].

[31] Rogers Corporation, “RO4000 Series High Frequency Circuit Materials,” RO4003 datasheet, 2018.

[32] Panwar, Harvesh & Khan, Firoz & Khanna, Puneet. (2013). Design & Analysis of Square Microstrip Patch Antenna. Artificial intelligence for engineering design analysis and manufacturing. 2. 79-81.

[33] S. V. Hum, J. Z. Chu, R. H. Johnston and M. Okoniewski, "Efficiency of a resistively loaded microstrip patch antenna," in IEEE Antennas and Wireless Propagation Letters, vol. 2, pp. 22-25, 2003, doi: 10.1109/LAWP.2003.810777.

[34] B. Syrett, Class Lecture, Topic: "7.0 Microwave Resonators." ELEC 4502, Department of Electronics, Carleton University, Ottawa, ON., 2016.

[35] Mini-Circuits, “Power Splitter/Combiner,” ZC4PD-153-S+ datasheet, [Revised Apr. 2014].

[36] Haroun, I. (Ibrahim), Hsu, Y.-C. (Yuan-Chia), Chang, D.-C. (Da-Chiang), and C Plett, """A novel reduced-size 60-GHz 180° coupler using LG-CPW transmission lines""", presented at the Asia-Pacific Microwave Conference, APMC 2011, 2011.

[37] Peregrine Semiconductor, "UltraCMOS SPDT RF Switch 9 kHz-13 GHz," PE42520 datasheet, 2021.

[38] W. Zhou, N. Javanbakht, S. Abdullah, J. Labossiere, J. Hyland and R. E. Amaya, "Dual Differential-Fed 2×2 Phased Array with Reconfigurable Polarization and Radiation Pattern Diversity," *2021 IEEE 19th International Symposium on Antenna Technology and Applied Electromagnetics (ANTEM)*, 2021, pp. 1-2, doi: 10.1109/ANTEM51107.2021.9518671.

[39] W. Zhou, J. Labossiere, N. Javanbakht, S. Abdullah and R. E. Amaya, "Mutual Coupling Reduction in Dual Differential-Fed 2×1 Phased Array with Polarization and Pattern Diversity," *2021 IEEE International Symposium on Antennas and Propagation and USNC-URSI Radio Science Meeting (APS/URSI)*, 2021, pp. 919-920, doi: 10.1109/APS/URSI47566.2021.9704461.